CHEMICAL REVIEWS

pubs.acs.org/CR

Review

# Structure and Mechanism of Respiratory III–IV Supercomplexes in Bioenergetic Membranes

Peter Brzezinski,* Agnes Moe, and Pia Ädelroth

Cite This: *Chem. Rev.* 2021, 121, 9644–9673

Read Online

ACCESS | Metrics & More | Article Recommendations

**ABSTRACT:** In the final steps of energy conservation in aerobic organisms, free energy from electron transfer through the respiratory chain is transduced into a proton electrochemical gradient across a membrane. In mitochondria and many bacteria, reduction of the dioxygen electron acceptor is catalyzed by cytochrome *c* oxidase (complex IV), which receives electrons from cytochrome $bc_1$ (complex III), via membrane-bound or water-soluble cytochrome *c*. These complexes function independently, but in many organisms they associate to form supercomplexes. Here, we review the structural features and the functional significance of the nonobligate $III_2IV_{1/2}$ *Saccharomyces cerevisiae* mitochondrial supercomplex as well as the obligate $III_2IV_2$ supercomplex from actinobacteria. The analysis is centered around the Q-cycle of complex III, proton uptake by CytcO, as well as mechanistic and structural solutions to the electronic link between complexes III and IV.

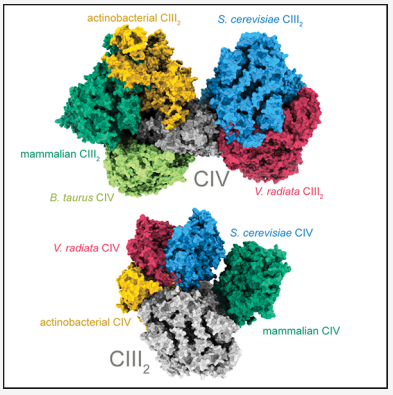


## CONTENTS



**Received:** February 18, 2021
**Published:** June 29, 2021

ACS Publications

© 2021 The Authors. Published by American Chemical Society



https://doi.org/10.1021/acs.chemrev.1c00140
*Chem. Rev.* 2021, 121, 9644–9673

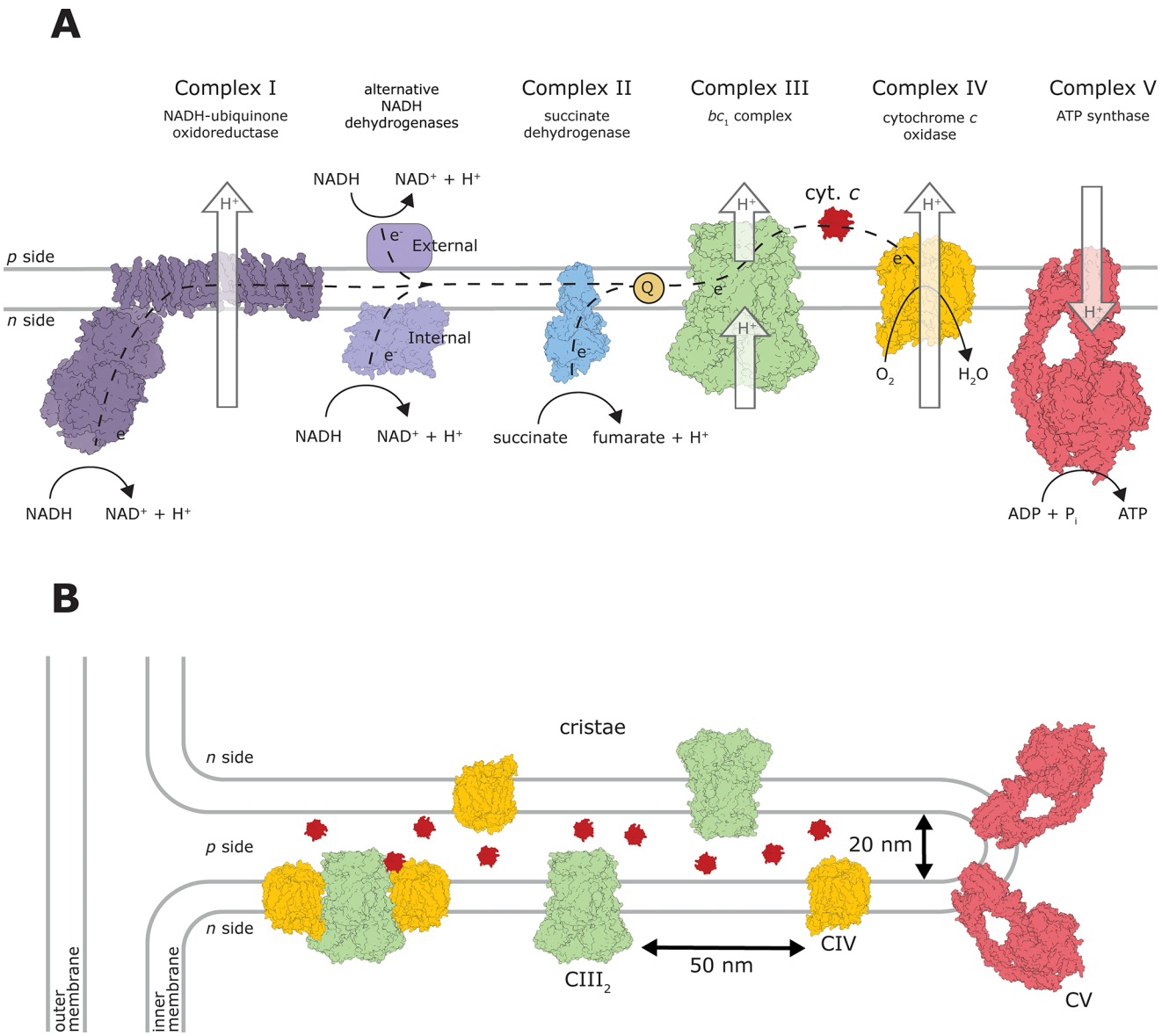


**Figure 1.** The mitochondrial respiratory chain. (A) Complex I of mammalian mitochondria is not present in *S. cerevisiae*. Instead, the external (Nde1, Nde2) and internal (Ndi1) membrane-associated NADH dehydrogenases catalyze the same NADH-oxidation:Q reduction reaction as complex I. All these enzymes are shown here in the same membrane only to illustrate the different pathways of NADH oxidation. The structures originate from different organisms: *T. thermophilus* complex I (PDB 3M9S), *S. cerevisiae* Ndi1 (PDB 4G9K), *S. scrofa* (pig) complex II (PDB 1ZOY), *S. cerevisiae* complex III and IV (PDB 6HU9), *S. cerevisiae* complex V (PDB 6CP6), and *S. cerevisiae* cyt. *c* (PDB 1YCC). (B) The respiratory chain is found in protrusions of the inner membrane that are called cristae. Here, the respiratory chain components I–IV (only complexes III and IV are shown) are located in the flat regions, while the ATP synthase (complex V) is restricted to the bent end regions. Approximate dimension and average distance are from refs 16,49–52. The cyt. *c*:Cyt*c*O ratio in *S. cerevisiae* is 2–4, which is equivalent to an average concentration of ~100 $\mu$M cyt. *c* in the intercristae space.[16,50]

## 1. INTRODUCTION

Aerobic organisms extract energy by linking oxidation of environmental compounds to production of ATP. In eukaryotes, these compounds are initially degraded to yield NADH, which is used to reduce molecular oxygen to water. Electrons from NADH are transferred through a number of enzymes that reside in the inner mitochondrial membrane. These enzymes are collectively referred to as the respiratory chain because they are wired to transfer electrons consecutively from low-potential electron donors, via a number of intermediate electron carriers, to the final, high-potential electron acceptor, $O_2$. The electron current through the respiratory chain drives proton translocation across the membrane, from the inside mitochondrial matrix (negative side, *n*) to the outside intermembrane space (positive side, *p*) (Figure 1A). As a result of this process, a difference in voltage and proton concentration is maintained across the membrane, referred to as an electrochemical proton gradient or protonmotive force (PMF).[1] The free energy that is stored in this electrochemical gradient is typically in the order ~0.2 eV,[2,3] and it is used for production of ATP from ADP by the ATP synthase (also known as $F_1F_o$-ATP-synthase and sometimes referred to as complex V) or for transport of molecules or ions across the membrane.[4]

In mitochondria, the energy-conversion machinery is found in protrusions of the inner membrane which define subcompartments called cristae. Here, the respiratory chain is located in the


https://doi.org/10.1021/acs.chemrev.1c00140
Chem. Rev. 2021, 121, 9644–9673

flat regions, while the ATP synthases are restricted mainly to the bent end regions[5,6] (Figure 1B). In aerobic bacteria the respiratory chain is found in the cytoplasmic membrane where protons are translocated from the cytoplasm to the periplasm (for review, see refs 2,7−9).

In mammalian mitochondria, the first component of the respiratory chain is an integral membrane protein called NADH:ubiquinone oxidoreductase (also named complex I), which catalyzes oxidation of NADH and reduction of quinone (Q) to quinol ($QH_2$) (Figure 1A). This electron-transfer reaction is linked to pumping of protons across the membrane. Many yeast species such as *Saccharomyces* (*S.*) *cerevisiae* do not harbor a complex I, but in these mitochondria, oxidation of NADH and reduction of Q is catalyzed by other, membrane peripheral NADH dehydrogenases located both on the inner (Ndi1) and outer (Nde1 and Nde2) surfaces of the inner mitochondrial membrane[10−12] (Figure 1A). Electron transfer to Q is also performed by succinate dehydrogenase (also named complex II). Reduced $QH_2$ diffuses within the membrane to donate electrons to ubiquinol-cytochrome *c* reductase (also named cytochrome (cyt.) $bc_1$ or complex III), which transfers electrons to water-soluble cyt. *c* that resides in the intermembrane space. Reduced cyt. *c* is an electron donor to cytochrome *c* oxidase (Cyt*c*O, also named complex IV), which catalyzes oxidation of cyt. *c* and reduction of molecular oxygen to water. Aerobic bacteria utilize a wide range of electron donors, and a specific organism may harbor many different respiratory chains that are expressed depending on environmental conditions and are often branched. General reviews of these pathways are found in refs 2,7,13−15.

Because the mobile electron carriers of the mitochondrial electron-transport chain, i.e., $QH_2$ and cyt. *c*, can diffuse freely in the membrane and water phases, respectively, a functional link between the components of the respiratory chain does not require a physical linkage between these complexes. Experimental data and theoretical analyses supported a model where all respiratory complexes diffuse independently in the membrane, as do the electron carriers Q and cyt. *c*.[16] This perception changed gradually with the invention of blue native polyacrylamide gel electrophoresis (BN-PAGE), which made it possible to identify larger complexes, referred to as respiratory supercomplexes, composed of different combinations of the respiratory enzymes with variable stoichiometry.[17] Functionally active respiratory supercomplexes were found in a wide range of organisms.[17−28] Recent structural studies of the inner mitochondrial membrane using electron cryo-tomography in situ demonstrated that the electron-transport chain components are organized in supercomplexes in mammals, yeast and plants,[29] i.e., the observation of supercomplexes is not a consequence of the isolation procedures used. A wide range of these supercomplexes with different composition and stoichiometry of the components have been isolated using "weak" detergents, and in recent years a number of high-resolution supercomplex structures have been obtained using electron cryomicroscopy (cryo-EM) (reviewed in refs 30,31 and listed in Table 1).

From the above discussion, it becomes apparent that the term "respiratory supercomplex" is used to describe a phenomenon, i.e., formation of membrane-bound clusters of respiratory complexes rather than entities with a well-defined composition (see Table 1). This variation in the constituents and their stoichiometry has contributed to the difficulty in uncovering a functional role of respiratory supercomplexes, which is reflected in ongoing discussions (e.g., refs 53−55).

**Table 1. Cryo-EM Structures of Supercomplexes That Contain Complexes $III_2$ and IV**

| composition | organism | reference | comment |
|---|---|---|---|
| $III_2IV_1$ | *Vigna radiata* (mung bean) | 32 | PDB 7JRP |
| $III_2IV_1$ and $III_2IV_2$ | *S. cerevisiae* | 33 | PDB 6T15, 6T0B |
| | | 34 | PDB 6HU9 |
| | | 35 | PDB 6GIQ |
| | | 36 | PDB 6YMX |
| | | 37 | EMD 23414 |
| $I_1III_2IV_1$ | *O. aries* (sheep) | 38 | PDB 5J4Z, 5J7Y |
| | *S. scrofa* (pig) | 39 | PDB 5GPN |
| | *S. scrofa* | 40 | PDB 5GUP |
| | *B. taurus* (cow) | 41 | PDB 5LUF |
| $I_1III_2IV_1$ and $I_2III_2IV_2$ | *H. sapiens* (human) | 42 | PDB 5XTH, 5XTI |
| $III_2IV_2$ | *M. smegmatis* | 43 | PDB 6ADQ |
| | | 44 | PDB 6HWH |
| $III_2IV_2$ | *C. glutamicum* | 45 | |
| $III_2IV_1$ | *R. capsulatus* | 46 | PDB 6XKW, 6XKX, 6XKZ<br>Cyt. $bc_1$ and $cbb_3$ type complex IV, including cyt. $c_y$ |
| $ACIII_1IV_1$ | *F. johnsoniae* | 47 | EMD-7447<br>alternative complex III from *R. marinus* also in ref 48 |

Many Gram-negative prokaryotes also harbor respiratory supercomplexes, but much less is known about their composition or structure (reviewed in ref 56). For example, in *Paracoccus* (*P.*) *denitrificans*, which under aerobic conditions harbors a respiratory chain similar to that of mitochondria, supercomplexes composed of complexes III and IV were isolated already in 1985,[57] and a larger supercomplex that included also complex I was identified later.[58] In a recent study, a complex III−IV supercomplex from *Rhodobacter* (*R.*) *sphaeroides* that contains a membrane-anchored cyt. $c_y$ was isolated and functionally characterized.[59] In another recent study, the cryo-EM structure of a *Rhodobacter capsulatus* supercomplex composed of complex III, a $cbb_3$-type complex IV and a membrane-anchored cyt. $c_y$ was presented.[46] Furthermore, in *Escherichia* (*E.*) *coli* cytoplasmic cell membranes a segregation of respiratory complexes into subdomains was observed *in vivo*, although these bacteria do not harbor supercomplexes.[60,61] Gram-positive bacteria, which belong to the phylum Actinobacteria, e.g., *Mycobacterium* (*M.*) *smegmatis*, *Mycobacterium tuberculosis*, and *Corynebacterium* (*C.*) *glutamicum*, lack small *c*-cytochromes and harbor an obligate supercomplex composed of a complex III dimer flanked by two monomers of complex IV (denoted $III_2IV_2$), which are electronically linked by the diheme cyt. *cc* domain of complex III.[62−67] A supercomplex composed of complexes III and IV was also isolated from the Gram-positive bacterium *Bacillus* PS3.[68]

The *S. cerevisiae* respiratory supercomplex is composed of a cyt. $bc_1$ dimer, flanked by either one or two Cyt*c*Os on each side


https://doi.org/10.1021/acs.chemrev.1c00140
Chem. Rev. 2021, 121, 9644−9673

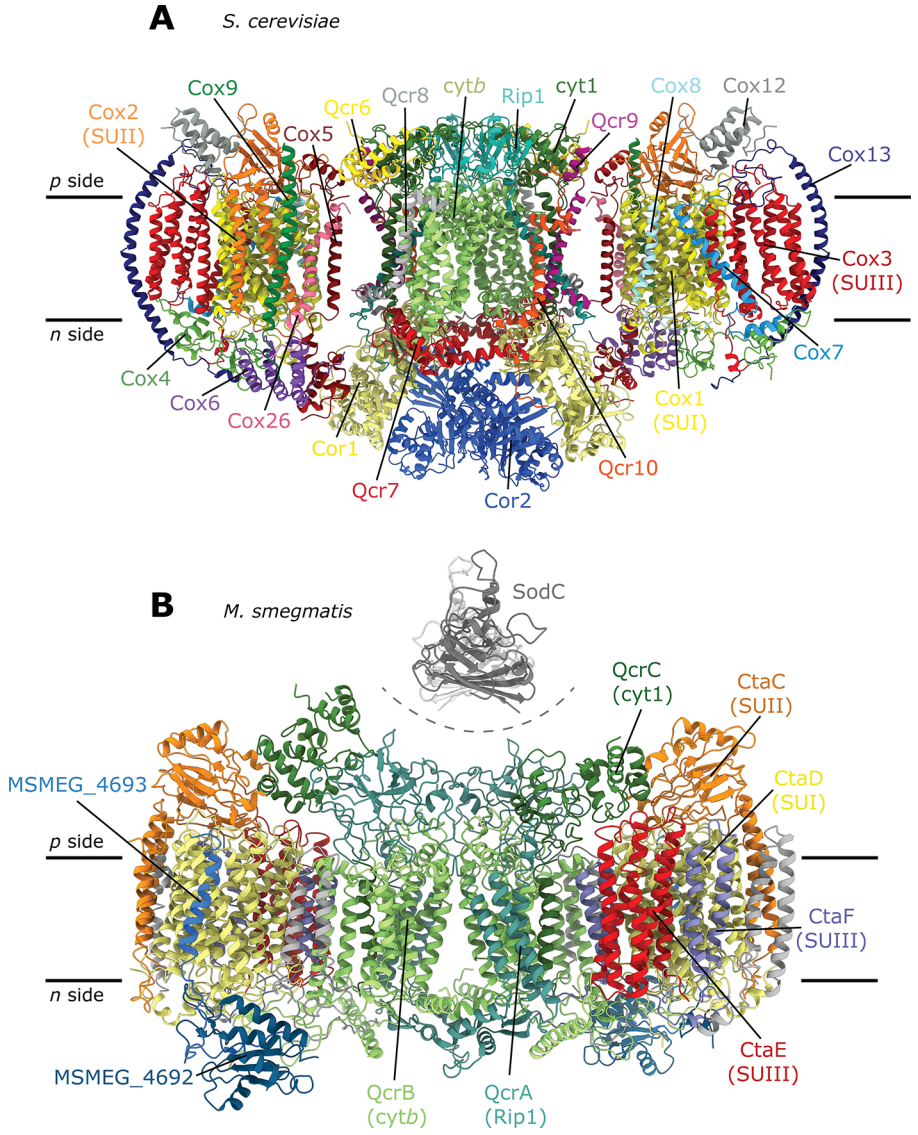


**Figure 2.** Structures of $III_2IV_2$supercomplexes. (A) *S. cerevisiae* supercomplex (PDB 6HU9). Catalytically important subunits of complexes III are cyt*b*, the Rieske iron−sulfur protein (also called Rip1 in *S. cerevisiae*) and cyt1, while those of complex IV are cox1−3 (also called SU I−III). (B) *M. smegmatis* supercomplex (PDB 6HWH, SodC is 1PZS). Catalytically important subunits of complexes III and IV are QcrA-C and CtaC-F (equivalent of SU I−III), respectively. The equivalent of canonical SU III is composed of two parts, CtaE and CtaF. Unidentified subunits are shown in gray. The SodC-type superoxide dismutase dimer subunit (PDB 1PZS) was identified in the structure.[43,44] It was less resolved in ref 44, which did not allow identification of a connection between the subunit and the rest of the supercomplex (illustrated by the dashed line).

of the central dimer.[17,18,69−77] Recently determined cryo-EM structures of this supercomplex[33−35,37] revealed its molecular architecture (Figure 2A) but also showed that the association of cyt. $bc_1$ and CytcO does not lead to any significant structural changes of the components. This observation suggests that the functionality of the *S. cerevisiae* supercomplex is simply that of the sum of the components, except that the components reside at a fixed intercomplex distance. In contrast, structural and functional studies of the *M. smegmatis*[43,44] (Figure 2B) and *C. glutamicum*[45,62,65] supercomplexes revealed intercomplex connections that presumably modulate the functionality of the components, consistent with the obligate nature of these supercomplexes.

Recent progress in development of methods to isolate pure respiratory supercomplexes has allowed functional studies using biochemical and biophysical techniques, previously employed in studies of the individual respiratory complexes. Major advancement in the field was contributed by the use of cryo-EM to determine the overall architecture of supercomplexes, high-resolution structures of their components as well as positions and distances between all cofactors (shown for the *S. cerevisiae* and *M. smegmatis* supercomplexes in Figure 3). These studies are still in an early phase, but the data available to date allows a discussion of possible links between the molecular architecture and function of respiratory supercomplexes. This review is centered around the *S. cerevisiae* supercomplex, but we also discuss the *M. smegmatis* and *C. glutamicum* obligate $III_2IV_2$ supercomplexes while focusing on functional similarities and differences to the mitochondrial counterpart. The emphasis is put on the biological processes at the molecular level in terms of physical mechanisms.


https://doi.org/10.1021/acs.chemrev.1c00140
*Chem. Rev.* 2021, 121, 9644−9673

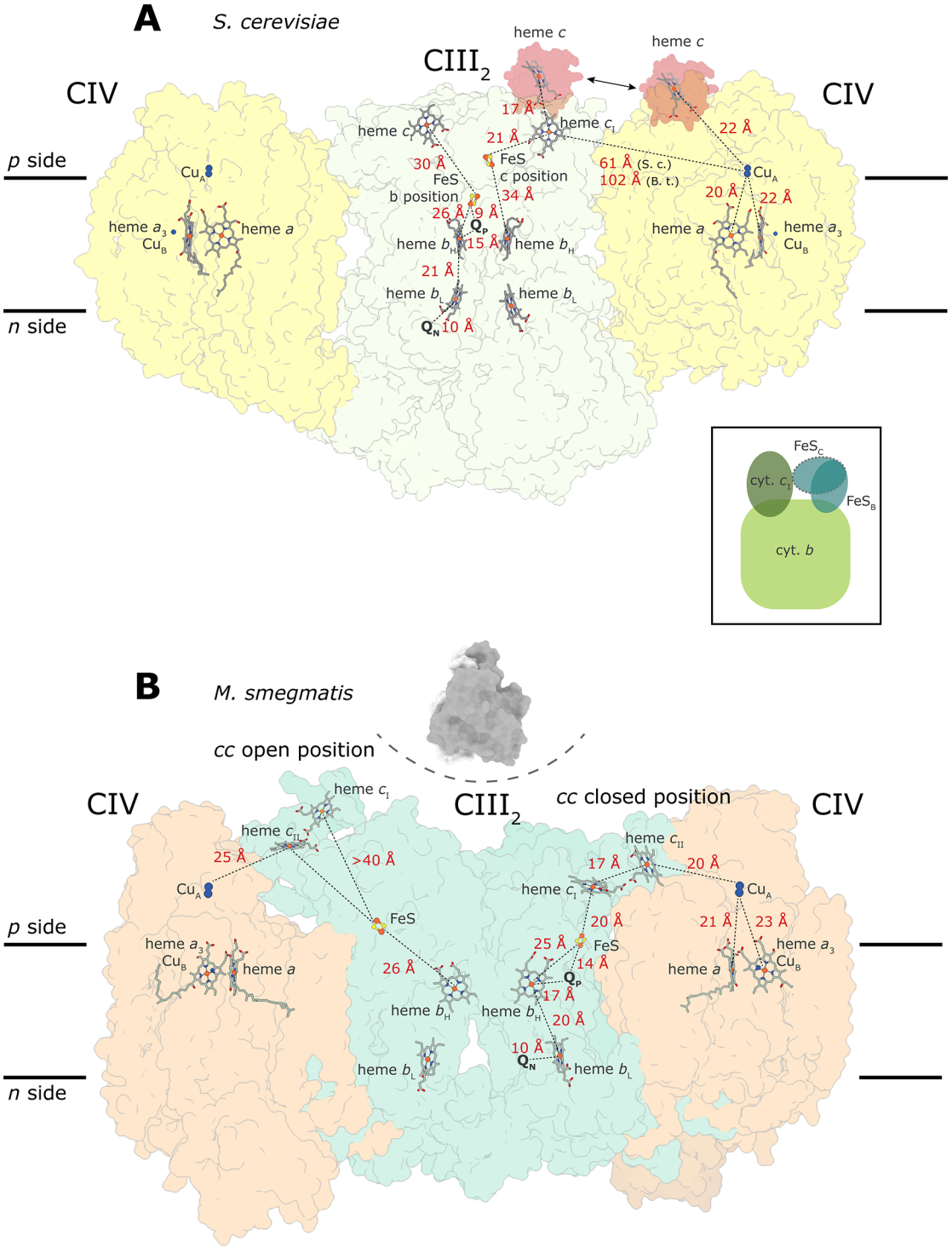


**Figure 3.** Distances between cofactors. (A) *S. cerevisiae* (PDB 6HU9) and (B) *M. smegmatis* (PDB 6HWH) supercomplexes. In (A), distances for the FeS center in the C ($FeS_C$) and B ($FeS_B$) positions, respectively (see inset), are indicated in the two halves of the complex $III_2$ dimer. Note that the arrangement shown in (A) is a fusion of two different structures where the FeS center is either in $FeS_B$ (left monomer) or $FeS_C$ (right monomer) (B position PDB is 1KYO, C position is PDB 3H1H). The positions of cyt. *c* bound to cyt. $bc_1$ or CytcO are indicated (cyt. *c* at complex III is PDB 1KYO, cyt. *c* at complex IV is PDB 5IY5), see also ref 37. In (B), the open and closed conformations of the cyt. *cc* domain, observed in a single supercomplex, are shown (SodC is PDB 1PZS).

## 2. COMPLEX III

Complex III (cyt. $bc_1$) is an obligate homodimer. Each monomer is composed of three main, functionally important catalytic subunits (Figure 4A): (*i*) cyt. *b* (QcrB in actinobacteria), which harbors two hemes B and two quinone-binding sites; (*ii*) cyt. $c_1$, which harbors a heme C (QcrC, which harbors two hemes C in actinobacteria); (*iii*) the Rieske iron−sulfur protein (ISP, called QcrA in actinobacteria or Rip1 in *S. cerevisiae*), which harbors a 2Fe-2S center (FeS) that is bound in an ectodomain on the *p* side of the membrane (reviewed, e.g., in ref 78−85). In addition to these three catalytic subunits, in *S. cerevisiae*, each cyt. $bc_1$


https://doi.org/10.1021/acs.chemrev.1c00140
Chem. Rev. 2021, 121, 9644−9673

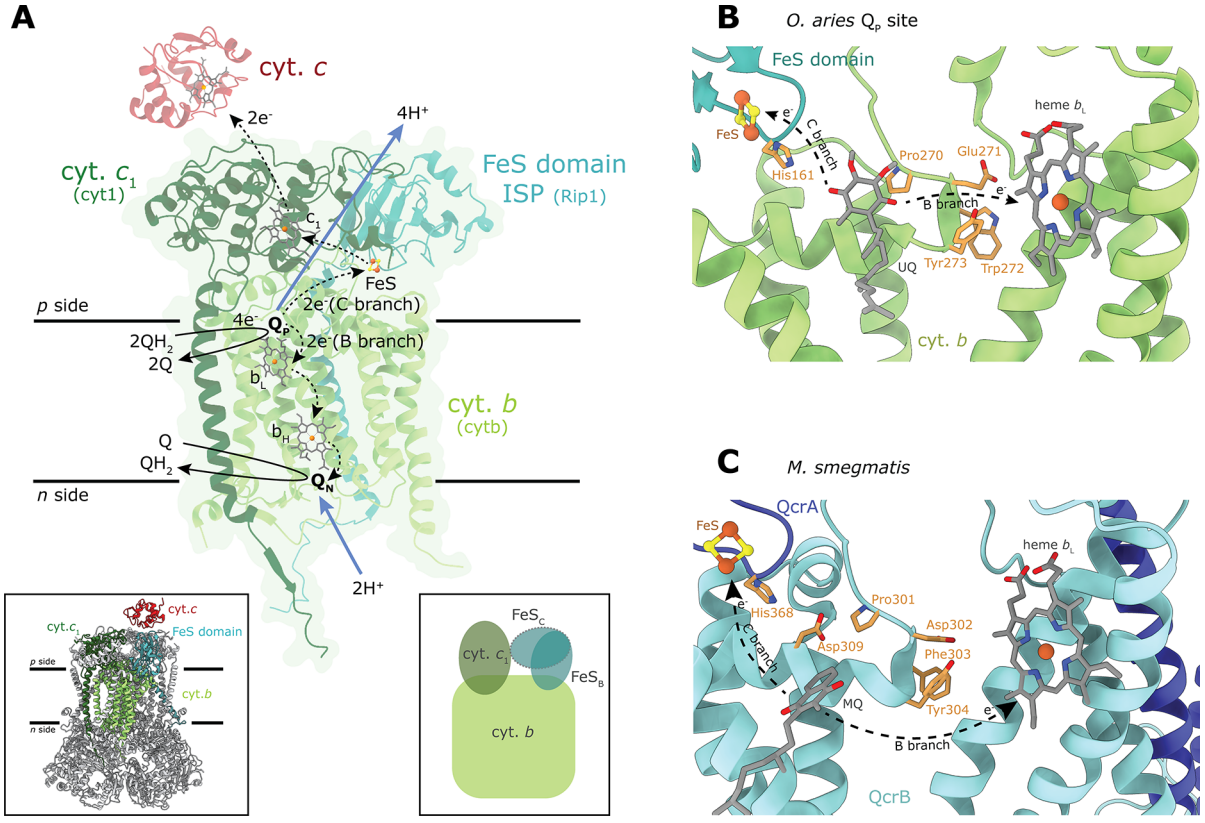


**Figure 4.** Complex III. (A) The catalytically important subunits of one monomer of complex $III_2$ (cyt. $bc_1$) from *S. cerevisiae* (PDB 6HU9) and the catalyzed reaction. The electron-transfer paths along the B and C branches are indicated with dashed lines, while proton uptake and release are shown with blue arrows. Note that the total stoichiometry of electron and proton transfer is indicated for oxidation of two $QH_2$. Upon oxidation of each $QH_2$ in the $Q_P$ site, two electrons are transferred, one electron along each of the B and C branches, respectively. One $H^+$ is transferred to His161 (His181 in *S. cerevisiae*) ligand of the FeS center (shown in B) and is transferred to the *p* side upon movement of the FeS-domain from the B position ($FeS_B$ in the right-hand side inset to A) to the C position ($FeS_C$). The second $H^+$ is transferred via protonatable residues of the cyt. *b* subunit (see text). The same sequence of electron and $H^+$ transfer is repeated upon binding of the second $QH_2$ in the $Q_P$ site. The inset on the lower left shows all subunits of the dimer, including accessory subunits in gray and bound cyt. *c* (PDB 1KYO). In main panel A, the FeS center is found in an intermediate B/C position. (B) The $Q_P$ binding site of *O. aries* (sheep, PDB 6Q9E) with a bound ubiquinone (UQ),[38] the only structure of a mitochondrial cyt. $bc_1$ in which the $Q_P$ site is occupied by Q. The $Q_P$ site and all functionally important residues are conserved in the *S. cerevisiae* cyt. $bc_1$. (C) The $Q_P$ site of *M. smegmatis* complex III (PDB 6ADQ).

monomer is composed of an additional 7 subunits (Figure 2A), collectively shown in gray in the inset to Figure 4A (lower left).

## 2.1. Catalytic Reaction and Quinone Binding

Complex III catalyzes net oxidation of $QH_2$ and reduction of cyt. *c* in a reaction sequence that is referred to as the proton-motive Q-cycle, which contributes to maintaining the proton electrochemical potential across the inner mitochondrial membrane.[86] The $QH_2$ electron donor binds in a Q-binding site referred to as $Q_P$, which is located near the *p* side of the membrane (also called $Q_o$) (Figure 4A). In the mitochondrial cyt. $bc_1$, this site is characterized by a conserved PEWY (Pro-Glu-Trp-Tyr) motif[87] (residues 270−273 in Figure 4B). The equivalent in *M. smegmatis* is PDFY (PDVY in *C. glutamicum*) residues 301−304 in Figure 4C. The first electron from $QH_2$ is transferred to the FeS center and then to cyt. $c_1$ along a branch that is referred to as the "C branch" (Figure 4A). This electron transfer is accompanied by release of two protons to the aqueous solution on the membrane *p* side. The second electron is transferred along the "B branch", consecutively to the low-potential heme $b_L$, the high-potential heme $b_H$ and a Q in the $Q_N$ site (also called $Q_i$), which forms a semiquinone, $SQ^{\bullet-}$. After oxidation of $QH_2$ in the $Q_P$ site, the product Q is replaced by another $QH_2$, and the sequence of electron and proton-transfer reactions is repeated.

As a result, a doubly reduced $QH_2$ is formed at the $Q_N$ site after proton uptake from the *n* side. The $QH_2$ is released from the $Q_N$ site by equilibration with the $Q/QH_2$ pool in the membrane. The overall reaction catalyzed by cyt. $bc_1$ is (see also Figure 4A):

Oxidation of first $QH_2$ in the $Q_P$ site:

$$(QH_2)_P + (Q)_N + (\text{cyt. } c^{3+})_P \rightarrow (Q)_P + 2H_p^+ + (SQ^{\bullet-})_N + (\text{cyt. } c^{2+})_P \quad (1a)$$

Oxidation of second $QH_2$ in the $Q_P$ site:

$$(QH_2)_P + (SQ^{\bullet-})_N + 2H_n^+ + (\text{cyt. } c^{3+})_P \rightarrow (Q)_P + 2H_p^+ + (QH_2)_N + (\text{cyt. } c^{2+})_P \quad (1b)$$

Overall reaction:

$$2(QH_2)_P + (Q)_N + 2H_n^+ + 2(\text{cyt. } c^{3+})_P \rightarrow 2(Q)_P + 4H_p^+ + (QH_2)_N + 2(\text{cyt. } c^{2+})_P \quad (1c)$$

where subscripts *n* and *p* refer to the two sides of the membrane, respectively, and *N* and *P* refer to the two Q-binding sites, respectively.



https://doi.org/10.1021/acs.chemrev.1c00140
Chem. Rev. 2021, 121, 9644−9673

Crystal structures of cyt. $bc_1$ complexes have revealed a single bound Q in the $Q_N$ site for each monomer, but the $Q_P$ site is typically empty. The putative position of the $Q_P$ site was instead revealed by the location of inhibitors such as stigmatellin or myxothiazol (reviewed in refs 78,81,84). In the cryo-EM structures of the *S. cerevisiae* cyt. $bc_1$ complexes[33−35,37] a Q could not be modeled convincingly in the $Q_P$ site, but a ubiquinone (UQ) was found to be bound in the $Q_N$ site, in line with the earlier structural studies using X-ray crystallography. A recent cryo-EM study of the mammalian $I_1III_2$ supercomplex[88] revealed a UQ in the $Q_P$ site, but only in one monomer of the cyt. $bc_1$ dimer (the other $Q_P$ site was empty). In another recent cryo-EM structure of complex $III_2$ from *C. albicans*, density for a UQ was found in both $Q_P$ sites of the dimer (as well as in the $Q_N$ sites), although at low occupancy.[89]

On the basis of the observation of an empty $Q_P$ site and a UQ bound in the $Q_N$ site in the *S. cerevisiae* complex III, it was recently suggested that a higher affinity for UQ at the $Q_N$ site would prevent release of a semiquinone that would give rise to superoxide upon reaction with $O_2$.[35] However, we note that (*i*) the difference in affinity for UQ at the two binding sites is not directly related to the affinity of the negatively charged semiquinone radical, $SQ^{\bullet-}$, at these sites,[90] (*ii*) $SQ^{\bullet-}$ is not released to the membrane, i.e., the reaction of $O_2$ with $SQ^{\bullet-}$ is more likely to occur *in situ*, but (*iii*) it occurs at the $Q_P$ rather than at the $Q_N$ site.[81,91,92] We instead suggest that observation of a bound UQ in the $Q_N$ site reflects a higher affinity for the substrate UQ in that site, compared to the product UQ in the $Q_P$ site (all structures were obtained with the oxidized state of complex III).

In the *M. smegmatis* and *C. glutamicum* $III_2IV_2$ supercomplexes, menaquinone (MQ) was observed in the $Q_P$ and $Q_N$ sites but also at additional sites on the *p* side of complex III.[43−45] The MQ in the $Q_P$ site of the *M. smegmatis* complex III overlaps in space with that of UQ in the mammalian complex III. In *C. glutamicum*, the $Q_P$ cavity is larger than in *M. smegmatis*, and the data suggest that MQ could also occupy a position just outside of the $Q_P$ site, suggesting two possible binding modes, one inside and one just outside of the $Q_P$ site.[45] Furthermore, in both *M. smegmatis*[44] and *C. glutamicum*[45] supercomplexes, clear density corresponding to an additional MQ on the *p* side was observed. In the *M. smegmatis* supercomplex, this MQ is positioned near the Tyr of the PDFY motif, at the vertex of a triangle formed the FeS center (at a distance of ∼20 Å) and heme $b_L$ (at a distance of ∼20 Å). In the *C. glutamicum* supercomplex structure, the second MQ is located at a distance of ∼14 Å from heme $b_L$ and ∼35 Å from the FeS center. The role of an additional MQ binding site on the *p* side is unknown, but identification of these Q-binding sites in both *C. glutamicum* and *M. smegmatis* suggests a functional role, for example, to bypass energy conservation in complex III at low $O_2$ concentrations.[45]

## 2.2. The Bifurcated Electron Transfer

A bifurcated electron transfer from $QH_2$ at the $Q_P$ site is required by the Q-cycle mechanism. As outlined above, in this process, one electron from $QH_2$ is transferred to FeS and one to heme $b_L$ along the C and B branches, respectively (Figure 4A), which is schematically outlined in the following equation, assuming a putative semiquinone intermediate:

$$QH_2FeSb_L \underset{k_{-1}}{\overset{k_1}{\rightleftarrows}} SQ^{\bullet-}FeS^{-}b_L \xrightarrow{k_2} QFeS^{-}b_L^{-} \qquad (2)$$

### 2.2.1. Canonical Complex III.

The detailed mechanism of this bifurcation at the $Q_P$ site remains enigmatic.[78,81,82] Transfer from $QH_2$ to FeS with a midpoint potential $E_m{}^7 \geq 300$ mV is thermodynamically more favorable than transfer to heme $b_L$ with $E_m{}^7 \cong 0$ mV (when heme $b_H$ is oxidized). Thus, oxidation of $QH_2$ results first in reduction of FeS along the C branch. The second electron could in principle also be transferred along the same C branch to FeS after reoxidation of $FeS^-$ by cyt. $c_1$, i.e., without energy conservation.[82] Instead, the electron is transferred along the B branch in a reaction that is strictly controlled yielding almost complete reduction of heme $b_L$. This phenomenon was clearly illustrated in an experiment where transfer to the $Q_N$ site, along the B branch, was inhibited by binding of the $Q_N$-site inhibitor antimycin. Even though, in principle, the enzyme could turnover by electron transfer via the C branch only, this block of the B branch resulted in reduction of both hemes $b_L$ and $b_H$ and almost full inhibition of the cyt. $bc_1$ turnover complex.[93]

Crystal structures of canonical cyt. $bc_1$ complexes revealed that the FeS ectodomain could adopt different positions where in the two extreme orientations the FeS cluster is found in proximity to either cyt. $c_1$ (C position) or heme $b_L$ (B position).[94−96] These two FeS ectodomain positions are indicated schematically in the right-hand side inset to Figure 4A (see also inset to Figure 3A). The distance spanned by the FeS cluster while moving between the B and C positions is almost 20 Å, and the structural data suggested that the FeS cluster could accept electrons from $QH_2$ (in site $Q_P$) only in the B position, while electron transfer to cyt. $c_1$ would occur only in the C position. However, the link between $Q/QH_2$ binding in the $Q_P$ site, the redox state of FeS and the equilibrium constant for the two FeS-domain positions remains enigmatic.[78,81,97]

Structural studies with different types of inhibitors bound in the $Q_P$ site indicate that the position of the FeS ectodomain depends on its interactions with the inhibitor as well as minor structural changes caused by the inhibitor binding.[78,89,95,97−103] There are two classes of $Q_P$-site inhibitors referred to as $P_f$ (*f* for fix) and $P_m$ (*m* for mobile), respectively. The $P_f$ class of inhibitors, such as the UQ analogue stigmatellin, fix the FeS ectodomain in the B position, presumably due to formation of a hydrogen bond between the inhibitor and the FeS ectodomain. The $P_m$ class of inhibitors, such as, e.g., myxothiazol or azoxystrobin, displace the FeS ectodomain from the B position yielding a mobile domain that adopts different positions, including the C position. A recent cryo-EM study with the $P_m$-type fungal complex $III_2$ inhibitor Inz-5 revealed the distribution of these positions.[89]

Crystal structures of complex $III_2$ revealed also intermediate positions of the ectodomain, in between the B and C positions.[104] This variability in the ectodomain position was explained by differences in crystal packing (summarized in ref 84). However, in the cryo-EM structures of the *S. cerevisiae* cyt. $bc_1$[34,35] the FeS ectodomain also adopts an intermediate position (shown in Figure 4A), i.e., the intermediate ectodomain position is not a consequence of protein crystallization. Interestingly, in a recent cryo-EM structure of the *C. albicans* cyt. $bc_1$ several classes of particles were observed in which the FeS head domain is either in the B position, C position, or in between these positions,[89] suggesting a statistical distribution of these states, which is consistent with spectroscopic data.[292] Similarly, in the cryo-EM structure of the *R. capsulatus* cyt. $bc_1$, subpopulations were identified with the FeS ectodomain either in the B or C position with an empty $Q_P$ site.[46] In the cryo-EM structure of the


https://doi.org/10.1021/acs.chemrev.1c00140
Chem. Rev. 2021, 121, 9644−9673

mammalian cyt. $bc_1$, only one $Q_P$ site of complex $III_2$ dimer is occupied,[88] but the FeS domain adopts the C position in both monomers. Furthermore, in the recently determined structure of the plant supercomplex from *Vigna* (*V.*) *radiata*, both FeS domain positions were observed in the absence of bound Q in the $Q_P$ site.[32] Hence, all these data suggest that the position of the FeS ectodomain is stochastic when the $Q_P$ site is empty or occupied by an oxidized Q.[78,81,88,97] On the other hand, binding of a reduced hydroquinone in the $Q_P$ site when the FeS cluster is oxidized may shift the equilibrium of the FeS domain toward the B position, similarly to binding of stigmatellin.[89,105−110]

Because movement of the FeS domain is involved in transfer of the first electron from $QH_2$ to cyt. $c_1$, the equilibrium constant and/or time constant for the FeS domain transition between the B and C positions determines the kinetics of this electron transfer.[82,84] A stochastic FeS domain movement after oxidation of $QH_2$ in the $Q_P$ site implies that the B−C transition is not required to accomplish the electron bifurcation from the $Q_P$ site,[107] i.e., electron branching in the Q-cycle is possible without movement of the FeS domain. Indeed, the FeS domain is permanently fixed near the B position in the *M. smegmatis* and *C. glutamicum* $III_2IV_2$ supercomplexes.[43−45] Rich and colleagues[107] discussed the thermodynamics and kinetics of electron bifurcation in the framework of eq 2 above and concluded that the mechanism could be explained by a concerted two-electron oxidation of $QH_2$.

**2.2.2. *M. smegmatis* and *C. glutamicum* Supercomplexes.** In the *M. smegmatis* supercomplex, the cyt. *cc* domain of complex III displayed two conformations in the two halves of the supercomplex, a closed conformation in which it is located near the electron acceptor at complex IV, and an open conformation where the electronic connection between the two complexes is interrupted[44] (Figure 3B). We hypothesized that movement of the cyt. *cc* domain, instead of movement of the FeS ectodomain, could mediate electron transfer from $MQH_2$ within the supercomplex.[44] However, at this point, it is unknown whether or not the cyt. *cc* domain movement is stochastic or linked to other reactions. In the *C. glutamicum* supercomplex[45] as well as in another structure of the *M. smegmatis* supercomplex,[43] all elements of the electron-transfer chain appear to be fixed, which suggests that the Q-cycle can be realized without any domain movements. Collectively, these data suggest a variability in the structural solution to a mechanistic realization of the Q cycle, which is discussed in the next subsection.

## 2.3. Proton Release from the $Q_P$ Site

**2.3.1. Canonical Complex III.** The electron bifurcation from $QH_2$ along the C and B branches, respectively, is functionally linked to proton release to the membrane *p* side.[82,87,97,110−114] In the canonical cyt. $bc_1$, binding of $QH_2$ at the $Q_P$ site has been suggested to shift the equilibrium of the FeS head domain toward the B position where one of the $QH_2$ protons would form a hydrogen bond with the FeS ligand His161 (mammalian complex III numbering, His181 in *S. cerevisiae*). It is well established that upon transfer of the first electron from $QH_2$ to FeS, the first proton is transferred to this His161.[82,87,97,111−114] The second proton has been suggested to be transferred to Glu271 (Glu272 in *S. cerevisiae*) of the PEWY motif (Figure 4B), followed by rotation of the protonated Glu271 toward the heme $b_L$ propionate upon electron transfer to heme $b_L$ (Figure 4B). After transfer of the second electron along the B branch, the FeS head domain would transiently adopt the C position (see discussion in the previous section), from where the first electron is transferred to cyt. $c_1$, linked to proton release from His161 to the *p* side of the membrane. In other words, this mechanism implies that part of the proton-transfer route for the first proton would involve the rotation of the FeS head domain.

It is likely that a spatial distribution of the two proton-transfer paths and the link between proton and electron transfer yields the bifurcated proton transfer. While the transfer route of the first proton from $QH_2$ is relatively well characterized, the route of the second proton remains to be explored. The proton from Glu271 has been suggested to be transferred consecutively to Arg79 (not shown in Figure 4B) and the *p* side aqueous phase.[111] However, functional studies of structural variants at position Glu271 indicate that this residue is not a unique proton acceptor from $QH_2$,[115,116] and there are presumably alternative proton-release pathways.[81] In the structure of *S. cerevisiae* complex III, residues Glu272 and Tyr274 (equivalent of Asp302 and Tyr304, respectively, in *M. smegmatis*, Figure 4BC), together with other residues, coordinate a network of water molecules between heme $b_L$ and the $Q_P$ site, which may be involved in proton transfer, and determines the dielectric environment of the site.

**2.3.2. *M. smegmatis* and *C. glutamicum* Supercomplexes.** The mechanism described above outlines that deprotonation of His161 to the *p* side occurs only when the FeS head domain had moved to transiently adopt the electron donating C position. Because in *M. smegmatis* and *C. glutamicum* the FeS domain is fixed in the B position, a different proton-release route is presumably utilized in these complexes. In complex III from *M. smegmatis* and *C. glutamicum*, a Q was found to be bound in a site equivalent to the canonical $Q_P$ site.[43−45] His368, the equivalent of His161, is presumably the acceptor of the first proton from $QH_2$ also in these complexes III (Figure 4C). In the *M. smegmatis* complex III, the equivalent of Glu271 is a shorter side chain Asp302, which cannot approach the $Q_P$ site sufficiently closely to act as an acceptor of the second proton. Instead, Asp309 (*M. smegmatis* numbering) is found in proximity to the second proton of $QH_2$ (Figure 4C). Furthermore, Asp309 is found at ∼4 Å from His368, suggesting a possible common proton-release route of the two $QH_2$ protons.[45] Many actinobacteria harbor a Glu residue instead of Asp309, which could also serve as a proton acceptor.

On the basis of this analysis of the structure, we speculated that a possible Q-cycle mechanism in *C. glutamicum* and *M. smegmatis* complex III may involve the following sequence of events:[45] (*i*) transfer of the first proton/electron to His368/FeS, (*ii*) transfer of the second proton/electron to Asp309/heme $b_L$, (*iii*) electron transfer from heme $b_L$ to heme $b_H$, linked to deprotonation of Asp309, and (*iv*) electron transfer from FeS to the nearest cyt. $c_I$ of the cyt. *cc* domain.

The electron transfer from FeS to cyt. $c_I$ in (*iv*) is assumed to occur only if it is linked to deprotonation of the FeS ligand His368, which is possible only after deprotonation of Asp309, i.e., *after* electron transfer from heme $b_L$ to heme $b_H$. Indeed, the electron transfer in (*iii*), from FeS to cyt. *cc* along the C branch, was shown to be rate-limiting for turnover of the *C. glutamicum* supercomplex,[65] i.e., it would occur after electron transfer along the B branch. In addition, on the basis of analysis of one of the *M. smegmatis* supercomplex structures, we hypothesize that the transition between the open and closed conformation of the cyt. *cc* domain (Figure 3B) may provide a mechanism to gate electron transfer from complex III to complex IV.[44] However, as indicated above, it is presently unclear how this movement would be linked to the binding of $QH_2$ at the $Q_P$ site and the


https://doi.org/10.1021/acs.chemrev.1c00140
Chem. Rev. 2021, 121, 9644−9673

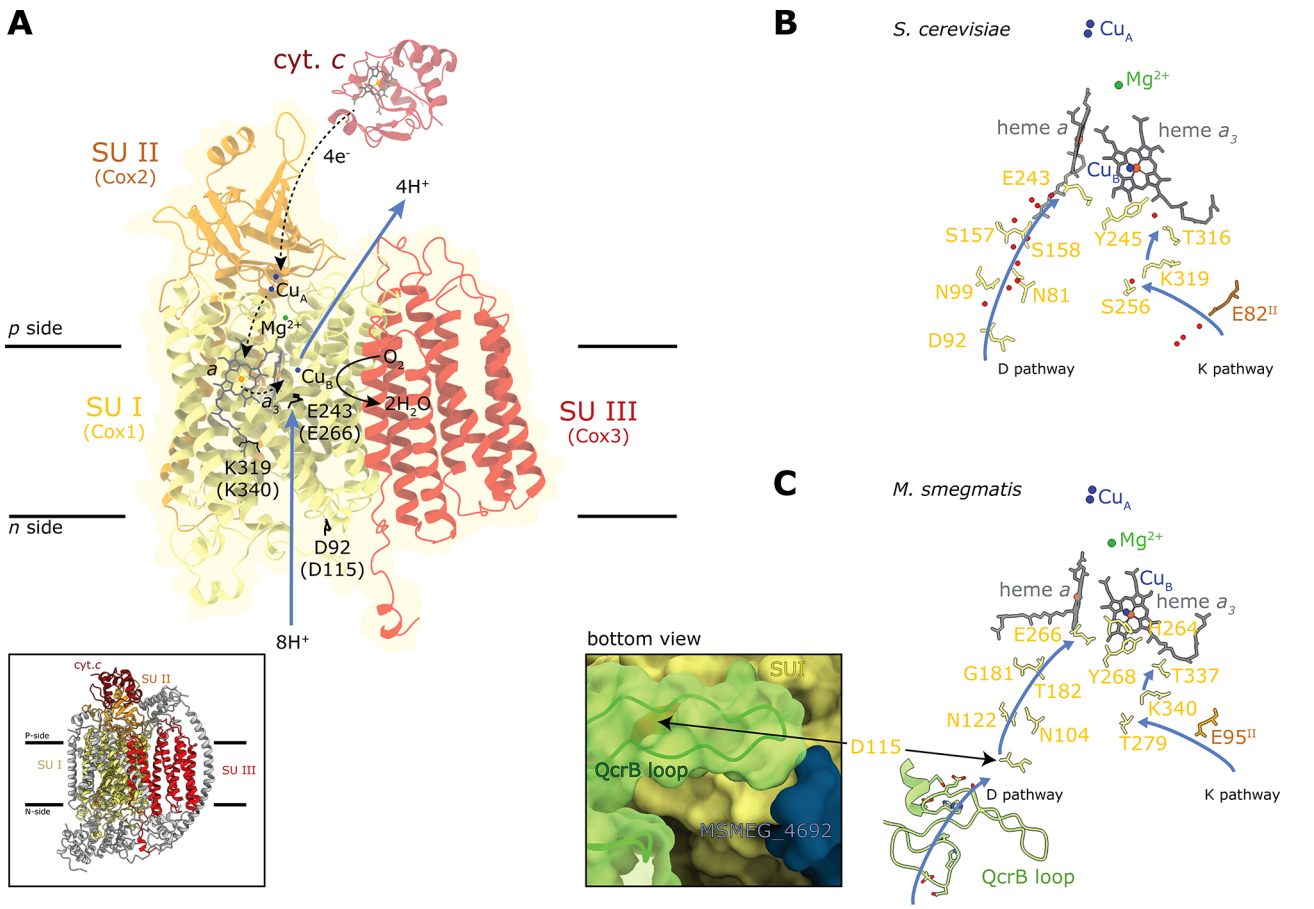


**Figure 5.** Complex IV. (A) The core subunits of the *S. cerevisiae* CytcO (complex IV, PDB 6HU9) and the catalyzed reaction. The inset shows all subunits of the *S. cerevisiae* CytcO, including accessory subunits in gray and bound cyt. *c* (based on the cyt. *c* position in the bovine CytcO, PDB 5IY5, which displays the same geometry as the *S. cerevisiae* cyt. *c*-CytcO cocomplex[37]). The D and K proton pathways of the *S. cerevisiae* (B) and *M. smegmatis* (PDB 6HWH) (C) CytcOs. In (B), water molecules seen in the crystal structures of bacterial and mammalian CytcOs are included. They were not resolved in the cryo-EM structures of the *S. cerevisiae* CytcO. (C) The QcrB "lid" of complex III, which covers the D pathway of CytcO in the *M. smegmatis* supercomplex. Amino acid residue side chains of QcrB that provide an alternative entry pathway to D115 are shown (along the blue arrow below the D pathway).

proton-transfer reactions. It should be stressed that the mechanism outlined above is based on analyses of structures and is presented only to serve as a guide in the design of experiments aimed at testing this hypothesis.

## 3. COMPLEX IV[117]

The mitochondrial complex IV is a member of the heme-copper oxidase family, which is characterized by a catalytic site that is composed of a heme group and a copper ion where dioxygen is reduced to water. Other oxidases, such as the $UQH_2$-$O_2$ oxidoreductases, cytochrome *bd*[118,119] and alternative oxidases[120] also catalyze reduction of $O_2$ to water in respiratory chains, but these oxidases harbor catalytic sites of different composition and do not belong to the heme-copper oxidase family. The heme-copper oxidase family is defined by homology in subunit I (Figure 5A), which harbors six conserved histidine residues that coordinate three redox-active metal sites: (*i*) a six-coordinated heme group with two axial His ligands (heme *a* in Figure 5A); (*ii*) a five-coordinated heme group with one axial His ligand (heme $a_3$ in Figure 5A); and (*iii*) a copper ion called $Cu_B$, which is coordinated by three His ligands. The latter heme and $Cu_B$ form a catalytic site where $O_2$ binds and is reduced. In bacteria, the two heme groups may be of the same or different types: hemes *a*, *b*, or *o*. In mitochondria both hemes are of the same *a* type, hence these complexes are sometimes also referred to as cytochromes $aa_3$.

The heme-copper oxidase family can be divided in two functional subgroups, based on the origin of the electron donor: quinol oxidases and CytcOs. The former receive electrons from membrane-soluble $QH_2$, while the latter receive electrons from cyt. *c*. The quinol oxidase from, e.g., *E. coli* (cytochrome $bo_3$) has an overall structure that is similar to those of bacterial CytcOs but lacks the electron acceptor metal site ($Cu_A$, see below) and instead harbors a Q-binding site at which $QH_2$ donates electrons.

The primary electron acceptor of the mitochondrial CytcOs, including that of *S. cerevisiae*, is a dinuclear Cu-center called $Cu_A$, located near the *p* side in subunit II (Figure 5A). Because electrons from cyt. *c* are donated at the *p* side of the membrane, while protons are taken up from the opposite, *n*, side of the membrane, the reaction yields a charge separation across the membrane that is equivalent to moving one positive charge from the *n* to the *p* side. In addition, for each electron transferred to the catalytic site, one proton is pumped from the *n* to the *p* side, thereby increasing the total charge-separation stoichiometry. The proton-pumping stoichiometry varies between CytcOs from different organisms. Thus, the reaction catalyzed by the CytcOs is


https://doi.org/10.1021/acs.chemrev.1c00140
Chem. Rev. 2021, 121, 9644−9673

$$2(\text{cyt. } c^{2+})_p + 1/2O_2 + 2(1+\delta)H_n^+ \rightarrow 2(\text{cyt. } c^{3+})_p + H_2O + (2\delta H_p^+)_{pump} \quad (3)$$

where $\delta$ is the proton-pumping stoichiometry, i.e., number of $H^+$ pumped per electron transferred to $O_2$, typically $0.5 \leq \delta \leq 1$ ($\delta$ = 1 for mitochondrial CytcOs), subscripts *n* and *p* refer to the two sides of the membrane, and the subscript "pump" refers to pumped protons released on the *p* side (for more detailed reviews on the structure and function of CytcOs, see refs 121−130).

It is worth noting that supercomplexes composed of cyt. $bc_1$ and CytcO catalyze the same reaction as that catalyzed by quinol oxidases mentioned above, i.e., oxidation of $QH_2$ and reduction of dioxygen to water. However, the energy-conservation efficiency is larger for the supercomplex than for, e.g., the *E. coli* cyt. $bo_3$ because, in addition to the charge separation and proton pumping by the CytcO part, in the supercomplex there is also a transmembrane charge separation generated by cyt. $bc_1$.

### 3.1. The Core Subunits

Bacterial heme−copper oxidases consist typically of two to four subunits. The minimum functional unit is composed of subunits I and II, which harbor all four redox-active cofactors that catalyze the reaction in eq 3. Subunits I−III (Cox1−3 in *S. cerevisiae*, Figure 5A) are often referred to as the "catalytic core" because upon removal of subunit III, many CytcOs lose their activity during turnover, referred to as suicide inactivation (reviewed in ref 131). The subunit I−III catalytic core is conserved and structurally almost identical in CytcOs from mammals, yeast, and many aerobic bacteria.

On the basis of an analysis of amino acid sequence homology as well as functionally important structural features, e.g., proton pathways (see below and ref 132), the CytcOs have been classified into three major families named A, B, and C.[133,134] Type A includes the mitochondrial as well as the "mitochondrial-like" bacterial cytochromes $aa_3$, e.g., from *P. denitrificans*, *R. sphaeroides*, and *M. smegmatis*. Type B includes e.g. the *Thermus* (*T.*) *thermophilus* $ba_3$ CytcO, while type C includes the $cbb_3$ oxidases found, e.g., in *R. sphaeroides*, *R. capsulatus*, and *P. denitrificans*, where a subunit with a diheme cyt. *c* is the primary electron acceptor instead of $Cu_A$.[132]

The A family CytcOs have two well characterized proton-transfer pathways; the K-pathway named after a conserved Lys (K319 or K340, *S. cerevisiae* or *M. smegmatis* numbering, respectively, Figure 5B,C), and the D-pathway named after a conserved Asp at its entrance (D92 or D115 in Figure 5B,C). The A-family is further divided into two subfamilies, A1 and A2. The former is characterized by a subunit I motif "XGHPEVY", found in, e.g., the mitochondrial CytcOs including that from *S. cerevisiae*, where "E" is Glu243 in the D proton pathway (Figure 5B), "H" is a ligand of $Cu_B$ (His241, not shown in Figure 5B), while "Y" is a catalytically active Tyr245 in the catalytic site. The imidazole group of His241 and the phenol group of Tyr245 (Y) are linked by a covalent bond. Similarly, the *M. smegmatis* CytcO belongs to the A1 subclass. Subclass A2 instead harbors an "YSHPXVY" motif where the Glu is replaced by a Tyr-Ser pair ("YS") at about the same position in space in the D pathway.

Subunit I in the *S. cerevisiae* (Cox1) CytcO comprises 12 transmembrane (TM) $\alpha$-helices. Subunit Cox2 is composed of two TM $\alpha$-helices and a head domain, which harbors the redox-active $Cu_A$ site (Figure 5A). Subunit Cox 3 is composed of seven TM $\alpha$-helices that form a V-shaped cleft, which has been suggested to funnel $O_2$ from the membrane to the catalytic site.[129,135] The putative $O_2$ channel in Cox 3 typically harbors three tightly bound lipid molecules, PG, PC, and PE, resolved in crystal structures of CytcO from *R. sphaeroides*, *P. denitrificans*, and *B. taurus*.[136] In the *S. cerevisiae* CytcO, two lipid molecules could be modeled in this cleft.[33,34]

### 3.2. The Catalytic Reaction and Proton Pathways

During turnover of CytcO, electron transfer from cyt. *c* to the $Cu_A$ site is followed in time by electron transfer to heme *a* and the heme $a_3$-$Cu_B$ catalytic site. Figure 6 illustrates schematically

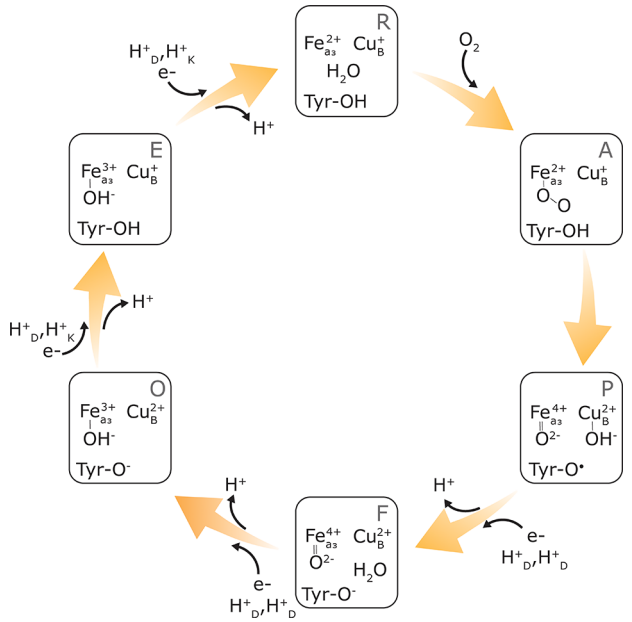


**Figure 6.** Reduction of $O_2$ at the catalytic site of CytcO. The first electron ($e^-$) from cyt. *c* to the oxidized CytcO (state **O**) is transferred to $Cu_B$ to form state **E**. It is accompanied by proton uptake from the *n* side solution though the K pathway ($H_K^+$) to Tyr245 (*S. cerevisiae* CytcO numbering, Tyr in the figure). Transfer of the second electron to heme $a_3$ and a proton through the K pathway to a hydroxide at heme $a_3$ leads to formation of state **R**, where the catalytic site is reduced by two electrons. Next, $O_2$ binds to heme $a_3$ forming state **A**. After transfer of one electron and one proton from the Tyr residue, a ferryl state is formed, called **P** ("peroxy", for historical reasons). Transfer of the third electron is accompanied by proton uptake through the D pathway ($H_D^+$) and formation of the ferryl state, **F**. After transfer of the fourth electron and another proton through the D pathway to the catalytic site, the oxidized state **O** is formed again. The four transitions **P** → **F**, **F** → **O**, **O** → **E**, and **E** → **R** are each associated with pumping of one proton across the membrane. These protons are taken up through the D pathway ($H_D^+$, each proton released to the *p* side is indicated as $H^+$).

the reaction cycle of the mitochondrial CytcOs. The oxidized state of CytcO is referred to as state **O**. Electron transfer from reduced cyt. *c* to the oxidized CytcO results in reduction of first $Cu_B$ and heme $a_3$, which is associated with uptake of two protons from the membrane *n* side through the K proton pathway (see Figure 5B) to the catalytic site. Each electron transfer from cyt. *c* to the catalytic site is associated with proton pumping across the membrane. The two-electron reduced catalytic site binds $O_2$ (state **A**), which results in breaking the O−O-bond by electron transfer from heme $a_3$ and $Cu_B$ as well as hydrogen transfer from Tyr245, which forms a radical (state **P**). In the following reaction steps one electron is transferred to the catalytic site in each of the **P** → **F** and **F** → **O** transitions. Each of these reduction steps is linked to uptake of two protons from the *n* side


https://doi.org/10.1021/acs.chemrev.1c00140
Chem. Rev. 2021, 121, 9644−9673

through the D proton pathway, one to the catalytic site and one is pumped across the membrane. The branching point from which the substrate and pumped protons are transferred along different trajectories is located at Glu243.

The structure and function of the K and D proton pathways have been studied in detail in bacterial A1-type CytcOs,[129,130,137−150] and their involvement in proton uptake also confirmed for the *S. cerevisiae* mitochondrial CytcO.[151,152] The K pathway starts near Glu82 in subunit II at the membrane *n* side (Figure 5B). It is connected via a water molecule to Ser256, which is hydrogen-bonded to the conserved Lys319. Proton transfer from the Lys residue requires a conformational change of the side chain toward the catalytic site.[135] From the "up-position" the proton is transferred, via a water molecule and Thr316 to Tyr245 at the catalytic site (see Figure 5B).

Residue Asp92 of the D pathway is positioned at the inside of a cleft at the *n*-side surface of subunit I. The pathway is composed of polar residues that coordinate ∼10 $H_2O$ molecules, which span the distance of ∼20 Å from Asp92 to Glu243 (Figure 5B). The maximum rate of proton uptake to the catalytic site, via the D pathway, is $\sim 10^4$ $s^{-1}$ at pH 7, and it drops with increasing pH displaying a p$K_a$ of 9.4,[153] which is attributed to titration of Glu243[153] (but, see ref 154). Replacement of the Asp or Glu residues by their nonprotonatable analogues, Asn or Gln, respectively, result in impaired activity and a complete block of proton uptake.[137,142,155−159]

Minor structural changes around the orifice of the D pathway influence the proton-uptake kinetics and proton pumping stoichiometry. For example, one-residue changes at Asp92 or in the vicinity of this residue in bacterial and *S. cerevisiae* CytcOs result in lower proton-pumping stoichiometry or complete uncoupling of proton pumping from the $O_2$-reduction reaction, often without altering the CytcO turnover or proton-uptake rate.[151,153,160] Similarly, changes in the surface-exposed loop of subunit I in the *R. sphaeroides* CytcO, outside of Asp92, yielded modified pH dependence and uncoupling of proton pumping.[161] Also, removal of *R. sphaeroides* subunit III, which has a loop of residues near Asp92 (*S. cerevisiae* numbering), resulted in a dramatic shift in the pH dependence of the proton-uptake rate[162] and allowed proton uptake via alternative surface protonatable groups, other than Asp92[163] (the two subunit I and III loops are found just below D92/D115 in Figure 5B,C, but are not shown in the figure). Collectively, these data indicate that moderate alteration of the D pathway near the entry point modulate proton-pumping stoichiometry and result in changes in the pH dependence of the proton-transfer kinetics through the D pathway.[164]

Interestingly, in the *M. smegmatis* and *C. glutamicum* $III_2IV_2$ supercomplexes, in addition to the subunit III (subunits CtaE/F) loop, another loop that extends from cytochrome *b* (QcrB subunit of complex III) covers the orifice of the D pathway[44] and presents an alternative route for proton entry into the D pathway, via protonatable groups of the QcrB loop[45] (Figure 5C, the subunit III loop is not shown in the figure, it is positioned between Asp115 and the QcrB loop). As outlined above, the D pathway entrance is highly conserved and the proton-uptake kinetics is controlled by an intricate web of interactions between the pathway residues. A modified architecture as a result from supramolecular interactions between complexes III and IV in the *C. glutamicum* and *M. smegmatis* $III_2IV_2$ supercomplexes suggests that proton uptake by complex IV could be modulated by structural changes in complex III.[65]

In the mammalian CytcO, a third proton pathway (H pathway) was suggested based on a structural analysis.[121,139] In bacterial CytcOs, the equivalent of this pathway is not involved in proton transfer.[165] Structural analyses and data from functional studies of structural variants in which putative residues of the H pathway were modified in the mitochondrial *S. cerevisiae* CytcO do not support a functional role of this pathway.[151,152,166] Furthermore, key residues of the suggested H pathway are not present in CytcO from plant mitochondria,[32] which suggest that its involvement in proton pumping would have to be restricted to the mammalian CytcOs.

### 3.3. Peripheral subunits of the *S. cerevisiae* CytcO

In addition to the three core subunits Cox1−3, the *S. cerevisiae* CytcO is also composed of nine peripheral subunits called Cox4−9, Cox12, Cox13, and Cox26,[33,34] where the latter was identified only recently[167,168] (Figure 2A). All of these accessory subunits, except Cox26, have subunit homologues in mammals. Some of these subunits have been suggested to be involved in regulation of the electron transfer and proton pumping activities of the CytcO.[169−172] A discussion of the role of all these subunits is beyond the scope of this review, but we briefly discuss those accessory subunits that are relevant in the context of supramolecular interactions with cyt. $bc_1$. A detailed description of all the accessory subunits in *S. cerevisiae* CytcO is found in ref 173 (see also ref 171).

Subunit Cox5 is the major interaction partner with cyt. $bc_1$ in the *S. cerevisiae* supercomplex (Figure 2A). It is homologous to mammalian CoxIV and is expressed as one of two isoforms, called Cox5A or Cox5B, which share 68% sequence identity.[173] Expression of the two isoforms depends on the oxygen concentration; the former version is expressed at normoxic conditions (∼200 $\mu$M $O_2$), while the latter is expressed at low oxygen concentrations (<0.5 $\mu$M).[174,175] Early data indicated that the catalytic turnover of CytcO is higher with Cox5B than with Cox5A.[176] However, more recent data indicate that the elevated CytcO activity is not simply a result of replacement of Cox5A by Cox5B because a genetic replacement of Cox5A by Cox5B did not yield any differences in the turnover activity nor of the affinity for $O_2$ or cyt. *c*.[177]

In the *S. cerevisiae* CytcO, subunit Cox13 is composed mainly of a single bow-shaped TM $\alpha$-helix at the periphery of CytcO.[34] In the cryo-EM structural model, it interacts with Cox1, Cox3, and Cox12 on the *p* side and with Cox4 on the *n* side of the membrane[34] (Figure 2A).

### 3.4. The *M. smegmatis* CytcO

The *M. smegmatis* CytcO core is composed of subunits CtaD (subunit I), CtaC (subunit II), as well as CtaE and CtaF, which together form the equivalent of subunit III. The structure of this subunit I−III core is very similar to that of the canonical CytcO. In addition, the *M. smegmatis* supercomplex harbors a number of accessory subunits (Figure 2B).[43,44] Even though some of these subunits are attached only to the CytcO part of the supercomplex, we consider them being components of the supercomplex rather than of CytcO itself. Furthermore, as already mentioned above, in the *M. smegmatis* supercomplex subunit QcrB of complex III is extended to interact with complex IV. Figures 2B and 3B show the open and closed positions of the cyt. *cc* domain (QcrC) in the two halves of the supercomplex.


https://doi.org/10.1021/acs.chemrev.1c00140
Chem. Rev. 2021, 121, 9644−9673

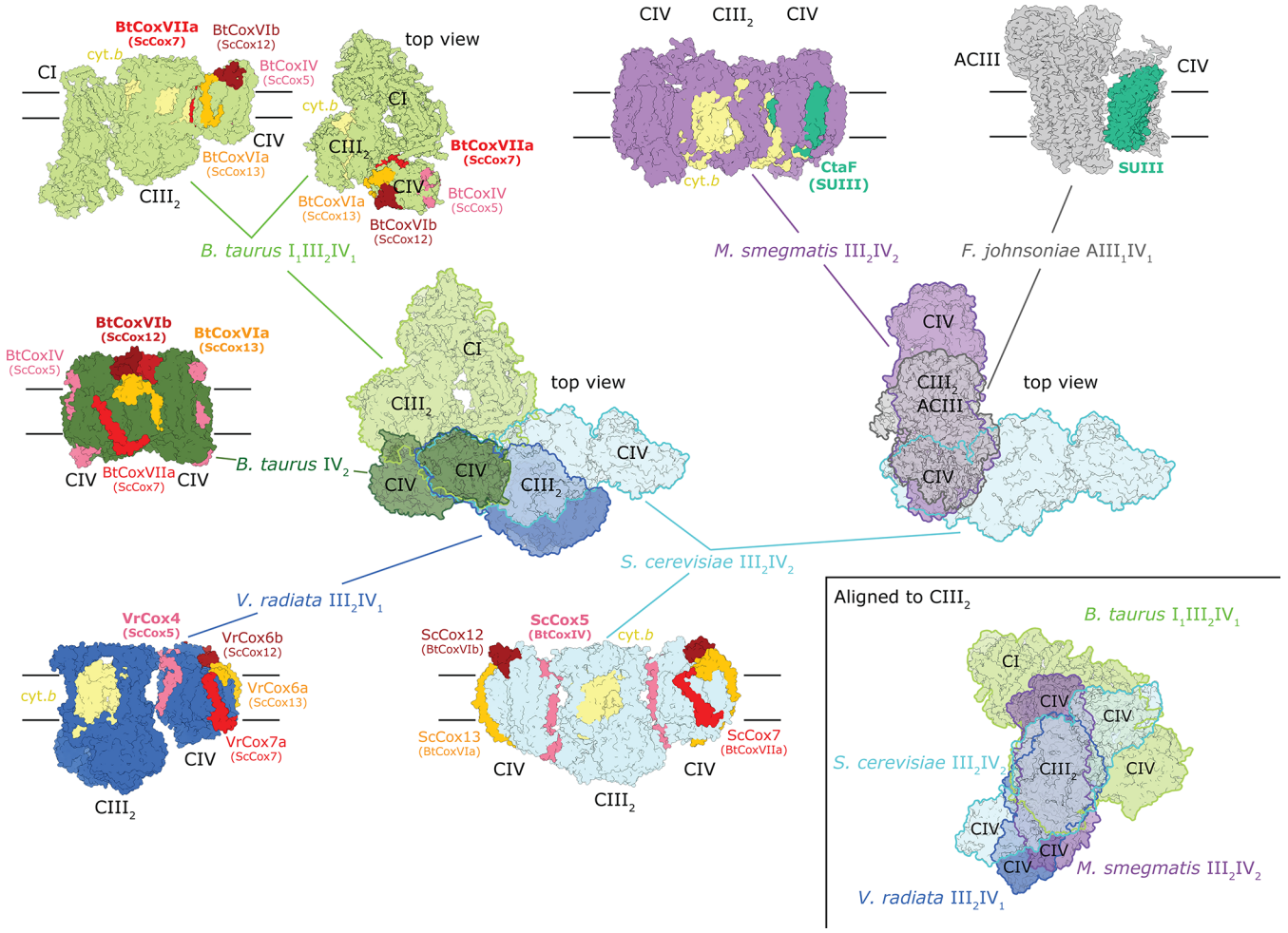


**Figure 7.** Arrangement of supercomplexes with known structures that contain complexes III and IV in different species. The *B. taurus* (cow) CytcO dimer is also shown (PDB 1OCC), other references are given in Table 1. The main panel in the middle shows the alignment of complex $III_2$ relative to the position of complex IV with its subunits at the interface of complex $III_2$ indicated in bold text and in different colors. All interacting subunits for all supercomplexes are marked in specific colors for reference in order to indicate their relative positions in all supercomplexes. The prefixes Bt (*B. taurus*), Sc (*S. cerevisiae*), and Vr (*V. radiata*) are added because of the different subunit numbering used for the equivalent subunits in different organisms. The mitochondrial supercomplexes are shown on the left, while the obligate *M. smegmatis* $III_2IV_2$ and the alternative complex III–IV supercomplexes are shown on the right. The *S. cerevisiae* supercomplex is encircled by a blue line; it is shown as reference for both the mitochondrial and bacterial supercomplexes. Top views and side views with approximate positions of the membrane with black lines. The inset shows the same supercomplexes but aligned to the complex $III_2$ dimer (alternative complex III in *F. johnsoniae* is not shown here).

### 3.5. Nonredox Active Metal Sites

In addition to the redox-active metal sites, A-type CytcOs harbor a number of nonredox active metal sites (Figure 5A). An $Mn^{2+}$/$Mg^{2+}$ (depending on the concentration of the metal in the growth medium) is located near the catalytic site of mammalian and bacterial A-type CytcOs[139,178,179] and was also identified in one cryo-EM structure of the *S. cerevisiae* CytcO.[34] In addition, a $Ca^{2+}$/$Na^{+}$ site was confirmed in the *S. cerevisiae* CytcO[34] (see also refs 139,179,180). These metal sites are presumably also present in the actinobacterial supercomplexes.[45] Furthermore, a $Zn^{2+}$ ion is bound in Cox4 of the *S. cerevisiae* CytcO[34] (see also ref 139). Added $Zn^{2+}$ also binds near the proton pathways to slow or impair proton uptake.[181−185]

### 3.6. The Putative CytcO Dimer

The bacterial CytcOs are typically monomers. The first crystal structures of the mammalian CytcO revealed a dimer,[139] which is consistent with earlier data from functional studies suggesting that formation of the dimer would be functionally relevant.[171] As seen in Figure 7, in the mammalian CytcO, the equivalent of subunit Cox12 and Cox13 in *S. cerevisiae*, i.e., subunits CoxVIb and CoxVIa, are found at the monomer−monomer interface in the crystal structure of the dimeric enzyme (interface subunits are marked in bold text in Figure 7). Here, the CoxVIa subunit adopts a structure different from that of Cox13 in *S. cerevisiae*.[139,186]

More recent structural and functional studies showed that the $O_2$-reduction activity of the CytcO monomer was not significantly different from that of the dimer, and only minor structural differences were observed between the monomeric and dimeric forms.[187] Furthermore, recent structures of supercomplexes composed of complexes I, III, and IV (sometimes also referred to as respirasomes) from mammals showed that the CytcO bound in these preparations is a monomer[38−41] (Figure 7), as also seen for supercomplexes *in situ* in mammals, yeast, and plants.[29]

In *S. cerevisiae*, almost all CytcO is found in supercomplexes.[17,72] In variants with only one CytcO ($III_2IV$), the enzyme is obviously a monomer, but also in the $III_2IV_2$ variant, the two CytcOs are maximally separated in the supercomplex


https://doi.org/10.1021/acs.chemrev.1c00140
Chem. Rev. 2021, 121, 9644−9673

(Figure 2A). The current data also suggest that the small fraction free CytcO in *S. cerevisiae* mitochondria is found in monomeric form.[17,72,188] Even though a fraction of CytcO dimer was observed upon reconstitution of the *S. cerevisiae* CytcO in liposomes,[189] this observation may be consequence of detergent solubilization of the enzyme prior to reconstitution in a membrane as well as a lipid composition that differs from that of the inner mitochondrial membrane.

## 4. COMPLEX III–IV SUPERCOMPLEXES

### 4.1. The *S. cerevisiae* Supercomplex

The interface surface between cyt. $bc_1$ and CytcO within the *S. cerevisiae* supercomplex is surprisingly small,[24] with a main part of the cyt. $bc_1$–CytcO interactions on the matrix (*n*) side of the supercomplex where the N-terminal domain of Cox5 binds to Cor1[34] (Figure 2). In addition, the C-terminal domain of Cox5 on the *p* side of the membrane interacts with the C terminus of Qcr6 and with the cyt. $c_1$ domain (Figure 2). The first supercomplex structures[34,35] were determined with the Cox5A isoform (in ref 34, Cox5B was removed genetically). Many of the residues of Cox5A that are involved in binding to cyt. $bc_1$ in the supercomplex are the same in the two isoforms of Cox5. Accordingly, a recent structural study of supercomplexes composed of CytcO with either Cox5A or Cox5B did not show any isoform-dependent interactions.[33]

Only minor structural changes result from formation of the supercomplex. The data suggest that the N terminus of the TM $\alpha$-helix of the Rieske iron–sulfur protein (Rip1) in cyt. $bc_1$ undergoes a conformational change upon interactions with a cardiolipin molecule within the supercomplex.[34] However, the authors also noted that this change would not impact the FeS-containing head domain of the iron–sulfur protein,[34] i.e., the function of cyt. $bc_1$ is unlikely to be altered as a result of supercomplex formation. Furthermore, the structural comparison of the N terminus of the iron–sulfur protein was made to the crystal structure of cyt. $bc_1$, i.e., any differences in interactions with cardiolipin may also reflect differences in the organization of cyt. $bc_1$ in crystals and in the cryo-EM sample, respectively. The conformation of the other cyt. $bc_1$ subunits that interact with CytcO (mainly Cor1, but also cyt. $c_1$ and Qcr8, see Figure 2A) are not altered by the supramolecular interactions.[33,34] Another difference in structure possibly caused by the supramolecular interaction is the configuration of the N-terminal domain of Cox5A. This protein segment may bind ATP, which has been suggested to allosterically regulate the CytcO activity.[190] Because upon forming a supercomplex this domain is shifted toward cyt. $bc_1$, the structural difference may be a consequence of binding of CytcO to cyt. $bc_1$ within the supercomplex.[34,35] However, because a structure of the *S. cerevisiae* CytcO alone (i.e., not part of a supercomplex) is not available, the structural comparison of subunit Cox5A was made for the equivalent subunit of the isolated mammalian (bovine heart) CytcO and the *S. cerevisiae* CytcO in a supercomplex.[34] Therefore, the structural difference may reflect that of the equivalent subunits in the different CytcOs. We also note that the turnover activity of free CytcO is the same as that of CytcO in a supercomplex with cyt. $bc_1$,[37] which suggests that the putative structural changes seen upon supercomplex formation are not functionally relevant. In conclusion, because the supramolecular interaction surface is small and any structural differences that may occur upon supercomplex formation are minor,[33−35] the activities of cyt. $bc_1$ and CytcO are unlikely to be "regulated" upon formation of the supercomplex.

As indicated above, the monomer–monomer interface in the mammalian dimer[139] involves subunits CoxVIa and CoxVIb[139] (Figure 7). The equivalent subunits in the *S. cerevisiae* CytcO, Cox13, and Cox12, respectively, were suggested to define a monomer–monomer interface also in a putative dimer of the *S. cerevisiae* CytcO.[173] Because in the *S. cerevisiae* supercomplex the cyt. $bc_1$–CytcO interface involves subunit Cox5, subunits Cox12 and Cox13 are exposed on the opposite side of the CytcO (see Figures 2 and 7). Therefore, if a CytcO dimer would be formed in *S. cerevisiae* by interactions through Cox12 and Cox13, a chain of supercomplexes would form in the membrane. Indeed, such a multisupercomplex structure was suggested by Schägger for yeast and mammalian mitochondria.[18] However, to our knowledge, there is no published data in support of such a scenario. Furthermore, Hartley *et al.* noted that the bow-shaped topology of Cox13 would hinder dimerization of CytcO.[34] In addition, the suggested binding of the respiratory supercomplex factor 2 (Rcf2, see below) at Cox13 would probably also prevent CytcO dimerization through interactions via Cox13.[33]

### 4.2. Other (I)$III_2IV_{1/2}$ Supercomplexes

Figure 7 shows known structures of supercomplexes in which complexes III and IV are in direct contact (see also Table 1), as well as the mammalian complex IV dimer. The orientation of the mitochondrial respiratory complexes in relation to complex IV is shown in the main left-hand side panel, with CytcO subunits that interact with the other complexes indicated in different colors (bold text is used to indicate interactions for each supercomplex). To the right are shown bacterial complex III-IV supercomplexes with known structures. The inset on lower right shows an overlay of all supercomplexes but instead aligned to the complex $III_2$ dimer.

As seen in Figure 7, there is a great variability in the relative orientation of complexes $III_2$ and IV, i.e., the interaction surfaces of these complexes in supercomplexes varies between different organisms. In the mammalian $I_1III_2IV_1$ supercomplex,[38] the surface of the homologous subunits of complex III that interact with complex IV in the *S. cerevisiae* supercomplex, instead bind to complex I. In this mammalian supercomplex, main interactions with cyt. $bc_1$ occur via CytcO subunit CoxVIIa (Cox7 in *S. cerevisiae*). The details of the cyt. $bc_1$–CytcO interactions in *S. cerevisiae* as well as interactions within the mammalian CytcO dimer are discussed in the previous sections.

In the plant supercomplex from *V. radiata* mitochondria the approximate relative orientation of complexes $III_2$ and IV is similar to that of *S. cerevisiae*. However, the protein–protein interaction sites differ and the orientation angle differs by 18° (defined by heme $b_H$s in complex $III_2$, and hemes *a* and $a_3$ in complex IV, Figure 7).[32] As with the *S. cerevisiae* supercomplex, subunit Cox5 (Cox4 in *V. radiata* mitochondria) faces toward complex III. However, on the matrix side the interactions between Cox5 and Cor1, observed in *S. cerevisiae*, are absent in *V. radiata* because the equivalent of Cox5 in the latter is shorter by ~100 amino acid residues at the N terminus. Instead, the main interactions are found on the cytosolic side between *V. radiata* Cox4 and Qcr6, which are more extensive in the *V. radiata* than in the *S. cerevisiae* mitochondrial supercomplex.[32]

In the *M. smegmatis* $III_2IV_2$ supercomplex the main $III_2$–IV interactions are mediated via complex IV subunits CtaE and CtaF, which together form the equivalent of CytcO subunit III, and QcrB (cytochrome *b*) of complex $III_2$, which is also bound


https://doi.org/10.1021/acs.chemrev.1c00140
Chem. Rev. 2021, 121, 9644−9673

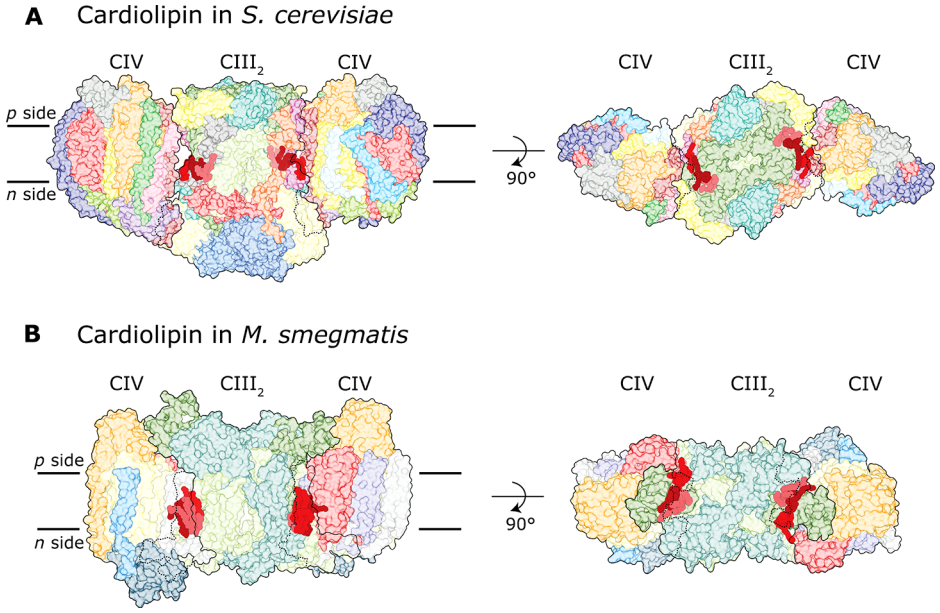


**Figure 8.** Cardiolipin in complex III–IV supercomplexes. All cardiolipin (shown in red) head groups face the *n* side. The boundaries of complexes III and IV are indicated by solid lines. The dashed lines indicate boundaries on the opposite side of each supercomplex. (A) The *S. cerevisiae* supercomplex. Subunits are colored as in Figure 2A. (B) The *M. smegmatis* supercomplex. Subunits are colored as in Figure 2B.

to complex IV via the extended QcrB loop on the periplasmic (*n*) side (Figure 7).[43,44]

In the structure of the *F. johnsoniae* supercomplex composed of an alternative complex III and CytcO, interactions are mediated via the CytcO subunit III.[47] The authors noted that this subunit III lacks TM $\alpha$-helices 1 and 2, i.e., consists of five TM $\alpha$-helices. These five TM $\alpha$-helices are equivalent to subunit CtaE of the *M. smegmatis* CytcO, which also interact with complex $III_2$ in this supercomplex. As noted above, in *M. smegmatis*, the equivalents of TM $\alpha$-helices 1 and 2 are present and formed by the CtaF subunit. This observation shows that subunit III of CytcO displays a structural variability that may be adopted to accommodate different interaction partners.[47]

The variability in the interaction surfaces of complexes III and IV most likely excludes a universal structure–function modulation that would be a consequence of $III_2$–IV supercomplex formation in mitochondria. The situation is different for actinobacterial supercomplexes where formation of the $III_2IV_2$ supercomplex introduces new architecture to otherwise conserved structural elements, for example, those involved in proton uptake and pumping in complex IV.

### 4.3. Cardiolipin in Supercomplexes

Cardiolipin is typically found in membranes that are involved in energy conversion, i.e., that maintain an electrochemical proton gradient.[191−193] The phospholipid is unique in having a dimeric structure consisting of two phosphatidyl moieties linked to glycerol and four acyl chains. The p$K_a$ values of the two phosphate groups were reported to be different with one p$K_a$ being above 8.0, i.e., the cardiolipin headgroup would carry only one negative charge at neutral pH.[194] The high-p$K_a$ headgroup was suggested to act as a proton trap near enzymes that maintain or utilize electrochemical proton gradients.[194] However, results from more recent studies indicate that the two p$K_a$s are similar ($\lesssim$ ~3) and that cardiolipin carries two negative charges at neutral pH.[195,196]

In mammalian cells, cardiolipin is found primarily in the mitochondrial inner membrane where the weight fraction of the lipid is ~18%[193] (16% in the *S. cerevisiae* inner mitochondrial membrane[197]). In addition, the lipid may be enriched in the inner leaflet of the inner mitochondrial membrane,[191] and it has been suggested to be involved in shaping the cristae.[52] Cardiolipin has been identified as an integral part of many membrane proteins,[198,199] and the enzymatic activities of, for example, detergent-solubilized mitochondrial cyt. $bc_1$ and CytcO are dependent on the presence of bound cardiolipin[200,201] (this effect is not observed with the *R. sphaeroides* CytcO[202]). In addition, cardiolipin is involved in apoptosis, where one step in the cascade of signaling reactions involves formation of a co-complex between the lipid and cyt. *c*, which results in cyt. *c* acquiring peroxidase activity.[203]

A discussion on the role of cardiolipin in supporting enzymatic activities of the respiratory complexes and its involvement in apoptosis is beyond the scope of this review. Instead, we discuss briefly cardiolipin's role in maintaining supramolecular interactions between cyt. $bc_1$ and CytcO in supercomplexes. The lipid is enriched in both the mammalian $I_1III_2IV_1$[204] and *S. cerevisiae* $III_2IV_{1/2}$[205] supercomplexes. In the presence of cardiolipin the fraction of supercomplexes is larger than in its absence.[71,204−208] Recent cryo-EM structures of the *S. cerevisiae* $III_2IV_{1/2}$ supercomplexes showed that a cardiolipin and presumably a phosphocholine are found at the cyt. $bc_1$–CytcO interface. Two other cardiolipins are found in the vicinity where they also may contribute to supporting the cyt. $bc_1$–CytcO interaction[34] (Figure 8A). The lipid is suggested to mediate interactions between cyt. $bc_1$ and CytcO acting as a "glue"[209] by simultaneously binding to specific sites at each of these two complexes.[199,210]

Involvement of cardiolipin in stabilizing binding of cyt. $bc_1$ to CytcO may, at least in part, explain why the fraction of supercomplexes and free complexes depends on *S. cerevisiae* growth conditions,[17] which often influence the lipid composition of mitochondria. Furthermore, it is likely that the fraction of the two supercomplex forms, i.e., $III_2IV_1$ and $III_2IV_2$, is not only determined by the concentration of the cyt. $bc_1$ and CytcO components in the membrane,[33] but also by the presence of


https://doi.org/10.1021/acs.chemrev.1c00140
Chem. Rev. 2021, 121, 9644−9673

cardiolipin,[189,205,206,208,209] which would modulate the cyt. $bc_1$−CytcO binding affinity.

In the obligate $III_2IV_2$ supercomplexes in *M. smegmatis* and *C. glutamicum* three cardiolipins are found at the interface of complexes III and IV (Figure 8B).[44,45] Similarly, to the *S. cerevisiae* supercomplex, the head groups of all these cardiolipin molecules face the *n* side of the membrane.

### 4.4. Respiratory Supercomplex Factors

Respiratory supercomplex factors, Rcf1 and Rcf2, physically associate with cyt. $bc_1$ and CytcO. Both Rcf1 and Rcf2 contain a hypoxia-induced gene domain 1 (HIGD1), which is conserved in a wide range of organisms.[211−214] In Rcf1, the HIGD1 is in the N terminus and the C terminus has a fungi-specific domain, composed of approximately 60 amino acid residues. In Rcf2, which is a fungi-specific protein, the HIGD1 is located at the C terminus, preceded by a subdomain composed of ∼100 amino acid residues, which forms two transmembrane helices.[215,216] The Rcf2 protein has been shown to be proteolytically processed to yield a stable C-terminal fragment that associates with CytcO.[217]

Data from early studies of the functional role of Rcf1 and Rcf2 were interpreted to indicate that these factors are required for formation of the cyt. $bc_1$−CytcO supercomplexes in *S. cerevisiae*.[73,188,214,217−220] The conclusion is in part based on observations that the ratio between supercomplexes and free components decreased upon genetic removal of Rcf1, which was also interpreted to suggest that this factor acts as a bridge between the components of the supercomplex. However, Rcf1 interacts with the Cox3 subunit and possibly also Cox13,[214,219,221−223] but the recently determined supercomplex structures show that these subunits are found at the opposite side of CytcO from the $III_2$−IV interaction surface (Figure 2A).[33−35,37] Hence, Rcf1 cannot bridge supramolecular interactions between cyt. $bc_1$ and CytcO. Similarly, a recently determined cryo-EM structure suggested binding of Rcf2 at the distal side of the supercomplex.[33]

More recent studies suggest that Rcf1 is instead involved in assembly of CytcO (reviewed in refs 54,224) and incompletely assembled CytcO would result in a smaller fraction of supercomplexes. In other words, the cyt. $bc_1$−CytcO supercomplexes can form also in the absence of Rcf1, but when Rcf1 is removed, a fraction of CytcO is modified, which yields less supercomplexes. Similarly, the Aim24 protein in *S. cerevisiae*[225] and mammalian homologue of Rcf1, HIGD2A, have recently been shown to be involved in the assembly of CytcO.[226,227] It is interesting to note that data from recent studies indicate that removal of Rcf1 or Rcf2 affects the ability of the CytcO to maintain a proton electrochemical potential across the membrane, possibly due to proton leaks across the incorrectly assembled fraction of CytcO in the absence of Rcf.[228]

Genetic deletion of Rcf1 yields a subpopulation of CytcO that is incorrectly assembled and a subpopulation that is correctly assembled.[219,229−231] In the absence of Rcf1, the correctly assembled CytcO subpopulation displays a lower activity and a modified heme $a_3$-$Cu_B$ catalytic site.[229−231] The activity of this subpopulation could be restored upon addition of recombinantly expressed Rcf1,[232] which suggests that in the correctly assembled CytcO reversible binding of Rcf1 can modulate the CytcO activity. This finding is further supported by recent data showing that Rcf1 positively modulates CytcO activity also in the intact mitochondrial membrane.[221]

Deletion of Rcf2 alone has a small effect on CytcO turnover,[214,219,221,233,234] but more recent data indicate that binding of Rcf2 results in lowering the CytcO activity.[221] Collectively, these data suggest that, in addition to being involved in assembly of CytcO, the binding of the Rcf proteins is linked to changes in the turnover activity.

Mass spectrometry revealed the presence of Rcf1 and Rcf2 in preparations of purified *S. cerevisiae* supercomplexes, but these proteins were not resolved in the first cryo-EM structures.[34,35] As indicated above, more recent cryo-EM data show additional density in a pocket formed by Cox1, Cox3, Cox12, and Cox13 that in the supercomplex containing the Cox5B isoform could be assigned to the processed C terminus (HIGD1) of Rcf2.[33] In CytcO containing the Cox5A isoform, the additional density could not be assigned with confidence. As the HIGD1 fragment is conserved to both Rcf1 and Rcf2, but is found in the C terminus of Rcf2 or the N terminus of Rcf1, the interaction between this segment and a putative conserved CytcO site would expose the remaining parts of the two Rcf proteins to different sides of HIGD1 (discussed in more detail in ref 215). In other words, any additional interactions with the supercomplex would be very different for the Rcf1 and Rcf2 proteins. This observation reveals how binding of Rcf1 and Rcf2 could differently modulate the activity of CytcO or the supercomplex. An interaction between the homologous bovine HIGD1A protein and bovine CytcO was also observed.[235] Furthermore, formation of the mammalian $III_2IV$ supercomplexes is dependent on another protein factor, COX7A2L.[27,28]

It is also interesting to note that interaction of Rcf1 with subunit Cox3 (subunit III) may modulate $O_2$ binding at catalytic site[221,228,234] because Cox3 harbors the lipid-containing V-shaped cleft suggested to be used for $O_2$ diffusion from the membrane phase into the CytcO catalytic site. Data from earlier studies with the *R. sphaeroides* CytcO showed that changes in lipid molecules in this cleft result in changes of the CytcO catalytic site.[236]

As evident from the discussion above, the Rcf proteins determine the structure and function of complex IV of the *S. cerevisiae* respiratory chain, however, their role at the molecular level is complex and presently not fully understood.

### 4.5. Superoxide Dismutase in the *M. smegmatis* Supercomplex

A copper-containing superoxide dismutase (SodC) dimer subunit was found to be bound in the *M. smegmatis* $III_2IV_2$ supercomplex, near the cyt. *cc* head domain of the QcrC subunit[43,44] (Figure 2B). As other SOD enzymes, it catalyzes the dismutation of the $O_2^{\bullet-}$ radical to $H_2O_2$ and $O_2$:

$$O_2^{\bullet-} + \text{SodC}-Cu^{2+} \rightarrow \text{SodC}-Cu^{+} + O_2 \quad (4a)$$

$$O_2^{\bullet-} + \text{SodC}-Cu^{+} + 2H^{+} \rightarrow \text{SodC}-Cu^{2+} + H_2O_2 \quad (4b)$$

The functional role of this SodC is unknown. Because the semiquinone formed as an intermediate at the $Q_P$ site of complex III may react with $O_2$ to form superoxide,[81,91,92] association of a SodC with the respiratory supercomplex could allow detoxification near the $O_2^{\bullet-}$ generation site.[44] In addition, the product $H_2O_2$ released by the SodC is a substrate for CytcO, which upon transfer of two electrons from cyt. *c* reduces $H_2O_2$ to water.[237] Alternatively, the reduced $Cu^+$ formed in SodC in the first reaction step (eq 4a) may transfer an electron to cyt. *cc* and then to $Cu_A$ in CytcO, where it would enter the respiratory chain


https://doi.org/10.1021/acs.chemrev.1c00140
Chem. Rev. 2021, 121, 9644−9673

thereby bypassing formation of $H_2O_2$.[44] In some anaerobic organisms, an essentially opposite reaction is catalyzed by a superoxide reductase, which reduces $O_2^{\bullet-}$ to $H_2O_2$ upon electron transfer from an external donor.[238] Recently, an integral-membrane superoxide oxidase was discovered in *E. coli*.[239] The *M. smegmatis* SodC has a similar orthologue in *M. tuberculosis*, where the subunit could remove $O_2^{\bullet-}$ generated by the host as a defense mechanism in the phagolysosomes of macrophages.[44]

## 5. INTERACTION OF COMPLEXES $III_2$ AND IV WITH CYTOCHROME *C*

In mitochondria cyt *c* is a small, typically ~12 kDa, water-soluble protein that diffuses in the three-dimensional (3D) intermembrane space (Figure 1B). Cytochrome *c* has a dipole moment and a net positive charge.[240,241] The edge of the heme group is positioned toward the positively charged protein surface, which docks either to cyt. $c_1$ or near $Cu_A$ at negatively charged surfaces of cyt. $bc_1$ or CytcO, respectively.[242−244] The orientation of cyt. *c* is the same when binding to either cyt. $bc_1$ or CytcO.[245,246]

It is generally assumed that the intracellular ionic strength is relatively high (80−150 mM), and it has been shown that at this ionic strength a major fraction of cyt *c* diffuses in three dimensions.[16,51] However, a recent analysis revealed that only the cation concentration is kept at high concentration, while the concentration of small anions is much lower and the remaining negative charges are found at the surfaces of polyanionic macromolecules.[247] As a consequence, the Debye screening radius in the intracellular medium is larger than that obtained for a monovalent salt electrolyte at 80−150 mM. Oliveberg, Wennerström, and coauthors estimated that a more reasonable mimic of the intracellular environment is the equivalent of ~20 mM of a 1:1-electrolyte. As a consequence, the electrostatic interactions between the positively charged cyt. *c*, and its negatively charged interaction partners are likely to be much stronger than those observed when mimicking the intracellular environment in a solution containing 80−150 mM monovalent salt. Below, we discuss the consequence of supercomplex-cyt. *c* interactions for electron transfer between complexes III and IV in supercomplexes, but first we briefly describe data from studies of interactions of cyt. *c* with complexes $III_2$ and IV, respectively.

### 5.1. Cyt. *c* Binding to Complexes III and IV

Early data from steady-state turnover measurements with the mammalian cyt. $bc_1$ suggested that cyt. *c* binds at a single site near cyt. $c_1$.[246] More recent data from NMR studies of the plant complex III identified an additional low-affinity distal binding site.[248] In the crystal structure of the *S. cerevisiae* cyt. $bc_1$−cyt. *c* co-complex, cyt. *c* was found bound to cyt. $c_1$.[243,249] In the structure of the *S. cerevisiae* $III_2IV_{1/2}$ supercomplex−cyt. *c* co-complex (see inset to Figure 4A), the position of cyt. *c* at cyt. $bc_1$ was only slightly shifted compared to that observed in the crystal structure.[37]

Interactions of cyt. *c* with CytcO are more complex. Results from studies of the steady-state turnover rate of mammalian CytcO were interpreted to indicate two cyt. *c* binding sites in CytcO.[245,250,251] This observation does not automatically imply the presence of two independent binding sites from which an electron is transferred to $Cu_A$. The same data could also be explained in terms of "nonproductive" binding of cyt. *c* that interferes with the "productive" binding site.[252] However, results from other experiments suggested that two cyt. *c* molecules can simultaneously bind to a monomer of the mammalian CytcO, with $K_D$ values of ~10 nM and ~1 μM, respectively.[245,250,251] Furthermore, covalent cross-linking of a cyt. *c* at the high-affinity site only had a minor effect on binding of a second cyt. *c* at the low-affinity site.[253] Binding at each site presumably results in electron transfer from cyt. *c* to $Cu_A$, but electron transfer from cyt. *c* at the high-affinity site is slower than that from the low-affinity site.[253]

Studies of the steady-state activity of the *S. cerevisiae* CytcO were initially interpreted to suggest binding of two cyt. *c* molecules with equal affinities, $K_M \cong 100$ nM.[254] However, more recent data revealed an additional $K_M$ of ~30 μM,[177] indicating a similar mechanism of cyt. *c* binding to the mammalian and *S. cerevisiae* CytcO.

The cryo-EM structure of the $III_2IV_{1/2}$ supercomplex-cyt. *c* co-complex in *S. cerevisiae*[37] showed that the cyt. *c* binding is similar to that seen in the crystal structure of the equivalent co-complex with the bovine CytcO[244] (see inset to Figure 5A).

### 5.2. The Electronic Link between Complexes III and IV

**5.2.1. Diffusion in 3D.** It is clear that association of cyt. $bc_1$ and CytcO to form a supercomplex leads to a decrease in the intercomplex distance. The distance between the electron donor site at cyt. $bc_1$ and the acceptor site near $Cu_A$ at CytcO within the *S. cerevisiae* supercomplex is ~60 Å (Figure 3A)[34,35] (see also refs 72,74), i.e., too long to yield a catalytically relevant electron-transfer rate through docking of a single cyt. *c* between the electron donor and acceptor sites.[255] Thus, the question arises whether or not a shorter diffusion distance via the water phase of the intermembrane space (defined as 3D diffusion) would result in a higher $QH_2$:$O_2$ oxidoreductase activity.[36,50] Considering a reasonable average distance between independently diffusing cyt. $bc_1$ and CytcO in the membrane (~50 nm, see Figure 1B), the 3D diffusion time of cyt. *c* between these complexes is in the order of 10 μs.[50] Hence, diffusion of cyt. *c* cannot be rate limiting for electron transfer from $QH_2$ to $O_2$ because the maximum turnover ($k_{cat}$) of cyt. $bc_1$ and CytcO in *S. cerevisiae* is ~$10^2$ $s^{-1}$ and ~$10^3$ $s^{-1}$, respectively.[17] Furthermore, the overall electron flux through the respiratory chain *in vivo* is lower than the lowest $k_{cat}$ value of the involved components, in the range 40 $s^{-1}$ to 140 $s^{-1}$ (Michel Rigoulet, personal communication). Nevertheless, the $QH_2$:$O_2$ oxidoreductase activity is dependent on the concentration of externally added cyt. *c* to mitoplasts[36] or purified supercomplexes at a cyt. *c*:supercomplex ratio similar to that found *in vivo*,[37] suggesting that the cyt. *c*-mediated electron transfer is rate limiting.

Results from a recent theoretical study showed that the electron flux between cyt. $bc_1$ and CytcO, mediated by 3D diffusion of cyt. *c*, is determined by the equilibration time of cyt. *c* with the cyt. *c* pool in the intermembrane space, rather than by the cyt. *c* diffusion time constant itself.[50] Furthermore, the data showed that this equilibration time increases with decreasing cyt. *c* concentration, i.e., the lower the cyt. *c* concentration, the stronger the distance dependence on activity. For freely diffusing components, a cyt. *c*:supercomplex ratio of 2−3 and an average cyt. $bc_1$−CytcO distance of 50 nm (Figure 1B), this scenario yields a cyt. *c*-mediated $QH_2$:$O_2$ oxidoreductase activity that is slower than the turnover of cyt. $bc_1$ and is dependent on the average cyt. $bc_1$−CytcO distance. Interestingly, on the basis of the data in ref 256, Maldonado *et al.* estimated that in plant mitochondria the cyt. *c*:supercomplex ratio is one,[32] suggesting an even stronger cyt. $bc_1$−CytcO distance dependence on the $QH_2$:$O_2$ oxidoreductase activity than in *S. cerevisiae* mitochondria. Taking into consideration the recent finding that the salt


https://doi.org/10.1021/acs.chemrev.1c00140
Chem. Rev. 2021, 121, 9644−9673

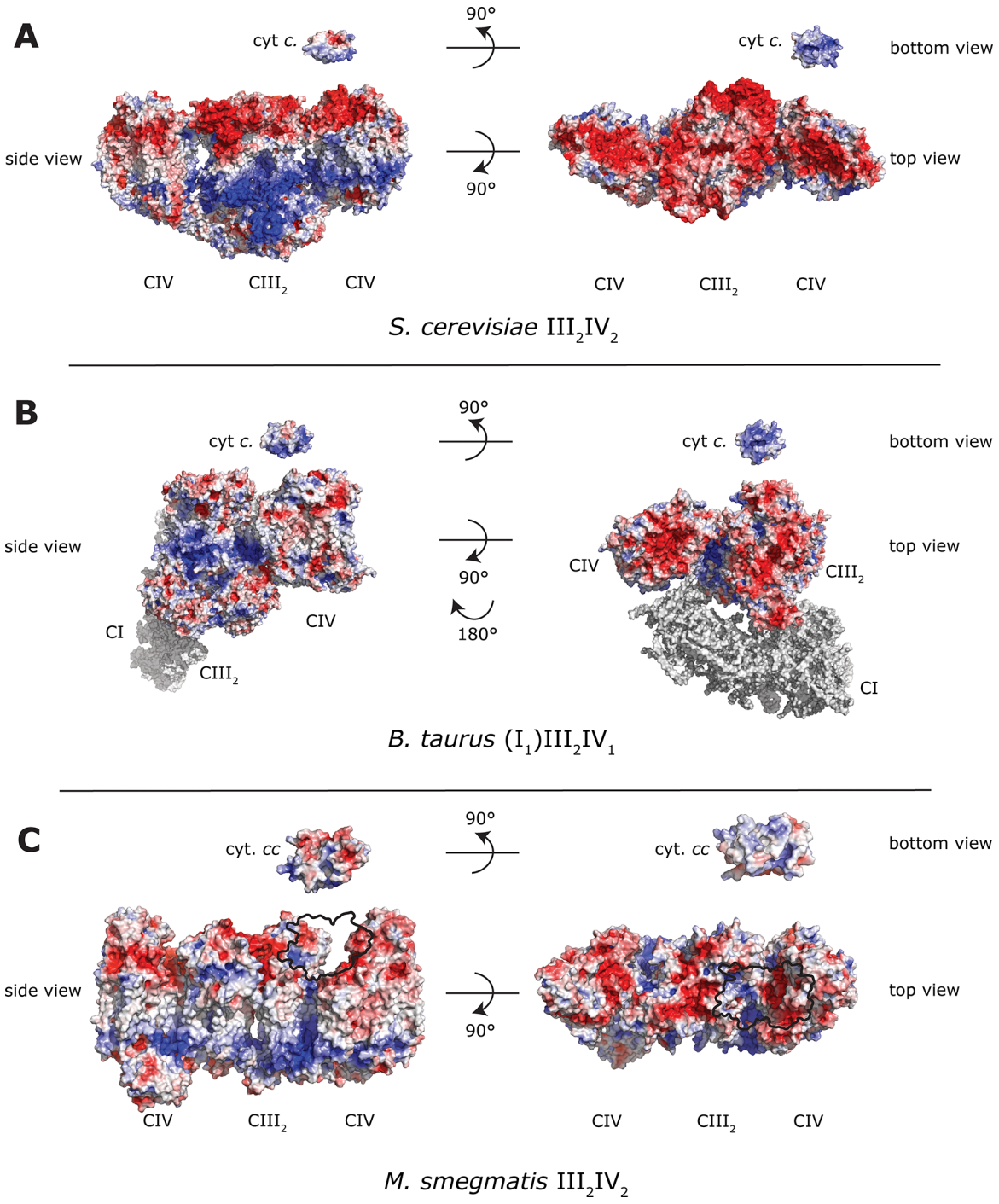


**Figure 9.** Surface representation of the electrostatic potential in III–IV supercomplexes. The *S. cerevisiae* (PDB 6HU9) (A), *B. taurus* (cow) (PDB 5LUF) (B), and *M. smegmatis* (PDB 6HWH) (C) supercomplexes are shown. Cyt. *c* is from either *S. cerevisiae* (A, PBD 1YCC) or *B. taurus* (B, PDB 2B4Z). For *M. smegmatis* (C), the cyt. *cc* head domain of QcrC in the closed conformation was separated from the supercomplex and the electrostatic potentials were calculated separately for the supercomplex and cyt. *cc* domain, respectively. The original position of the cyt. *cc* domain at the top of the supercomplex is encircled by a black line in (C). Color range from red to blue for an electrostatic potential from −5 to +5 $k_BT/q$, where $k_B$ is the Boltzmann constant, $T$ is the absolute temperature, and $q$ is a the unit charge. The figure was prepared using the APBS tool[270] with standard settings of the PyMOL software (*Molecular Graphics System*, version 2.4; Schrödinger, LLC).[271]

concentration equivalent of the intracellular environment is estimated to be ∼20 mM[247] rather than the 150 mM used in the theoretical study,[50] the diffusion coefficient for cyt. *c* in mitochondria would be a factor of ∼$10^2$ lower[51] than that used in the theoretical study in ref 50. This effect further emphasizes the kinetic advantage in forming supercomplexes, under the assumption that electron transfer occurs via 3D diffusion.

**5.2.2. Diffusion in 2D.** Many Gram-negative bacteria, e.g., *R. capsulatus*, *R. sphaeroides*, and *P. denitrificans* harbor a membrane-anchored cyt. $c_y$ in addition to a water-soluble cyt. *c*.[46,257,258] A cyt. $c_y$ homologue is the only cyt. *c* present in *Rickettsia prowazekii*.[257,259] Restriction of cyt. *c* diffusion to the


https://doi.org/10.1021/acs.chemrev.1c00140
Chem. Rev. 2021, 121, 9644−9673

two-dimensional (2D) space of the membrane surface yields shorter diffusion times than for 3D diffusion at the same concentrations of the involved components.[50] Furthermore, integration of a membrane-anchored cyt. *c* into a cyt. $bc_1$−Cyt*c*O supercomplex allows direct electron transfer from the donor at cyt. $bc_1$ to the acceptor at Cyt*c*O,[59,260] even though the linker between the membrane domain and the cytochrome domain in cyt. $c_y$ is too long to distinguish between 2D and restricted 3D diffusion. In a recent study, the normally water-soluble cyt. *c* was attached to a membrane-bound protein in *S. cerevisiae* mitochondria, which allowed electron transfer between complexes III and IV over a time scale similar to that *in vivo*.[261]

Some Gram-positive bacteria, which lack an outer membrane, harbor membrane-associated cyt *c*s that are attached either via a transmembrane polypeptide or a lipid anchor.[262] In *Bacillus* PS3, a supercomplex composed of cyt. $bc_1$, Cyt*c*O and a cyt. *c* was identified and shown to display quinol oxidase activity, i.e., electron transfer from quinol to oxygen.[68] In the Gram-positive actinobacteria from, e.g., *M. smegmatis* and *C. glutamicum* electron transfer between cyt. *bcc* and Cyt*c*O occurs via the diheme cyt. *c* ectodomain of the QcrC subunit of the cyt. *bcc* complex (Figures 2B and 3B). Because these bacteria lack any water-soluble or membrane-anchored free cyt. *c*, a supercomplex composed of cyt. *bcc* and Cyt*c*O is required for electron transfer from $MQH_2$ to dioxygen.[62,64,65,263] Disruption of the supercomplex using detergent results in a decrease in activity.[263]

Electron transfer between cyt. $bc_1$ and Cyt*c*O by 2D diffusion of cyt. *c* that is bound to the supercomplex surface or weakly associated with the membrane has been discussed also in organisms that harbor a water-soluble cyt. *c*[37,50,77,264−268] (see also ref 53). The surface between the cyt. *c*-binding sites at cyt. $bc_1$ and Cyt*c*O in the *S. cerevisiae* supercomplex is negatively charged (Figure 9A), and one cyt. *c* per Cyt*c*O is tightly bound to the supercomplex[204,234,269] *in situ* (but not in purified complexes). Assuming the same scenario in plant mitochondria, an estimated cyt. *c*:supercomplex ratio of one in *V. radiata*[32] suggests that the entire cyt. *c* pool would be associated with supercomplexes but presumably at equilibrium. Recent Cryo-EM structures of the supercomplex with added cyt. *c* revealed distinct states where cyt. *c* is bound either to cyt. $bc_1$ or Cyt*c*O, or resides at intermediate positions at the supercomplex surface.[37] Measurement of the supercomplex activity as a function of the concentration of added cyt. *c* yielded apparent $K_M$ values of ≤6 nM and ∼1.7 μM, i.e., much smaller than those obtained with isolated *S. cerevisiae* Cyt*c*O (∼100 nM and ∼30 μM, respectively, see above). These data suggest a stronger binding to the supercomplex than to Cyt*c*O, which is consistent with the large negatively charged binding surface for cyt. *c* between cyt. $bc_1$ and Cyt*c*O. The $QH_2$:$O_2$ oxidoreductase activity of the supercomplex is ∼20 $e^-$/s for a supercomplex with a single bound cyt. *c*. This rate decreased upon dissociation of the supercomplex, i.e., when increasing the average distance between cyt. $bc_1$ and Cyt*c*O. Collectively, the structural and kinetic data showed that electron transfer within the supercomplex is mediated by 2D diffusion of a single surface-associated cyt. *c*. It is also interesting to note that the rate of electron transfer between cyt. $bc_1$ and Cyt*c*O with a single bound cyt. *c* is near the lower limit of the electron flux through the respiratory chain *in vivo*. It is also worth mentioning that the above-described experiments were performed at the assumed near-physiological monovalent salt concentration of ∼150 mM, which was also required to prevent protein aggregation on the cryo-EM grids.[37] Considering the novel finding that a better mimic of physiological conditions is 20 mM monovalent salt,[247] the cyt. *c*−supercomplex interactions are most likely even stronger *in vivo* than those experimentally observed.[37]

In conclusion, the combined cryo-EM and kinetic data show that supercomplex formation in *S. cerevisiae* does not result in increasing the electron transfer rate by decreasing the cyt. *c* 3D diffusion distance, as recently suggested.[36] Rather, formation of $III_2IV_{1/2}$ supercomplexes in *S. cerevisiae* results in switching to a different mechanism that involves 2D diffusion from the electron donor to the electron acceptor.[37] In other systems electron transfer between complexes III and IV may occur by 3D diffusion and the theoretical studies show that also under these conditions, there is a kinetic advantage in decreasing the intercomplex distance by formation of supercomplexes.[50] The 2D-diffusion mechanism in *S. cerevisiae* is similar to that suggested for electron transfer from cyt. $bc_1$ to the $cbb_3$ Cyt*c*O via a movable membrane-anchored cyt. $c_y$ domain in *R. capsulatus*.[46]

Electron transfer from cyt. $bc_1$ to Cyt*c*O by 2D diffusion of cyt. *c* along the supercomplex surface resembles a "substrate channeling" model, which has been criticized based on the finding that cyt. *c* diffusion in *S. cerevisiae* is unrestricted.[269] However, 2D diffusion of cyt. *c* is not in conflict with this finding because it assumes only weak electrostatic interactions between cyt. *c* and the supercomplex surface, and cyt. *c* remains in equilibrium with the cyt. *c* pool during the electron-transfer process[16] (see Figure 10).

In mammalian mitochondria, complexes $III_2$ and IV are not only part of respirasomes but also assemble independently to form $III_2IV$ supercomplexes.[27,28,272] The structure of these supercomplexes is presently not known. Figure 9B shows the electrostatic potential surface of the cyt. $bc_1$−Cyt*c*O part of the mammalian respirasome. As seen in the figure, the negatively charged cyt. *c* binding sites at cyt. $bc_1$ and Cyt*c*O are less connected by negative charges on the surface in between the sites than in the *S. cerevisiae* supercomplex (Figure 9A). This difference in charge distribution may reflect the much lower fraction of Cyt*c*O that is part of supercomplexes in mammalian (15−30%[54]) than in *S. cerevisiae* yeast (∼90%,[72]) mitochondria. In other words, in the mammalian respiratory chain electron transfer between cyt. $bc_1$ and Cyt*c*O occurs primarily via 3D diffusion.

It is also interesting to note that in the *M. smegmatis* $III_2IV_2$ supercomplex, interactions between the movable cyt. *cc* domain[44] (see Figure 2B) and complex IV most likely occur by electrostatic interactions between positive charges on the cyt. *cc* surface and negative charges at complex IV (Figure 9C). However, the extracellular surface of complex III is positively charged, which indicates that the cyt. *cc* domain is held in place by its TM α-helix rather than by electrostatic interactions.

**5.2.3. Effects of Cox5/cyt. *c* Isoforms.** Because subunit Cox5 is located at the interface of cyt. $bc_1$ and Cyt*c*O in the supercomplex[33−35,37] (Figure 2A), it is positioned at the diffusion path of cyt. *c*. Expression of the two interchangeable isoforms of Cox5, i.e., Cox5A and Cox5B, correlates with the expression of the two cyt. *c* isoforms, iso-1 and iso-2, respectively; Cox5A and iso-1 cyt. *c* are expressed under normoxia, while Cox5B and iso-2 cyt. *c* are expressed under hypoxia.[174,273,274] This correlation may be coincidental, but we discuss briefly its possible consequences. The supercomplex structure was essentially the same with either Cox5A or Cox5B,[33] and no effects were observed on the supercomplex activity. In addition, the maximum catalytic activity of Cyt*c*O


https://doi.org/10.1021/acs.chemrev.1c00140
Chem. Rev. 2021, 121, 9644−9673

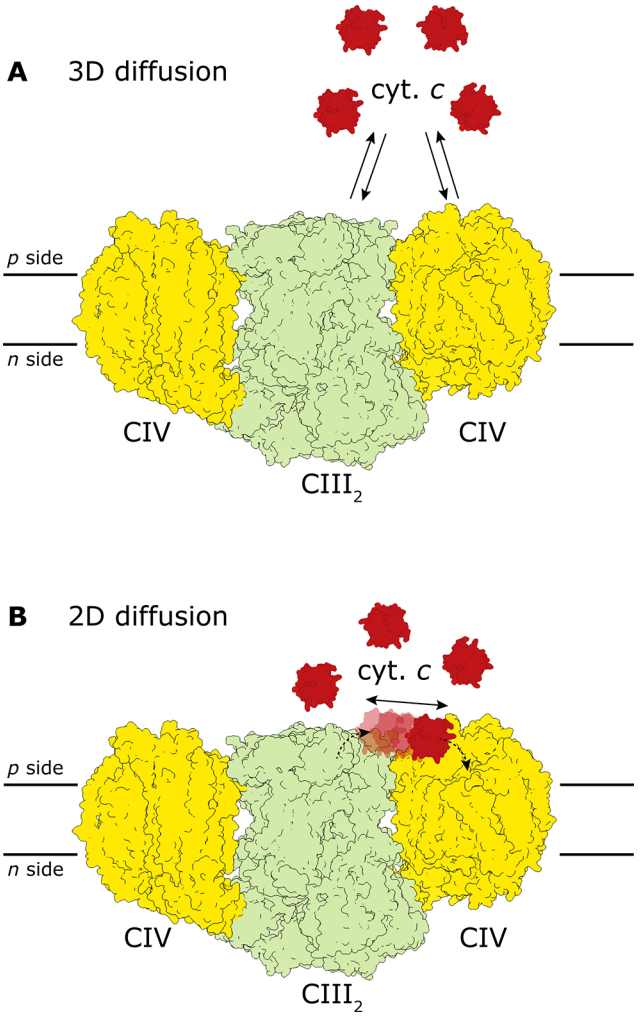


**Figure 10.** Model for electron transfer from cyt.$bc_1$ to CytcO in the *S. cerevisiae* supercomplex. (A) Electron transfer via 3D diffusion of cyt. *c*. (B) Electron transfer via 2D diffusion of cyt. *c*. Note that the surface-attached cyt. *c* is assumed to be in equilibrium with the cyt. *c* pool, but the time constant for equilibration of the surface-attached cyt. *c* with the pool cyt. *c* (as well as electron transfer between the surface-attached cyt. *c* and pool cyt. *c*) is assumed to be slower than diffusion between the binding sites at cyt. $bc_1$ and CytcO (modeled after ref 37). *S. cerevisiae* supercomplex and cyt. *c* are PDBs 6HU9 and 1YCC, respectively.

and its affinity for both cyt. *c* isoforms and $O_2$ were unaffected upon replacement of Cox5A by Cox5B.[177] However, the supercomplex activity was measured at a cyt. *c*:supercomplex ratio of $>10^3$,[34] where the electron-transfer rate saturates at a maximum value, $k_{cat}$. It is possible that at the much smaller cyt. *c*:supercomplex ratio of ~2−3, found in *S. cerevisiae* mitochondria *in vivo* (cf. ref 37), an effect on the intercomplex electron transfer would be observed depending on cyt. *c* and Cox5 isoforms. In other words, it cannot be excluded that electron transfer between cyt. $bc_1$ and CytcO within the supercomplex is regulated by altering the pairwise expression levels of Cox5 and cyt. *c* isoforms.

**5.2.4. Binding of cyt. *c* to Rcf1.** Cytochrome *c* has also been shown to bind to Rcf1.[232,234,275,276] The original suggestion that Rcf1 could be found at the interface of complexes III and IV prompted us to suggest that formation of a putative Rcf1−cyt. *c* co-complex would play a similar role to that of cyt. $c_y$, i.e., mediate electron transfer via a membrane-associated cyt. *c*.[234] However, this particular consequence of the Rcf1−cyt. *c* interaction appears less likely in *S. cerevisiae* in view of the putative binding of Rcf1 to Cox3/Cox13 (see above), and the position of these subunits at the distal edge of the supercomplex, rather than between cyt. $bc_1$ and CytcO (Figure 2A). On the other hand, assuming that Rcf1 would bind at the same position as Rcf2,[33] cyt. *c* binding to an Rcf1−CytcO cocomplex would position the cyt. *c* near the cyt. *c*-binding cleft defined by CytcO subunits Cox12 and Cox2. Interaction of cyt. *c* with Rcf1 at this position would result in increasing the affinity for cyt. *c* to CytcO to allow electron transfer between complexes III and IV via two transiently bound cyt. *c*s, as discussed previously.[37,264] Similarly, interaction of cyt. *c* with HIGD1 in mammalian mitochondria has also been observed and discussed.[227,235,277]

As outlined above, the Rcf proteins appear to support a range of functions in respiration, one of which involves binding of cyt. *c*. However, additional data is needed to fully understand the functional significance of the cyt. *c*−Rcf1 interactions at the molecular level.

## 6. WHY SUPERCOMPLEXES?

When considering complexes III and IV, the answer to the question above is rather trivial in the case of the Gram-positive actinobacteria, which do not harbor any water-soluble cyt. *c*. We therefore focus the discussion on the mitochondrial $III_2IV_{1/2}$ supercomplexes. A discussion of a functional significance of these mitochondrial supercomplexes is complicated by the variability in their composition, the variable distribution of free complexes and supercomplexes in different organisms,[54,278] and the differences in relative orientation of the respiratory complexes within the supercomplexes, i.e., the flexibility in the interaction surfaces of the supercomplex components among different species (Figure 7). Nevertheless, it is well established that supercomplexes do form in a wide range of organisms and are likely to have functional significance. As already indicated above, various physiological roles of supercomplexes have been discussed (e.g., refs 23,53−55,279,280), and below we summarize some specific suggestions with a focus on cyt. $bc_1$−CytcO supercomplexes.

### 6.1. Changes in Structure or Activity upon Formation of Supercomplexes

The lack of well-defined structural changes of the respiratory enzymes upon association into supercomplexes, and the differences in the relative orientation of the components in different organisms (Figure 7) suggest that formation of supercomplexes does not result in changes in functionality of individual components. Changes in turnover activity of individual respiratory complexes upon forming supercomplexes have been reported, but they are typically too small to yield any functionally relevant changes in the overall electron flux through the respiratory chain (see refs 53,54). Furthermore, as outlined above, the electron flux through the respiratory chain *in vivo* is typically lower than the $k_{cat}$ values of the components. Therefore, formation−dissociation of the mitochondrial supercomplexes is unlikely to comprise a universal mechanism to modulate function through changes of the activity of complexes III or IV themselves.

A similar problem is associated with identifying specific effects of supercomplex formation on the "stability" of the components, which has been suggested in the past, although mainly for complex I (reviewed in refs 53,54). As pointed out by


https://doi.org/10.1021/acs.chemrev.1c00140
Chem. Rev. 2021, 121, 9644−9673

Milenkovic *et al.*,[53] many of the studies addressing this issue are based on observation of correlations of effects on function, structure and morphology, and it is at present not possible to deduce any specific mechanistic effects at a molecular level.

### 6.2. Protein Distribution and Aggregation

Blaza *et al.*[281] proposed that formation of supercomplexes is a consequence of the very high protein density of the inner mitochondrial membrane (~2/3 protein); formation of supercomplexes would outcompete irreversible, unspecific aggregation of respiratory complexes with other membrane components.[53,281] However, as also noted by these authors, in mammalian mitochondria only 15−30% of Cyt*c*O is part of supercomplexes.[54] This equilibrium of free complexes and supercomplexes indicates that association of respiratory complexes to form supercomplexes is realized through relatively weak reversible interactions. Because a reversible equilibrium of supercomplexes and free complexes could not block irreversible formation of aggregates between respiratory complexes and other membrane proteins, we consider this role of supercomplexes to be less likely.

In *S. cerevisiae*, a larger fraction (~90%) of the Cyt*c*O population is part of supercomplexes.[72] An equilibrium constant between supercomplex-bound and free Cyt*c*O in the order of 10 suggests that also in *S. cerevisiae*, the $III_2IV_{1/2}$ supercomplexes are held together by weak interactions. This conclusion is further supported by the necessity to use weak detergents for isolation of supercomplexes (e.g., digitonin or glyco-diosgenin, GDN) and the observation that they dissociate into components upon addition of *n*-dodecyl-*β*-D-maltoside (DDM).[37] Thus, also in *S. cerevisiae* the cyt. $bc_1$−Cyt*c*O interactions are reversible and could not outcompete irreversible nonspecific aggregation with other membrane-bound proteins.

Another suggestion for the role of supercomplexes originates from an observation of the preference for respiratory complexes for specific membrane topology.[282] Fedor and Hirst[283] suggested that formation of supercomplexes would ensure an even distribution of the respiratory complexes in the membrane, a plausible proposal that could be tested experimentally in future studies.

### 6.3. Production of ROS

Formation of supercomplexes has been suggested to decrease the amount of produced reactive oxygen species (ROS) (e.g., refs 73,284). Here, we briefly discuss this proposed role in the framework of effects at a molecular level. This discussion requires a definition of the term ROS as it does not describe a single chemical entity, but rather a range of molecules or ions that are formed upon incomplete reduction of $O_2$ (i.e., reduction by <4 electrons), including superoxide, peroxide, and hydroxyl radicals.[285] The reactivity of these species differs and therefore the term ROS only depicts a generally reactive molecule or ion. Reduction of $O_2$ by one electron at a time yields first the superoxide anion ($O_2^{\bullet-}$), which is the precursor of other ROS.[285,286] The main sites of initial $O_2^{\bullet-}$ formation in mitochondria are at complexes I and III.[285,286]

The amount formed $O_2^{\bullet-}$ at a specific redox site at a particular $O_2$ concentration is determined by the relative rates of $O_2^{\bullet-}$ formation ("side reaction") and the rate by which the electron is transferred from that site to the next acceptor in the electron-transfer chain (physiological reaction). When assuming that formation of supercomplexes would yield less ROS, the implicit assumption is that the electron-transfer rate away from the ROS-forming site would be slower for individually diffusing complexes than for supercomplexes.

Data from studies of model systems suggest that the amount of ROS at complex I decreases upon supercomplex formation.[284] However, Fedor and Hirst[283] recently showed that $QH_2$ produced by complex I in supercomplexes is oxidized to Q more rapidly outside the supercomplex than by the acceptor within the supercomplex (complex III). In other words, electrons from complex I are removed more rapidly in the absence than in the presence of supercomplexes. As a consequence, formation of supercomplexes that involve complex I would not *per se* result in decreasing the fraction of reduced ROS-forming sites at complex I.

A postulate that formation of supercomplexes composed of cyt. $bc_1$ and Cyt*c*O would yield less ROS implies that association of the components would result in a faster reoxidation of cyt. $bc_1$ because ROS is mainly formed at cyt. $bc_1$. Indeed, as discussed above, reduction−oxidation of cyt. *c* is the rate-limiting step of electron transfer from $QH_2$ (complex III) to $O_2$ (complex IV) in *S. cerevisiae*. Therefore, a decrease in this transfer rate upon dissociation of the $III_2IV_{1/2}$ supercomplexes would result in a larger fraction of reduced complex III, which could result in accumulation of electrons at the $Q_P$ site where nonphysiological reduction of $O_2$ to $O_2^{\bullet-}$ is most likely to take place.[81] Hence, we consider it possible that $O_2^{\bullet-}$ production is indeed lowered upon formation of $III_2IV_{1/2}$ supercomplexes.

In the above discussion, we consider a fully functional respiratory chain. However, in the native membrane, new respiratory complexes are continuously produced, and at a given time there are also partly assembled respiratory complexes with incompletely connected electron-transfer chains. These partly assembled complexes could accumulate electrons at their redox sites, which upon interaction with $O_2$ may form ROS. It is possible that association of these partly assembled complexes with other fully functional partner complexes to form supercomplexes[287] would provide a route for dissipation of these reducing equivalents. In so doing, the probability for ROS formation from partly assembled respiratory complexes would be diminished.

### 6.4. Free Energy Conservation

As already discussed above, early hypotheses suggesting "substrate channeling", i.e., direct transfer of confined $Q/QH_2$ or cyt. *c* between respiratory complexes within a supercomplex, have been rejected.[38,53,88,269,281,283] Yet, supercomplexes have been proposed to allow a "more efficient" transport of electrons and an increase in the "efficiency" of respiration allowing higher "yields" of energy conservation (see e.g., refs 25,36,56,76,282,288). Therefore, a consideration of effects of supercomplex formation on "efficiency" and "yield", terms frequently used in the discussions, requires a definition of these terms and a more detailed analysis.

The free energy available at each respiratory complex (energy input) is defined by the difference in standard redox potentials of the electron donor and acceptor, the concentration ratio of reduced and oxidized donor, as well as the concentration ratio of reduced and oxidized acceptor. The free energy conserved at each respiratory complex (energy output) is determined by the number of protons transferred across the membrane and the charge separation upon oxidation of the electron donor and reduction of the acceptor. The term efficiency typically depicts the ratio of free energy output and free energy input in a given system. An assumption that association of respiratory−chain


https://doi.org/10.1021/acs.chemrev.1c00140
Chem. Rev. 2021, 121, 9644−9673

complexes into supercomplexes results in an increased efficiency of respiration implies that the efficiency of at least one component would increase. However, as discussed above, changes in the charge-separation stoichiometry of individual complexes are unlikely to occur upon association into supercomplexes and therefore the overall efficiency of the system is not expected to change upon forming supercomplexes.

The terms "yield" and "efficiency" are in principle equivalent but are often used in different context. The former is often used to depict the amount of ATP formed for a given amount of oxidized substrate of the respiratory chain (cf., the so-called P/O ratio). This parameter is also determined by the efficiency of each component, including the ATP synthase and, hence, it is not expected to change upon association of respiratory complexes into supercomplexes.

It is relevant to note that the yield of ATP formation is also dependent on proton leaks across the membrane. Proton leaks often occur at protein−membrane interface surfaces, which become smaller upon association of respiratory complexes into supercomplexes. However, the protein−protein interaction surface upon formation of a supercomplex comprises only a very small fraction of the sum of all protein−membrane interaction surfaces of all membrane proteins of the inner mitochondrial membrane. Therefore, the effect of decreasing the protein−membrane interaction surface upon forming supercomplexes would most likely not result in increasing the yield of ATP production. That said, it is clear that an intricate web of regulatory pathways in mitochondria controls energy conservation in respiratory complexes and the overall P/O ratio, depending on environmental conditions.[289] These regulatory pathways may also involve formation and dissociation of supercomplexes. However, changes in the energy-conversion efficiency or yield cannot simply be a direct consequence of changing the distance between respiratory complexes to form supercomplexes.

If "more efficient" incorrectly alludes to an increase in the electron-transfer rate between respiratory complexes, the suggestion that supercomplex formation would result in "more efficient" electron transfer is plausible, at least when considering association of complexes III and IV (see above).

### 6.5. The Redox State and Binding of cyt. *c*

We consider electron transfer between complexes III and IV via cyt. *c* diffusion and discuss two scenarios: (*i*) freely diffusing complexes III and IV where after reduction at cyt. $bc_1$, cyt. *c* equilibrates with the cyt. *c* pool in the intermembrane space and electrons are transferred to Cyt*c*O from this cyt. *c* pool (Figure 10A); (*ii*) electron transfer from cyt. $bc_1$ to Cyt*c*O by 2D diffusion along the surface of a $CIII_2CIV_{1/2}$ supercomplex (Figure 10B). According to scenario (*i*), the redox state of the cyt. *c* pool in the intermembrane space is determined by the relative rates of cyt. *c* reduction at cyt. $bc_1$ and oxidation at Cyt*c*O. According to scenario (*ii*), the redox state of the cyt. *c* pool is determined by the equilibrium constant of cyt. *c* bound to the supercomplex surface and free cyt. *c* in the bulk solution, i.e., the probability that a surface-associated cyt. *c* in the reduced state is replaced by a bulk oxidized cyt. *c*. In addition, cyt. *c* from the cyt. *c* pool may transiently interact and exchange electrons with any of the complexes or the bound cyt. *c* during the 2D electron transfer. Nevertheless, the reduction level of the cyt. *c* pool is expected to depend on the fractions cyt. $bc_1$ and Cyt*c*O that are part of a supercomplex because the nature of the electronic link changes upon supercomplex formation/dissociation. As proposed by Moe *et al.*,[37] the scenario suggests yet another possible functional role of supercomplex formation, i.e., to alter the reduced:oxidized ratio of cyt. *c*. Because cyt. *c* is involved in an intricate web of cellular interactions,[290,291] there may be a link between assembly of cyt. $bc_1$ and Cyt*c*O into supercomplexes, changes in environmental conditions, and cellular redox-signaling pathways.

Yet another possibility is that formation of supramolecular assemblies is not directly linked to functional properties of the respiratory chain. Cytochrome *c* is a positively charged dipolar molecule, which resides in an environment containing negatively charged proteins.[247] Association of cyt. *c* with the supercomplex surface by electrostatic interactions may be necessary to outcompete nonspecific reversible binding to other negatively charged proteins and membrane surfaces in the intermembrane space. Formation of supercomplexes that allow electron transfer by 2D diffusion along the supercomplex surface could thus be a consequence of the electrostatic binding of cyt. *c* to cyt. $bc_1$ and Cyt*c*O.

The discussion above leaves us with a question: why do mitochondria use a soluble, diffusible cyt. *c* rather than a membrane-anchored counterpart? In this context, it is interesting to recapitulate that *R. prowazekii*, the closest known microbe relative of mitochondria,[257,259] harbors only a membrane-anchored cyt. $c_y$ homologue.[257,259] We speculate that if the role of cyt. *c* is only to shuttle electrons between cyt. $bc_1$ and Cyt*c*O, then at a minimal cyt. *c* concentration, the highest possible electron-transfer rate is maintained by a membrane-anchored cyt. *c*. However, evolution has given also other, regulatory functions to cyt. *c*, such as, e.g., being a messenger in apoptosis,[203,291] which is linked to the redox properties of this electron carrier and may require a water-soluble, diffusible variant. A "best of both worlds" scenario, e.g., in *S. cerevisiae*, would therefore be to keep the same electron-transfer mechanism as that in *R. prowazekii* by association of cyt. *c* with a cyt. $bc_1$−Cyt*c*O supercomplex surface, but to use a water-soluble cyt. *c* that can also sustain other mitochondrial functions.

## 7. FINAL REMARKS

Respiratory supercomplexes are found in a wide range of organisms. Structures of the bacterial and mitochondrial $III_2IV_{1/2}$ supercomplexes show a great variability in their overall composition and relative orientations of the components, which suggests that the only common structural characteristics of the supramolecular assemblies is proximity of the components. Cryo-EM structures of the $III_2IV_{1/2}$ supercomplexes show that the components are connected via a small number of protein−protein interactions as well as interfacial cardiolipin, and the structures of cyt. $bc_1$ and Cyt*c*O remain essentially unaltered upon association. Collectively, the data suggest that the functional role of the supramolecular assemblies is to minimize the distance between the components. We suggest that this organization supports a mechanism that allows electron transfer by 2D diffusion of cyt. *c* across the merged negatively charged surface of the supercomplex.[37] The consequence of electron transfer by 2D diffusion upon forming a supercomplex is a change in the fraction of reduced/oxidized cyt. *c* in the intermembrane space, which may be sensed by multiple regulatory pathways of the cell. Alternatively, the 2D diffusion mechanism may be a consequence of tight binding of cyt. *c* to cyt. $bc_1$ and Cyt*c*O in order to outcompete nonspecific interactions between cyt. *c* and negatively charged proteins and membrane surfaces in the intermembrane space. In


https://doi.org/10.1021/acs.chemrev.1c00140
Chem. Rev. 2021, 121, 9644−9673

actinobacteria, electron transfer from complex III to complex IV is conducted via the diheme cyt. *cc* domain of subunit QcrC. In these supercomplexes, there is an additional effect from the intricate intertwining and shared structural domains, which suggests that the supercomplex functions as a single unit. This unit also comprises novel key structural features such as an FeS domain that is locked at a fixed position in complex III and a complex III "lid" that shapes a novel proton pathway orifice in complex IV. Future studies will hopefully reveal the functional significance of these novel structural features and offer further general insights into the functional significance of respiratory supercomplexes at a molecular level.

## AUTHOR INFORMATION


### Corresponding Author

**Peter Brzezinski** − *Department of Biochemistry and Biophysics, The Arrhenius Laboratories for Natural Sciences, Stockholm University, SE-106 91 Stockholm, Sweden;* orcid.org/0000-0003-3860-4988; Phone: +46 70 609 2642; Email: peterb@dbb.su.se

### Authors

**Agnes Moe** − *Department of Biochemistry and Biophysics, The Arrhenius Laboratories for Natural Sciences, Stockholm University, SE-106 91 Stockholm, Sweden*

**Pia Ädelroth** − *Department of Biochemistry and Biophysics, The Arrhenius Laboratories for Natural Sciences, Stockholm University, SE-106 91 Stockholm, Sweden*

Complete contact information is available at: https://pubs.acs.org/10.1021/acs.chemrev.1c00140


### Notes

The authors declare no competing financial interest.

### Biographies

Peter Brzezinski, born in 1961, received his Degree of Master of Science in Engineering Physics from Chalmers University of Technology (CTH) in Göteborg, Sweden. He received his Ph.D. in Physics and Biophysics in 1989 at CTH, working with Tore Vänngård and Bo Malmström. The thesis was focused on mechanistic studies of mammalian cytochrome *c* oxidase. He was a postdoctoral fellow at the Physics Department at UCSD (1989−1991), working in the group of George Feher, where he studied bacterial photosynthetic reaction centers. In 1991, Brzezinski joined the Faculty at the Department of Biochemistry and Biophysics at Göteborg University. His studies were focused on plant photosystems I and II, respiratory oxidases and interactions of biomolecules with surfaces. In 1998, he was appointed as Chair Professor of Biochemistry at Stockholm University, where his research is focused on broader aspects of molecular Bioenergetics.

Agnes Moe completed her B.Sc. in Chemistry in 2016 and M.Sc. in Biochemistry in 2018 at Stockholm University. She is currently a Ph.D. student at the Department of Biochemistry and Biophysics at Stockholm University under the supervision of Professor Peter Brzezinski. Her Ph.D. studies are focused on investigating the significance of respiratory supercomplexes by combining the use of cryo-EM with spectroscopy and functional assays.

Pia Ädelroth, born in 1970, received her Master's Degree in Chemistry in 1993 from Göteborg University, Sweden. She received her Ph.D. in Biochemistry in 1998 from Göteborg University with a thesis entitled "Pathways and Mechanisms of Proton transfer in Cytochrome *c* oxidase", which was focussed on the *R. sphaeroides* $aa_3$ oxidase. In 1999, she joined the group of Professor Mel Okamura at the Physics Department at UCSD as a postdoctoral fellow and stayed there for two years, working on the mechanistic details of proton transfer reactions in photosynthetic reaction centers. In 2001, Ädelroth joined the Department of Biochemistry and Biophysics at Stockholm University, first as an Assistant Professor, and since 2012 she holds a Professor position. The research in the Ädelroth lab is focussed mainly on the diversity of bacterial respiratory chains.

## ACKNOWLEDGMENTS

We thank Mikael Oliveberg, Lars Hederstedt, Michel Rigoulet, and Robert B. Gennis for valuable discussions. This work was supported by the Knut and Wallenberg Foundation grant 2019.0043 and the Swedish Research Council grant 2018-04619. Figures were prepared with UCSF ChimeraX, developed by the Resource for Biocomputing, Visualization, and Informatics at the University of California, San Francisco, with support from National Institutes of Health R01-GM129325 and the Office of Cyber Infrastructure and Computational Biology, National Institute of Allergy and Infectious Diseases.[293]

## REFERENCES


(1) Mitchell, P. Coupling of phosphorylation to electron and hydrogen transfer by a chemiosmotic type of mechanism. *Nature* **1961**, *191*, 144−148.

(2) Schoepp-Cothenet, B.; Van Lis, R.; Atteia, A.; Baymann, F.; Capowiez, L.; Ducluzeau, A. L.; Duval, S.; Ten Brink, F.; Russell, M. J.; Nitschke, W. On the universal core of bioenergetics. *Biochim. Biophys. Acta, Bioenerg.* **2013**, *1827*, 79−93.

(3) Calisto, F.; Sousa, F. M.; Sena, F. V.; Refojo, P. N.; Pereira, M. M. Mechanisms of energy transduction by charge translocating membrane proteins. *Chem. Rev.* **2021**, *121*, 1804−1844.

(4) Zelle, E.; Pfelzer, N.; Oldiges, M.; Koch-Koerfges, A.; Bott, M.; Nöh, K.; Wiechert, W. An energetic profile of *Corynebacterium glutamicum* underpinned by measured biomass yield on ATP. *Metab. Eng.* **2021**, *65*, 66−78.

(5) Davies, K. M.; Anselmi, C.; Wittig, I.; Faraldo-Gómez, J. D.; Kühlbrandt, W. Structure of the yeast $F_1F_o$-ATP synthase dimer and its role in shaping the mitochondrial cristae. *Proc. Natl. Acad. Sci. U. S. A.* **2012**, *109*, 13602−13607.

(6) Walker, J. E. The ATP synthase: The understood, the uncertain and the unknown. *Biochem. Soc. Trans.* **2013**, *41*, 1−16.

(7) Refojo, P. N.; Sena, F. V.; Calisto, F.; Sousa, F. M.; Pereira, M. M. The plethora of membrane respiratory chains in the phyla of life. *Adv. Microb. Physiol.* **2019**, *74*, 331−414.

(8) Marreiros, B. C.; Calisto, F.; Castro, P. J.; Duarte, A. M.; Sena, F. V.; Silva, A. F.; Sousa, F. M.; Teixeira, M.; Refojo, P. N.; Pereira, M. M. Exploring membrane respiratory chains. *Biochim. Biophys. Acta, Bioenerg.* **2016**, *1857*, 1039−1067.

(9) Simon, J.; van Spanning, R. J. M.; Richardson, D. J. The organisation of proton motive and non-proton motive redox loops in prokaryotic respiratory systems. *Biochim. Biophys. Acta, Bioenerg.* **2008**, *1777*, 1480−1490.

(10) Joseph-Horne, T.; Hollomon, D. W.; Wood, P. M. Fungal respiration: a fusion of standard and alternative components. *Biochim. Biophys. Acta, Bioenerg.* **2001**, *1504*, 179−195.

(11) Luttik, M. A. H.; Overkamp, K. M.; Kötter, P.; De Vries, S.; Van Dijken, J. P.; Pronk, J. T. The *Saccharomyces cerevisiae* NDE1 and NDE2 genes encode separate mitochondrial NADH dehydrogenases catalyzing the oxidation of cytosolic NADH. *J. Biol. Chem.* **1998**, *273*, 24529−24534.

(12) Matus-Ortega, M. G.; Cárdenas-Monroy, C. A.; Flores-Herrera, O.; Mendoza-Hernández, G.; Miranda, M.; González-Pedrajo, B.; Vázquez-Meza, H.; Pardo, J. P. New complexes containing the internal alternative NADH dehydrogenase (Ndi1) in mitochondria of *Saccharomyces cerevisiae*. *Yeast* **2015**, *32*, 629−641.

(13) Hards, K.; Cook, G. M. Targeting bacterial energetics to produce new antimicrobials. *Drug Resist. Updates* **2018**, *36*, 1−12.
(14) Cook, G. M.; Hards, K.; Vilchèze, C.; Hartman, T.; Berney, M. Energetics of respiration and oxidative phosphorylation in mycobacteria. *Microbiol. Spectrum* **2014**, *2*, 1−23.
(15) Eggeling, L.; Bott, M. *Handbook of Corynebacterium glutamicum*; CRC Press, 2005.
(16) Hackenbrock, C. R.; Chazotte, B.; Gupte, S. S. The random collision model and a critical assessment of diffusion and collision in mitochondrial electron transport. *J. Bioenerg. Biomembr.* **1986**, *18*, 331−368.
(17) Schägger, H.; Pfeiffer, K. Supercomplexes in the respiratory chains of yeast and mammalian mitochondria. *EMBO J.* **2000**, *19*, 1777−1783.
(18) Schägger, H. Respiratory chain supercomplexes. *IUBMB Life* **2001**, *52*, 119−128.
(19) Eubel, H.; Jänsch, L.; Braun, H.-P. New insights into the respiratory chain of plant mitochondria. supercomplexes and a unique composition of complex II. *Plant Physiol.* **2003**, *133*, 274−286.
(20) Enriquez, J. A. Supramolecular organization of respiratory complexes. *Annu. Rev. Physiol.* **2016**, *78*, 533−561.
(21) Acín-Pérez, R.; Fernández-Silva, P.; Peleato, M. L.; Pérez-Martos, A.; Enriquez, J. A. Respiratory active mitochondrial supercomplexes. *Mol. Cell* **2008**, *32*, 529−539.
(22) Schäfer, E.; Seelert, H.; Reifschneider, N. H.; Krause, F.; Dencher, N. A.; Vonck, J. Architecture of active mammalian respiratory chain supercomplexes. *J. Biol. Chem.* **2006**, *281*, 15370−15375.
(23) Boekema, E. J.; Braun, H. P. Supramolecular structure of the mitochondrial oxidative phosphorylation system. *J. Biol. Chem.* **2007**, *282*, 1−4.
(24) Sousa, J. S.; Vonck, J. Respiratory supercomplexes $III_2IV_2$ come into focus. *Nat. Struct. Mol. Biol.* **2019**, *26*, 87−89.
(25) Vonck, J.; Schäfer, E. Supramolecular organization of protein complexes in the mitochondrial inner membrane. *Biochim. Biophys. Acta, Mol. Cell Res.* **2009**, *1793*, 117−124.
(26) Vartak, R.; Porras, C. A.-M. e.; Bai, Y. Respiratory supercomplexes: structure, function and assembly. *Protein Cell* **2013**, *4*, 582−590.
(27) Mourier, A.; Matic, S.; Ruzzenente, B.; Larsson, N. G.; Milenkovic, D. The respiratory chain supercomplex organization is independent of COX7A2L isoforms. *Cell Metab.* **2014**, *20*, 1069−1075.
(28) Pérez-Pérez, R.; Lobo-Jarne, T.; Milenkovic, D.; Mourier, A.; Bratic, A.; García-Bartolomé, A.; Fernández-Vizarra, E.; Cadenas, S.; Delmiro, A.; García-Consuegra, I.; et al. COX7A2L is a mitochondrial complex III binding protein that stabilizes the $III_2$+IV supercomplex without affecting respirasome formation. *Cell Rep.* **2016**, *16*, 2387−2398.
(29) Davies, K. M.; Blum, T. B.; Kühlbrandt, W. Conserved in situ arrangement of complex i and $III_2$ in mitochondrial respiratory chain supercomplexes of mammals, yeast, and plants. *Proc. Natl. Acad. Sci. U. S. A.* **2018**, *115*, 3024−3029.
(30) Letts, J. A.; Sazanov, L. A. Clarifying the supercomplex: the higher-order organization of the mitochondrial electron transport chain. *Nat. Struct. Mol. Biol.* **2017**, *24*, 800−808.
(31) Caruana, N. J.; Stroud, D. A. The road to the structure of the mitochondrial respiratory chain supercomplex. *Biochem. Soc. Trans.* **2020**, *48*, 621−629.
(32) Maldonado, M.; Guo, F.; Letts, J. A. Atomic structures of respiratory complex $III_2$, complex IV, and supercomplex $III_2$-IV from vascular plants. *eLife* **2021**, *10*, No. e62047.
(33) Hartley, A. M.; Meunier, B.; Pinotsis, N.; Maréchal, A. Rcf2 revealed in cryo-EM structures of hypoxic isoforms of mature mitochondrial III-IV supercomplexes. *Proc. Natl. Acad. Sci. U. S. A.* **2020**, *117*, 9329−9337.
(34) Hartley, A. M.; Lukoyanova, N.; Zhang, Y.; Cabrera-Orefice, A.; Arnold, S.; Meunier, B.; Pinotsis, N.; Maréchal, A. Structure of yeast cytochrome *c* oxidase in a supercomplex with cytochrome $bc_1$. *Nat. Struct. Mol. Biol.* **2019**, *26*, 78−83.
(35) Rathore, S.; Berndtsson, J.; Marin-Buera, L.; Conrad, J.; Carroni, M.; Brzezinski, P.; Ott, M. Cryo-EM structure of the yeast respiratory supercomplex. *Nat. Struct. Mol. Biol.* **2019**, *26*, 50−57.
(36) Berndtsson, J.; Aufschnaiter, A.; Rathore, S.; Marin-Buera, L.; Dawitz, H.; Diessl, J.; Kohler, V.; Barrientos, A.; Büttner, S.; Fontanesi, F.; Ott, M. Respiratory supercomplexes enhance electron transport by decreasing cytochrome *c* diffusion distance. *EMBO Rep.* **2020**, *21*, No. e51015.
(37) Moe, A.; Di Trani, J.; Rubinstein, J. L.; Brzezinski, P. Cryo-EM structure and kinetics reveal electron transfer by 2D diffusion of cytochrome *c* in the yeast III-IV respiratory supercomplex. *Proc. Natl. Acad. Sci. U. S. A.* **2021**, *118*, No. e2021157118.
(38) Letts, J. A.; Fiedorczuk, K.; Sazanov, L. A. The architecture of respiratory supercomplexes. *Nature* **2016**, *537*, 644−648.
(39) Gu, J.; Wu, M.; Guo, R.; Yan, K.; Lei, J.; Gao, N.; Yang, M. The architecture of the mammalian respirasome. *Nature* **2016**, *537*, 639−643.
(40) Wu, M.; Gu, J.; Guo, R.; Huang, Y.; Yang, M. Structure of Mammalian Respiratory Supercomplex $I_1III_2IV_1$. *Cell* **2016**, *167*, 1598−1609 e10.
(41) Sousa, J. S.; Mills, D. J.; Vonck, J.; Kühlbrandt, W. Functional asymmetry and electron flow in the bovine respirasome. *eLife* **2016**, *5*, No. e21290.
(42) Guo, R.; Zong, S.; Wu, M.; Gu, J.; Yang, M. Architecture of human mitochondrial respiratory megacomplex $I_2III_2IV_2$. *Cell* **2017**, *170*, 1247−1257 e12.
(43) Gong, H.; Li, J.; Xu, A.; Tang, Y.; Ji, W.; Gao, R.; Wang, S.; Yu, L.; Tian, C.; Li, J.; et al. An electron transfer path connects subunits of a mycobacterial respiratory supercomplex. *Science* **2018**, *362*, eaat8923.
(44) Wiseman, B.; Nitharwal, R. G.; Fedotovskaya, O.; Schäfer, J.; Guo, H.; Kuang, Q.; Benlekbir, S.; Sjöstrand, D.; Ädelroth, P.; Rubinstein, J. L.; et al. Structure of a functional obligate complex $III_2IV_2$ respiratory supercomplex from *Mycobacterium smegmatis*. *Nat. Struct. Mol. Biol.* **2018**, *25*, 1128−1136.
(45) Moe, A.; Kovalova, T.; Król, S.; Yanofsky, D.; Bott, M.; Sjöstrand, D.; Rubinstein, J. L.; Högbom, M.; Brzezinski, P. The respiratory supercomplex from *C. glutamicum*. *bioRxiv* **2021**, 2021.05.18.444650.
(46) Steimle, S.; van Eeuwen, T.; Ozturk, Y.; Kim, H. J.; Braitbard, M.; Selamoglu, N.; Garcia, B. A.; Schneidman-Duhovny, D.; Murakami, K.; Daldal, F. Cryo-EM structures of engineered active $bc_1$-$cbb_3$ type $CIII_2CIV$ super-complexes and electronic communication between the complexes. *Nat. Commun.* **2021**, *12*, 929.
(47) Sun, C.; Benlekbir, S.; Venkatakrishnan, P.; Wang, Y.; Hong, S.; Hosler, J.; Tajkhorshid, E.; Rubinstein, J. L.; Gennis, R. B. Structure of the alternative complex III in a supercomplex with cytochrome oxidase. *Nature* **2018**, *557*, 123−126.
(48) Sousa, J. S.; Calisto, F.; Langer, J. D.; Mills, D. J.; Refojo, P. N.; Teixeira, M.; Kühlbrandt, W.; Vonck, J.; Pereira, M. M. Structural basis for energy transduction by respiratory alternative complex III. *Nat. Commun.* **2018**, *9*, 1728.
(49) Kühlbrandt, W. Structure and function of mitochondrial membrane protein complexes. *BMC Biol.* **2015**, *13*, 89.
(50) Stuchebrukhov, A.; Schäfer, J.; Berg, J.; Brzezinski, P. Kinetic advantage of forming respiratory supercomplexes. *Biochim. Biophys. Acta, Bioenerg.* **2020**, *1861*, 148193.
(51) Gupte, S. S.; Hackenbrock, C. R. Multidimensional diffusion modes and collision frequencies of cytochrome *c* with its redox partners. *J. Biol. Chem.* **1988**, *263*, 5241−5247.
(52) Ikon, N.; Ryan, R. O. Cardiolipin and mitochondrial cristae organization. *Biochim. Biophys. Acta, Biomembr.* **2017**, *1859*, 1156−1163.
(53) Milenkovic, D.; Blaza, J. N.; Larsson, N. G.; Hirst, J. The enigma of the respiratory chain supercomplex. *Cell Metab.* **2017**, *25*, 765−776.
(54) Lobo-Jarne, T.; Ugalde, C. Respiratory chain supercomplexes: structures, function and biogenesis. *Semin. Cell Dev. Biol.* **2018**, *76*, 179−190.
(55) Barrientos, A.; Ugalde, C. I Function, therefore I am: overcoming skepticism about mitochondrial supercomplexes. *Cell Metab.* **2013**, *18*, 147−149.


https://doi.org/10.1021/acs.chemrev.1c00140
*Chem. Rev.* 2021, 121, 9644−9673

(56) Melo, A. M. P.; Teixeira, M. Supramolecular organization of bacterial aerobic respiratory chains: from cells and back. *Biochim. Biophys. Acta, Bioenerg.* **2016**, *1857*, 190−197.
(57) Berry, E. A.; Trumpower, B. L. Isolation of ubiquinol oxidase from *Paracoccus denitrificans* and resolution into cytochrome $bc_1$ and cytochrome $c$-$aa_3$ complexes. *J. Biol. Chem.* **1985**, *260*, 2458−2467.
(58) Stroh, A.; Anderka, O.; Pfeiffer, K.; Yagi, T.; Finel, M.; Ludwig, B.; Schägger, H. Assembly of respiratory complexes I, III, and IV into NADH oxidase supercomplexs stabilizes complex I in *Paracoccus denitrificans*. *J. Biol. Chem.* **2004**, *279*, 5000−5007.
(59) Fedotovskaya, O.; Albertsson, I.; Nordlund, G.; Hong, S.; Gennis, R. B.; Brzezinski, P.; Ädelroth, P. Identification of a cytochrome $bc_1$-$aa_3$ supercomplex in *Rhodobacter sphaeroides*. *Biochim. Biophys. Acta, Bioenerg.* **2021**, *1862*, 148433.
(60) Llorente-Garcia, I.; Lenn, T.; Erhardt, H.; Harriman, O. L.; Liu, L. N.; Robson, A.; Chiu, S. W.; Matthews, S.; Willis, N. J.; Bray, C. D.; et al. Single-molecule in vivo imaging of bacterial respiratory complexes indicates delocalized oxidative phosphorylation. *Biochim. Biophys. Acta, Bioenerg.* **2014**, *1837*, 811−824.
(61) Erhardt, H.; Dempwolff, F.; Pfreundschuh, M.; Riehle, M.; Schäfer, C.; Pohl, T.; Graumann, P.; Friedrich, T. Organization of the *Escherichia coli* aerobic enzyme complexes of oxidative phosphorylation in dynamic domains within the cytoplasmic membrane. *MicrobiologyOpen* **2014**, *3*, 316−326.
(62) Kao, W. C.; Kleinschroth, T.; Nitschke, W.; Baymann, F.; Neehaul, Y.; Hellwig, P.; Richers, S.; Vonck, J.; Bott, M.; Hunte, C. The obligate respiratory supercomplex from Actinobacteria. *Biochim. Biophys. Acta, Bioenerg.* **2016**, *1857*, 1705−1714.
(63) Sone, N.; Nagata, K.; Kojima, H.; Tajima, J.; Kodera, Y.; Kanamaru, T.; Noguchi, S.; Sakamoto, J. A novel hydrophobic diheme $c$-type cytochrome. Purification from *Corynebacterium glutamicum* and analysis of the QcrCBA operon encoding three subunit proteins of a putative cytochrome reductase complex. *Biochim. Biophys. Acta, Bioenerg.* **2001**, *1503*, 279−290.
(64) Niebisch, A.; Bott, M. Purification of a cytochrome $bc_1$-$aa_3$ supercomplex with quinol oxidase activity from *Corynebacterium glutamicum*: Identification of a fourth subunit of cytochrome $aa_3$ oxidase and mutational analysis of diheme cytochrome $c_1$. *J. Biol. Chem.* **2003**, *278*, 4339−4346.
(65) Graf, S.; Fedotovskaya, O.; Kao, W. C.; Hunte, C.; Ädelroth, P.; Bott, M.; Von Ballmoos, C.; Brzezinski, P. Rapid electron transfer within the III-IV supercomplex in *Corynebacterium glutamicum*. *Sci. Rep.* **2016**, *6*, 34098.
(66) Bott, M.; Niebisch, A. The respiratory chain of *Corynebacterium glutamicum*. *J. Biotechnol.* **2003**, *104*, 129−153.
(67) Niebisch, A.; Bott, M. Molecular analysis of the cytochrome $bc_1$-$aa_3$ branch of the *Corynebacterium glutamicum* respiratory chain containing an unusual diheme cytochrome $c_1$. *Arch. Microbiol.* **2001**, *175*, 282−294.
(68) Sone, N.; Sekimachi, M.; Kutoh, E. Identification and properties of a quinol oxidase super-complex composed of a $bc_1$ complex and cytochrome oxidase in the thermophilic bacterium PS3. *J. Biol. Chem.* **1987**, *262*, 15386−15391.
(69) Cruciat, C. M.; Brunner, S.; Baumann, F.; Neupert, W.; Stuart, R. A. The cytochrome $bc_1$ and cytochrome $c$ oxidase complexes associate to form a single supracomplex in yeast mitochondria. *J. Biol. Chem.* **2000**, *275*, 18093−18098.
(70) Stuart, R. A. Supercomplex organization of the oxidative phosphorylation enzymes in yeast mitochondria. *J. Bioenerg. Biomembr.* **2008**, *40*, 411−417.
(71) Chaban, Y.; Boekema, E. J.; Dudkina, N. V. Structures of mitochondrial oxidative phosphorylation supercomplexes and mechanisms for their stabilisation. *Biochim. Biophys. Acta, Bioenerg.* **2014**, *1837*, 418−426.
(72) Heinemeyer, J.; Braun, H. P.; Boekema, E. J.; Kouřil, R. A structural model of the cytochrome $c$ reductase/oxidase supercomplex from yeast mitochondria. *J. Biol. Chem.* **2007**, *282*, 12240−12248.
(73) Winge, D. R. Sealing the mitochondrial respirasome. *Mol. Cell. Biol.* **2012**, *32*, 2647−2652.
(74) Mileykovskaya, E.; Penczek, P. A.; Fang, J.; Mallampalli, V. K. P. S.; Sparagna, G. C.; Dowhan, W. Arrangement of the respiratory chain complexes in *Saccharomyces cerevisiae* supercomplex $III_2IV_2$ revealed by single particle cryo-electron microscopy. *J. Biol. Chem.* **2012**, *287*, 23095−23103.
(75) Genova, M. L.; Lenaz, G. Functional role of mitochondrial respiratory supercomplexes. *Biochim. Biophys. Acta, Bioenerg.* **2014**, *1837*, 427−443.
(76) Acin-Perez, R.; Enriquez, J. A. The function of the respiratory supercomplexes: the plasticity model. *Biochim. Biophys. Acta, Bioenerg.* **2014**, *1837*, 444−450.
(77) Boumans, H.; Grivell, L. A.; Berden, J. A. The respiratory chain in yeast behaves as a single functional unit. *J. Biol. Chem.* **1998**, *273*, 4872−4877.
(78) Sarewicz, M.; Pintscher, S.; Pietras, R.; Borek, A.; Bujnowicz, Ł.; Hanke, G.; Cramer, W. A.; Finazzi, G.; Osyczka, A. Catalytic reactions and energy conservation in the cytochrome $bc_1$ and $b_6f$ complexes of energy-transducing membranes. *Chem. Rev.* **2021**, *121*, 2020−2108.
(79) Crofts, A. R. The cytochrome $bc_1$ complex: function in the context of structure. *Annu. Rev. Physiol.* **2004**, *66*, 689−733.
(80) Crofts, A. R.; Lhee, S.; Crofts, S. B.; Cheng, J.; Rose, S. Proton pumping in the $bc_1$ complex: a new gating mechanism that prevents short circuits. *Biochim. Biophys. Acta, Bioenerg.* **2006**, *1757*, 1019−1034.
(81) Sarewicz, M.; Osyczka, A. Electronic connection between the quinone and cytochrome $c$ redox pools and its role in regulation of mitochondrial electron transport and redox signaling. *Physiol. Rev.* **2015**, *95*, 219−243.
(82) Mulkidjanian, A. Y. Ubiquinol oxidation in the cytochrome $bc_1$ complex: reaction mechanism and prevention of short-circuiting. *Biochim. Biophys. Acta, Bioenerg.* **2005**, *1709*, 5−34.
(83) Mulkidjanian, A. Y. Activated Q-cycle as a common mechanism for cytochrome $bc_1$ and cytochrome $b_6f$ complexes. *Biochim. Biophys. Acta, Bioenerg.* **2010**, *1797*, 1858−1868.
(84) Berry, E. A.; De Bari, H.; Huang, L. S. Unanswered questions about the structure of cytochrome $bc_1$ complexes. *Biochim. Biophys. Acta, Bioenerg.* **2013**, *1827*, 1258−1277.
(85) Cramer, W. A.; Hasan, S. S.; Yamashita, E. The Q cycle of cytochrome $bc$ complexes: a structure perspective. *Biochim. Biophys. Acta, Bioenerg.* **2011**, *1807*, 788−802.
(86) Mitchell, P. Possible molecular mechanisms of the protonmotive function of cytochrome systems. *J. Theor. Biol.* **1976**, *62*, 327−367.
(87) Kao, W. C.; Hunte, C. The molecular evolution of the $Q_o$ Motif. *Genome Biol. Evol.* **2014**, *6*, 1894−1910.
(88) Letts, J. A.; Fiedorczuk, K.; Degliesposti, G.; Skehel, M.; Sazanov, L. A. Structures of rspiratory supercomplex I+$III_2$ reveal functional and conformational crosstalk. *Mol. Cell* **2019**, *75*, 1131−1146 e6.
(89) Di Trani, J. M.; Liu, Z.; Whitesell, L.; Brzezinski, P.; Cowen, L. E.; Rubinstein, J. L. Rieske head domain dynamics and indazole-derivative inhibition of *Candida albicans* complex III. *bioRxiv* **2021** 2021.05.18.444650. DOI: 10.1101/2021.05.18.444650
(90) Pietras, R.; Sarewicz, M.; Osyczka, A. Distinct properties of semiquinone species detected at the ubiquinol oxidation $Q_o$ site of cytochrome $bc_1$ and their mechanistic implications. *J. R. Soc., Interface* **2016**, *13*, 20160133.
(91) Husen, P.; Solov'Yov, I. A. Spontaneous binding of molecular oxygen at the $Q_o$-site of the $bc_1$ complex could stimulate superoxide formation. *J. Am. Chem. Soc.* **2016**, *138*, 12150−12158.
(92) Muller, F.; Crofts, A. R.; Kramer, D. M. Multiple Q-cycle bypass reactions at the $Q_o$ site of the cytochrome $bc_1$ complex. *Biochemistry* **2002**, *41*, 7866−7874.
(93) Slater, E. C. The mechanism of action of the respiratory inhibitor, antimycin. *Biochim. Biophys. Acta, Rev. Bioenerg.* **1973**, *301*, 129−154.
(94) Darrouzet, E.; Moser, C. C.; Dutton, P. L.; Daldal, F. Large scale domain movement in cytochrome $bc_1$: a new device for electron transfer in proteins. *Trends Biochem. Sci.* **2001**, *26*, 445−451.
(95) Zhang, Z.; Huang, L.; Shulmeister, V. M.; Chi, Y. I.; Kim, K. K.; Hung, L. W.; Crofts, A. R.; Berry, E. A.; Kim, S. H. Electron transfer by domain movement in cytochrome $bc_1$. *Nature* **1998**, *392*, 677−684.

(96) Esser, L.; Gong, X.; Yang, S.; Yu, L.; Yu, C.-A.; Xia, D. Surface-modulated motion switch: capture and release of iron-sulfur protein in the cytochrome $bc_1$ complex. *Proc. Natl. Acad. Sci. U. S. A.* **2006**, *103*, 13045.
(97) Berry, E. A.; Huang, L. S. Observations concerning the quinol oxidation site of the cytochrome $bc_1$ complex. *FEBS Lett.* **2003**, *555*, 13−20.
(98) Kim, H.; Xia, D.; Yu, C. A.; Xia, J. Z.; Kachurin, A. M.; Zhang, L.; Yu, L.; Deisenhofer, J. Inhibitor binding changes domain mobility in the iron-sulfur protein of the mitochondrial $bc_1$ complex from bovine heart. *Proc. Natl. Acad. Sci. U. S. A.* **1998**, *95*, 8026−8033.
(99) Esser, L.; Quinn, B.; Li, Y.-F.; Zhang, M.; Elberry, M.; Yu, L.; Yu, C.-A.; Xia, D. Crystallographic studies of quinol oxidation site inhibitors: a modified classification of inhibitors for the cytochrome $bc_1$ complex. *J. Mol. Biol.* **2004**, *341*, 281−302.
(100) Esser, L.; Zhou, F.; Yu, C. A.; Xia, D. Crystal structure of bacterial cytochrome $bc_1$ in complex with azoxystrobin reveals a conformational switch of the Rieske iron-sulfur protein subunit. *J. Biol. Chem.* **2019**, *294*, 12007−12019.
(101) Xia, D.; Esser, L.; Tang, W. K.; Zhou, F.; Zhou, Y.; Yu, L.; Yu, C. A. Structural analysis of cytochrome $bc_1$ complexes: implications to the mechanism of function. *Biochim. Biophys. Acta, Bioenerg.* **2013**, *1827*, 1278−1294.
(102) Schoepp, B.; Brugna, M.; Riedel, A.; Nitschke, W.; Kramer, D. M. The $Q_o$-site inhibitor DBMIB favours the proximal position of the chloroplast Rieske protein and induces a p*K*-shift of the redox-linked proton. *FEBS Lett.* **1999**, *450*, 245−250.
(103) Osyczka, A.; Moser, C. C.; Dutton, P. L. Fixing the Q cycle. *Trends Biochem. Sci.* **2005**, *30*, 176−182.
(104) Iwata, S.; Lee, J. W.; Okada, K.; Lee, J. K.; Iwata, M.; Rasmussen, B.; Link, T. A.; Ramaswamy, S.; Jap, B. K. Complete structure of the 11-Subunit bovine mitochondrial cytochrome $bc_1$ complex. *Science* **1998**, *281*, 64−71.
(105) Crofts, A. R.; Wang, Z. How rapid are the internal reactions of the ubiquinol:cytochrome $c_2$ oxidoreductase? *Photosynth. Res.* **1989**, *22*, 69−87.
(106) Link, T. A.; Iwata, S. Functional implications of the structure of the 'Rieske' iron-sulfur protein of bovine heart mitochondrial cytochrome $bc_1$ complex. *Biochim. Biophys. Acta, Bioenerg.* **1996**, *1275*, 54−60.
(107) Jünemann, S.; Heathcote, P.; Rich, P. R. On the mechanism of quinol oxidation in the $bc_1$ complex. *J. Biol. Chem.* **1998**, *273*, 21603−21607.
(108) Millett, F.; Havens, J.; Rajagukguk, S.; Durham, B. Design and use of photoactive ruthenium complexes to study electron transfer within cytochrome $bc_1$ and from cytochrome $bc_1$ to cytochrome *c*. *Biochim. Biophys. Acta, Bioenerg.* **2013**, *1827*, 1309−1319.
(109) Link, T. A. The role of the 'Rieske' iron sulfur protein in the hydroquinone oxidation ($Q_p$) site of the cytochrome $bc_1$ complex. *FEBS Lett.* **1997**, *412*, 257−264.
(110) Rich, P. R. The quinone chemistry of *bc* complexes. *Biochim. Biophys. Acta, Bioenerg.* **2004**, *1658*, 165−171.
(111) Hunte, C.; Palsdottir, H.; Trumpower, B. L. Protonmotive pathways and mechanisms in the cytochrome $bc_1$ complex. *FEBS Lett.* **2003**, *545*, 39−46.
(112) Iwaki, M.; Yakovlev, G.; Hirst, J.; Osyczka, A.; Dutton, P. L.; Marshall, D.; Rich, P. R. Direct observation of redox-linked histidine protonation changes in the iron-sulfur protein of the cytochrome $bc_1$ complex by ATR-FTIR spectroscopy. *Biochemistry* **2005**, *44*, 4230−4237.
(113) Brandt, U.; Okun, J. G. Role of deprotonation events in ubihydroquinone:cytochrome *c* oxidoreductase from bovine heart and yeast mitochondria. *Biochemistry* **1997**, *36*, 11234−11240.
(114) Crofts, A. R.; Hong, S. J.; Ugulava, N.; Barquera, B.; Gennis, R.; Guergova-Kuras, M.; Berry, E. A. Pathways for proton release during ubihydroquinone oxidation by the bc(1) complex. *Proc. Natl. Acad. Sci. U. S. A.* **1999**, *96*, 10021−10026.
(115) Brasseur, G.; Saribaş, A. S.; Daldal, F. A compilation of mutations located in the cytochrome *b* subunit of the bacterial and mitochondrial $bc_1$ complex. *Biochim. Biophys. Acta, Bioenerg.* **1996**, *1275*, 61−69.
(116) Seddiki, N.; Meunier, B.; Lemesle-Meunier, D.; Brasseur, G. Is cytochrome *b* glutamic acid 272 a quinol binding residue in the $bc_1$ complex of *Saccharomyces cerevisiae*? *Biochemistry* **2008**, *47*, 2357−2368.
(117) The core subunits of cytochrome *c* oxidase are referred to as "subunit I-III". Other subunits are named according to conventions for the different organisms.
(118) Borisov, V. B.; Gennis, R. B.; Hemp, J.; Verkhovsky, M. I. The cytochrome *bd* respiratory oxygen reductases. *Biochim. Biophys. Acta, Bioenerg.* **2011**, *1807*, 1398−1413.
(119) Safarian, S.; Rajendran, C.; Müller, H.; Preu, J.; Langer, J. D.; Ovchinnikov, S.; Hirose, T.; Kusumoto, T.; Sakamoto, J.; Michel, H. Structure of a *bd* oxidase indicates similar mechanisms for membraneintegrated oxygen reductases. *Science* **2016**, *352*, 583−586.
(120) May, B.; Young, L.; Moore, A. L. Structural insights into the alternative oxidases: are all oxidases made equal? *Biochem. Soc. Trans.* **2017**, *45*, 731−740.
(121) Yoshikawa, S.; Shimada, A. Reaction mechanism of cytochrome *c* oxidase. *Chem. Rev.* **2015**, *115*, 1936−1989.
(122) Hosler, J. P.; Ferguson-Miller, S.; Mills, D. A. Energy transduction: Proton transfer through the respiratory complexes. *Annu. Rev. Biochem.* **2006**, *75*, 165−187.
(123) Namslauer, A.; Brzezinski, P. Structural elements involved in electron-coupled proton transfer in cytochrome *c* oxidase. *FEBS Lett.* **2004**, *567*, 103−110.
(124) Brzezinski, P.; Ädelroth, P. Design principles of proton-pumping haem-copper oxidases. *Curr. Opin. Struct. Biol.* **2006**, *16*, 465−472.
(125) Richter, O. M. H.; Ludwig, B. Electron transfer and energy transduction in the terminal part of the respiratory chain-lessons from bacterial model systems. *Biochim. Biophys. Acta, Bioenerg.* **2009**, *1787*, 626−634.
(126) Ferguson-Miller, S.; Hiser, C.; Liu, J. Gating and regulation of the cytochrome *c* oxidase proton pump. *Biochim. Biophys. Acta, Bioenerg.* **2012**, *1817*, 489−494.
(127) Rich, P. R.; Maréchal, A. Functions of the hydrophilic channels in protonmotive cytochrome *c* oxidase. *J. R. Soc., Interface* **2013**, *10*, 20130183.
(128) Kaila, V. R. I.; Verkhovsky, M. I.; Wikström, M. Proton-coupled electron transfer in cytochrome oxidase. *Chem. Rev.* **2010**, *110*, 7062−7081.
(129) Wikström, M.; Krab, K.; Sharma, V. Oxygen activation and energy conservation by cytochrome *c* oxidase. *Chem. Rev.* **2018**, *118*, 2469−2490.
(130) Wikström, M.; Sharma, V.; Kaila, V. R. I.; Hosler, J. P.; Hummer, G. New perspectives on proton pumping in cellular respiration. *Chem. Rev.* **2015**, *115*, 2196−2221.
(131) Varanasi, L.; Hosler, J. P. Subunit III-depleted cytochrome *c* oxidase provides insight into the process of proton uptake by proteins. *Biochim. Biophys. Acta, Bioenerg.* **2012**, *1817*, 545−551.
(132) Lee, H. J.; Reimann, J.; Huang, Y.; Ädelroth, P. Functional proton transfer pathways in the heme-copper oxidase superfamily. *Biochim. Biophys. Acta, Bioenerg.* **2012**, *1817*, 537−544.
(133) Pereira, M. M.; Santana, M.; Teixeira, M. A novel scenario for the evolution of haem-copper oxygen reductases. *Biochim. Biophys. Acta, Bioenerg.* **2001**, *1505*, 185−208.
(134) Hemp, J.; Gennis, R. B. Diversity of the heme-copper superfamily in archaea: insights from genomics and structural modeling. *Results Probl. Cell Differ.* **2008**, *45*, 1−31.
(135) Hofacker, I.; Schulten, K. Oxygen and proton pathways in cytochrome *c* oxidase. *Proteins: Struct., Funct., Genet.* **1998**, *30*, 100−107.
(136) Qin, L.; Sharpe, M. A.; Garavito, R. M.; Ferguson-Miller, S. Conserved lipid-binding sites in membrane proteins: a focus on cytochrome *c* oxidase. *Curr. Opin. Struct. Biol.* **2007**, *17*, 444−450.
(137) Fetter, J. R.; Qian, J.; Shapleigh, J.; Thomas, J. W.; García-Horsman, A.; Schmidt, E.; Hosler, J.; Babcock, G. T.; Gennis, R. B.;


https://doi.org/10.1021/acs.chemrev.1c00140
*Chem. Rev.* 2021, 121, 9644−9673

Ferguson-Miller, S. Possible proton relay pathways in cytochrome *c* oxidase. *Proc. Natl. Acad. Sci. U. S. A.* **1995**, *92*, 1604−1608.
(138) Iwata, S.; Ostermeier, C.; Ludwig, B.; Michel, H. Structure at 2.8 Å resolution of cytochrome *c* oxidase from *Paracoccus denitrificans*. *Nature* **1995**, *376*, 660−669.
(139) Tsukihara, T.; Aoyama, H.; Yamashita, E.; Tomizaki, T.; Yamaguchi, H.; Shinzawa-Itoh, K.; Nakashima, R.; Yaono, R.; Yoshikawa, S. The whole structure of the 13-subunit oxidized cytochrome *c* oxidase at 2.8 Å. *Science* **1996**, *272*, 1136−1144.
(140) Svensson-Ek, M.; Abramson, J.; Larsson, G.; Tornroth, S.; Brzezinski, P.; Iwata, S. The X-ray crystal structures of wild-type and EQ(I-286) mutant cytochrome *c* oxidases from *Rhodobacter sphaeroides*. *J. Mol. Biol.* **2002**, *321*, 329−339.
(141) Qin, L.; Hiser, C.; Mulichak, A.; Garavito, R. M.; Ferguson-Miller, S. Identification of conserved lipid/detergent-binding sites in a high-resolution structure of the membrane protein cytochrome *c* oxidase. *Proc. Natl. Acad. Sci. U. S. A.* **2006**, *103*, 16117−16122.
(142) Ädelroth, P.; Svensson Ek, M.; Mitchell, D. M.; Gennis, R. B.; Brzezinski, P. Glutamate 286 in cytochrome $aa_3$ from *Rhodobacter sphaeroides* is involved in proton uptake during the reaction of the fully-reduced enzyme with dioxygen. *Biochemistry* **1997**, *36*, 13824−13829.
(143) Ädelroth, P.; Gennis, R. B.; Brzezinski, P. Role of the pathway through K(I-362) in proton transfer in cytochrome *c* oxidase from *R. sphaeroides*. *Biochemistry* **1998**, *37*, 2470−2476.
(144) Konstantinov, A. A.; Siletsky, S.; Mitchell, D.; Kaulen, A.; Gennis, R. B. The roles of the two proton input channels in cytochrome *c* oxidase from Rhodobacter sphaeroides probed by the effects of site-directed mutations on time-resolved electrogenic intraprotein proton transfer. *Proc. Natl. Acad. Sci. U. S. A.* **1997**, *94*, 9085−9090.
(145) Brzezinski, P.; Ädelroth, P. Pathways of proton transfer in cytochrome *c* oxidase. *J. Bioenerg. Biomembr.* **1998**, *30*, 99−107.
(146) Sharma, V.; Wikström, M. The role of the K-channel and the active-site tyrosine in the catalytic mechanism of cytochrome *c* oxidase. *Biochim. Biophys. Acta, Bioenerg.* **2016**, *1857*, 1111−1115.
(147) Hosler, J. P.; Shapleigh, J. P.; Mitchell, D. M.; Kim, Y.; Pressler, M. A.; Georgiou, C.; Babcock, G. T.; Alben, J. O.; Ferguson-Miller, S.; Gennis, R. B. Polar residues in helix VIII of subunit I of cytochrome *c* oxidase influence the activity and the structure of the active site. *Biochemistry* **1996**, *35*, 10776−10783.
(148) Blomberg, M. R. A. Mechanism of oxygen reduction in cytochrome *c* oxidase and the role of the active site tyrosine. *Biochemistry* **2016**, *55*, 489−500.
(149) Poiana, F.; von Ballmoos, C.; Gonska, N.; Blomberg, M. R. A.; Ädelroth, P.; Brzezinski, P. Splitting of the O-O bond at the heme-copper catalytic site of respiratory oxidases. *Science Advances* **2017**, *3*, No. e1700279.
(150) Blomberg, M. R. A.; Siegbahn, P. E. M. Proton pumping in cytochrome *c* oxidase: energetic requirements and the role of two proton channels. *Biochim. Biophys. Acta, Bioenerg.* **2014**, *1837*, 1165−1177.
(151) Maréchal, A.; Xu, J. Y.; Genko, N.; Hartley, A. M.; Haraux, F.; Meunier, B.; Rich, P. R. A common coupling mechanism for A-type heme-copper oxidases from bacteria to mitochondria. *Proc. Natl. Acad. Sci. U. S. A.* **2020**, *117*, 9349−9355.
(152) Björck, M. L.; Vilhjálmsdóttir, J.; Hartley, A. M.; Meunier, B.; Näsvik Öjemyr, L.; Maréchal, A.; Brzezinski, P. Proton-transfer pathways in the mitochondrial *S. cerevisiae* cytochrome *c* oxidase. *Sci. Rep.* **2019**, *9*, 20207.
(153) Namslauer, A.; Pawate, A. S.; Gennis, R. B.; Brzezinski, P. Redox-coupled proton translocation in biological systems: Proton shuttling in cytochrome *c* oxidase. *Proc. Natl. Acad. Sci. U. S. A.* **2003**, *100*, 15543−15547.
(154) Wikström, M.; Verkhovsky, M. I. The D-channel of cytochrome oxidase: an alternative view. *Biochim. Biophys. Acta, Bioenerg.* **2011**, *1807*, 1273−1278.
(155) Mitchell, D. M.; Aasa, R.; Ädelroth, P.; Brzezinski, P.; Gennis, R. B.; Malmström, B. G. EPR studies of wild-type and several mutants of cytochrome *c* oxidase from *Rhodobacter sphaeroides*: Glu286 is not a bridging ligand in the cytochrome $a_3$-$Cu_B$ center. *FEBS Lett.* **1995**, *374*, 371−374.
(156) Smirnova, I. A.; Ädelroth, P.; Gennis, R. B.; Brzezinski, P. Aspartate-132 in cytochrome *c* oxidase from *Rhodobacter sphaeroides* is involved in a two-step proton transfer during oxo-ferryl formation. *Biochemistry* **1999**, *38*, 6826−6833.
(157) Johansson, A. L.; Högbom, M.; Carlsson, J.; Gennis, R. B.; Brzezinski, P. Role of aspartate 132 at the orifice of a proton pathway in cytochrome *c* oxidase. *Proc. Natl. Acad. Sci. U. S. A.* **2013**, *110*, 8912−8917.
(158) Watmough, N. J.; Katsonouri, A.; Little, R. H.; Osborne, J. P.; Furlong-Nickels, E.; Gennis, R. B.; Brittain, T.; Greenwood, C. A conserved glutamic acid in helix VI of cytochrome $bo_3$ influences a key step in oxygen reduction. *Biochemistry* **1997**, *36*, 13736−13742.
(159) Svensson-Ek, M.; Thomas, J. W.; Gennis, R. B.; Nilsson, T.; Brzezinski, P. Kinetics of electron and proton transfer during the reaction of wild type and helix VI mutants of cytochrome $bo_3$ with oxygen. *Biochemistry* **1996**, *35*, 13673−80.
(160) Brändén, G.; Pawate, A. S.; Gennis, R. B.; Brzezinski, P. Controlled uncoupling and recoupling of proton pumping in cytochrome *c* oxidase. *Proc. Natl. Acad. Sci. U. S. A.* **2006**, *103*, 317−22.
(161) Berg, J.; Liu, J.; Svahn, E.; Ferguson-Miller, S.; Brzezinski, P. Structural changes at the surface of cytochrome *c* oxidase alter the proton-pumping stoichiometry. *Biochim. Biophys. Acta, Bioenerg.* **2020**, *1861*, 148116.
(162) Gilderson, G.; Salomonsson, L.; Aagaard, A.; Gray, J.; Brzezinski, P.; Hosler, J. Subunit III of cytochrome *c* oxidase of *Rhodobacter sphaeroides* is required to maintain rapid proton uptake through the D pathway at physiologic pH. *Biochemistry* **2003**, *42*, 7400−7409.
(163) Ädelroth, P.; Hosler, J. Surface proton donors for the D-pathway of cytochrome *c* oxidase in the absence of subunit III. *Biochemistry* **2006**, *45*, 8308−8318.
(164) Brzezinski, P.; Johansson, A. L. Variable proton-pumping stoichiometry in structural variants of cytochrome *c* oxidase. *Biochim. Biophys. Acta, Bioenerg.* **2010**, *1797*, 710−723.
(165) Lee, H. M.; Das, T. K.; Rousseau, D. L.; Mills, D.; Ferguson-Miller, S.; Gennis, R. B. Mutations in the putative H-channel in the cytochrome *c* oxidase from *Rhodobacter sphaeroides* show that this channel is not important for proton conduction but reveal modulation of the properties of heme *a*. *Biochemistry* **2000**, *39*, 2989−2996.
(166) Näsvik Öjemyr, L.; Maréchal, A.; Vestin, H.; Meunier, B.; Rich, P. R.; Brzezinski, P. Reaction of wild-type and Glu243Asp variant yeast cytochrome *c* oxidase with $O_2$. *Biochim. Biophys. Acta, Bioenerg.* **2014**, *1837*, 1012−1018.
(167) Levchenko, M.; Wuttke, J. M.; Römpler, K.; Schmidt, B.; Neifer, K.; Juris, L.; Wissel, M.; Rehling, P.; Deckers, M. Cox26 is a novel stoichiometric subunit of the yeast cytochrome *c* oxidase. *Biochim. Biophys. Acta, Mol. Cell Res.* **2016**, *1863*, 1624−1632.
(168) Strecker, V.; Kadeer, Z.; Heidler, J.; Cruciat, C. M.; Angerer, H.; Giese, H.; Pfeiffer, K.; Stuart, R. A.; Wittig, I. Supercomplex-associated Cox26 protein binds to cytochrome *c* oxidase. *Biochim. Biophys. Acta, Mol. Cell Res.* **2016**, *1863*, 1643−1652.
(169) Arnold, S. The power of life-cytochrome *c* oxidase takes center stage in metabolic control, cell signalling and survival. *Mitochondrion* **2012**, *12*, 46−56.
(170) Vogt, S.; Rhiel, A.; Koch, V.; Kadenbach, B. Regulation of oxidative phosphorylation by inhibition of its enzyme complexes via reversible phosphorylation. *Curr. Enzyme Inhib.* **2007**, *3*, 189−206.
(171) Kadenbach, B.; Huttemann, M.; Arnold, S.; Lee, I.; Bender, E. Mitochondrial energy metabolism is regulated via nuclear-coded subunits of cytochrome *c* oxidase. *Free Radical Biol. Med.* **2000**, *29*, 211−221.
(172) Kadenbach, B.; Hüttemann, M. The subunit composition and function of mammalian cytochrome *c* oxidase. *Mitochondrion* **2015**, *24*, 64−76.
(173) Maréchal, A.; Meunier, B.; Lee, D.; Orengo, C.; Rich, P. R. Yeast cytochrome *c* oxidase: a model system to study mitochondrial forms of


https://doi.org/10.1021/acs.chemrev.1c00140
*Chem. Rev.* 2021, 121, 9644−9673

the haem-copper oxidase superfamily. *Biochim. Biophys. Acta, Bioenerg.* **2012**, *1817*, 620−628.
(174) Burke, P. V.; Raitt, D. C.; Allen, L. A.; Kellogg, E. A.; Poyton, R. O. Effects of oxygen concentration on the expression of cytochrome *c* and cytochrome *c* oxidase genes in yeast. *J. Biol. Chem.* **1997**, *272*, 14705−14712.
(175) Hodge, M. R.; Kim, G.; Singh, K.; Cumsky, M. G. Inverse regulation of the yeast COX5 genes by oxygen and heme. *Mol. Cell. Biol.* **1989**, *9*, 1958−1964.
(176) Allen, L. A.; Zhao, X. J.; Caughey, W.; Poyton, R. O. Isoforms of yeast cytochrome *c* oxidase subunit V affect the binuclear reaction center and alter the kinetics of interaction with the isoforms of yeast cytochrome *c*. *J. Biol. Chem.* **1995**, *270*, 110−118.
(177) Dodia, R.; Meunier, B.; Kay, C. W. M.; Rich, P. R. Comparisons of subunit 5A and 5B isoenzymes of yeast cytochrome *c* oxidase. *Biochem. J.* **2014**, *464*, 335−342.
(178) Hosler, J. P.; Espe, M. P.; Zhen, Y.; Babcock, G. T.; Ferguson-Miller, S. Analysis of site-directed mutants locates a non-redox-active metal near the active site of cytochrome *c* oxidase of *Rhodobacter sphaeroides*. *Biochemistry* **1995**, *34*, 7586−7592.
(179) Ostermeier, C.; Harrenga, A.; Ermler, U.; Michel, H. Structure at 2.7 Å resolution of the *Paracoccus denitrificans* two-subunit cytochrome *c* oxidase complexed with an antibody $F_V$ fragment. *Proc. Natl. Acad. Sci. U. S. A.* **1997**, *94*, 10547−10553.
(180) Pfitzner, U.; Kirichenko, A.; Konstantinov, A. A.; Mertens, M.; Wittershagen, A.; Kolbesen, B. O.; Steffens, G. C.; Harrenga, A.; Michel, H.; Ludwig, B. Mutations in the $Ca^{2+}$ binding site of the *Paracoccus denitrificans* cytochrome *c* oxidase. *FEBS Lett.* **1999**, *456*, 365−369.
(181) Muramoto, K.; Hirata, K.; Shinzawa-Itoh, K.; Yoko-O, S.; Yamashita, E.; Aoyama, H.; Tsukihara, T.; Yoshikawa, S. A histidine residue acting as a controlling site for dioxygen reduction and proton pumping by cytochrome *c* oxidase. *Proc. Natl. Acad. Sci. U. S. A.* **2007**, *104*, 7881−7886.
(182) Kannt, A.; Ostermann, T.; Muller, H.; Ruitenberg, M. $Zn^{2+}$ binding to the cytoplasmic side of *Paracoccus denitrificans* cytochrome *c* oxidase selectively uncouples electron transfer and proton translocation. *FEBS Lett.* **2001**, *503*, 142−146.
(183) Qin, L.; Mills, D. A.; Hiser, C.; Murphree, A.; Garavito, R. M.; Ferguson-Miller, S.; Hosler, J. Crystallographic location and mutational analysis of Zn and Cd inhibitory sites and role of lipidic carboxylates in rescuing proton path mutants in cytochrome *c* oxidase. *Biochemistry* **2007**, *46*, 6239−6248.
(184) Aagaard, A.; Brzezinski, P. Zinc ions inhibit oxidation of cytochrome *c* oxidase by oxygen. *FEBS Lett.* **2001**, *494*, 157−160.
(185) Aagaard, A.; Namslauer, A.; Brzezinski, P. Inhibition of proton transfer in cytochrome c oxidase by zinc ions: delayed proton uptake during oxygen reduction. *Biochim. Biophys. Acta, Bioenerg.* **2002**, *1555*, 133−139.
(186) Zhou, S.; Pettersson, P.; Björck, M. L.; Dawitz, H.; Brzezinski, P.; Mäler, L.; Ädelroth, P. NMR structural analysis of the yeast cytochrome c oxidase subunit Cox13 and its interaction with ATP. *BMC Biol.* **2021**, *19*, 98.
(187) Shinzawa-Itoh, K.; Sugimura, T.; Misaki, T.; Tadehara, Y.; Yamamoto, S.; Hanada, M.; Yano, N.; Nakagawa, T.; Uene, S.; Yamada, T.; et al. Monomeric structure of an active form of bovine cytochrome *c* oxidase. *Proc. Natl. Acad. Sci. U. S. A.* **2019**, *116*, 19945−19951.
(188) Cui, T. Z.; Conte, A.; Fox, J. L.; Zara, V.; Winge, D. R. Modulation of the respiratory supercomplexes in yeast: enhanced formation of cytochrome oxidase increases the stability and abundance of respiratory supercomplexes. *J. Biol. Chem.* **2014**, *289*, 6133−6141.
(189) Bazán, S.; Mileykovskaya, E.; Mallampalli, V. K. P. S.; Heacock, P.; Sparagna, G. C.; Dowhan, W. Cardiolipin-dependent reconstitution of respiratory supercomplexes from purified Saccharomyces cerevisiae complexes III and IV. *J. Biol. Chem.* **2013**, *288*, 401−411.
(190) Napiwotzki, J.; Kadenbach, B. Extramitochondrial ATP/ADP-ratios regulate cytochrome *c* oxidase activity via binding to the cytosolic domain of subunit IV. *Biol. Chem.* **1998**, *379*, 335−339.
(191) Kagan, V. E.; Chu, C. T.; Tyurina, Y. Y.; Cheikhi, A.; Bayir, H. Cardiolipin asymmetry, oxidation and signaling. *Chem. Phys. Lipids* **2014**, *179*, 64−69.
(192) Paradies, G.; Paradies, V.; De Benedictis, V.; Ruggiero, F. M.; Petrosillo, G. Functional role of cardiolipin in mitochondrial bioenergetics. *Biochim. Biophys. Acta, Bioenerg.* **2014**, *1837*, 408−417.
(193) Horvath, S. E.; Daum, G. Lipids of mitochondria. *Prog. Lipid Res.* **2013**, *52*, 590−614.
(194) Haines, T. H.; Dencher, N. A. Cardiolipin: a proton trap for oxidative phosphorylation. *FEBS Lett.* **2002**, *528*, 35−39.
(195) Olofsson, G.; Sparr, E. Ionization constants $pK_a$ of cardiolipin. *PLoS One* **2013**, *8*, No. e73040.
(196) Kooijman, E. E.; Swim, L. A.; Graber, Z. T.; Tyurina, Y. Y.; Bayir, H.; Kagan, V. E. Magic angle spinning $^{31}P$ NMR spectroscopy reveals two essentially identical ionization states for the cardiolipin phosphates in phospholipid liposomes. *Biochim. Biophys. Acta, Biomembr.* **2017**, *1859*, 61−68.
(197) Zinser, E.; Sperka-Gottlieb, C. D.; Fasch, E. V.; Kohlwein, S. D.; Paltauf, F.; Daum, G. Phospholipid synthesis and lipid composition of subcellular membranes in the unicellular eukaryote *Saccharomyces cerevisiae*. *J. Bacteriol.* **1991**, *173*, 2026−2034.
(198) Planas-Iglesias, J.; Dwarakanath, H.; Mohammadyani, D.; Yanamala, N.; Kagan, V. E.; Klein-Seetharaman, J. Cardiolipin interactions with proteins. *Biophys. J.* **2015**, *109*, 1282−1294.
(199) Corradi, V.; Sejdiu, B. I.; Mesa-Galloso, H.; Abdizadeh, H.; Noskov, S. Y.; Marrink, S. J.; Tieleman, D. P. Emerging diversity in lipid-protein interactions. *Chem. Rev.* **2019**, *119*, 5775−5848.
(200) Gomez Jr, B.; Robinson, N. C. Phospholipase digestion of bound cardiolipin reversibly inactivates bovine cytochrome $bc_1$. *Biochemistry* **1999**, *38*, 9031−9038.
(201) Sedlák, E.; Robinson, N. C. Phospholipase A2 digestion of cardiolipin bound to bovine cytochrome *c* oxidase alters both activity and quaternary structure. *Biochemistry* **1999**, *38*, 14966−14972.
(202) Zhang, X.; Tamot, B.; Hiser, C.; Reid, G. E.; Benning, C.; Ferguson-Miller, S. Cardiolipin deficiency in *Rhodobacter sphaeroides* alters the lipid profile of membranes and of crystallized cytochrome oxidase, but structure and function are maintained. *Biochemistry* **2011**, *50*, 3879−3890.
(203) Kagan, V. E.; Bayir, H. A.; Belikova, N. A.; Kapralov, O.; Tyurina, Y. Y.; Tyurin, V. A.; Jiang, J.; Stoyanovsky, D. A.; Wipf, P.; Kochanek, P. M.; et al. Cytochrome *c*/cardiolipin relations in mitochondria: a kiss of death. *Free Radical Biol. Med.* **2009**, *46*, 1439−1453.
(204) Althoff, T.; Mills, D. J.; Popot, J. L.; Kühlbrandt, W. Arrangement of electron transport chain components in bovine mitochondrial supercomplex $I_1III_2IV_1$. *EMBO J.* **2011**, *30*, 4652−4664.
(205) Zhang, M.; Mileykovskaya, E.; Dowhan, W. Cardiolipin is essential for organization of complexes III and IV into a supercomplex in intact yeast mitochondria. *J. Biol. Chem.* **2005**, *280*, 29403−29408.
(206) Pfeiffer, K.; Gohil, V.; Stuart, R. A.; Hunte, C.; Brandt, U.; Greenberg, M. L.; Schägger, H. Cardiolipin stabilizes respiratory chain supercomplexes. *J. Biol. Chem.* **2003**, *278*, 52873−52880.
(207) Wenz, T.; Hielscher, R.; Hellwig, P.; Schägger, H.; Richers, S.; Hunte, C. Role of phospholipids in respiratory cytochrome $bc_1$ complex catalysis and supercomplex formation. *Biochim. Biophys. Acta, Bioenerg.* **2009**, *1787*, 609−616.
(208) Mileykovskaya, E.; Dowhan, W. Cardiolipin-dependent formation of mitochondrial respiratory supercomplexes. *Chem. Phys. Lipids* **2014**, *179*, 42−48.
(209) Zhang, M.; Mileykovskaya, E.; Dowhan, W. Gluing the respiratory chain together: cardiolipin is required for supercomplex formation in the inner mitochondrial membrane. *J. Biol. Chem.* **2002**, *277*, 43553−43556.
(210) Arnarez, C.; Mazat, J. P.; Elezgaray, J.; Marrink, S. J.; Periole, X. Evidence for cardiolipin binding sites on the membrane-exposed surface of the cytochrome $bc_1$. *J. Am. Chem. Soc.* **2013**, *135*, 3112−3120.
(211) Ameri, K.; Jahangiri, A.; Rajah, A. M.; Tormos, K. V.; Nagarajan, R.; Pekmezci, M.; Nguyen, V.; Wheeler, M. L.; Murphy, M. P.; Sanders, T. A.; et al. HIGD1A regulates oxygen consumption, ROS production,


https://doi.org/10.1021/acs.chemrev.1c00140
*Chem. Rev.* 2021, 121, 9644−9673

and AMPK activity during glucose deprivation to modulate cell survival and tumor growth. *Cell Rep.* **2015**, *10*, 891−899.
(212) Bedó, G.; Vargas, M.; Ferreiro, M. J.; Chalar, C.; Agrati, D. Characterization of hypoxia induced gene 1: Expression during rat central nervous system maturation and evidence of antisense RNA expression. *Int. J. Dev. Biol.* **2005**, *49*, 431−436.
(213) Wang, J.; Cao, Y.; Chen, Y.; Chen, Y.; Gardner, P.; Steiner, D. F. Pancreatic $\beta$ cells lack a low glucose and $O_2$-inducible mitochondrial protein that augments cell survival. *Proc. Natl. Acad. Sci. U. S. A.* **2006**, *103*, 10636−10641.
(214) Strogolova, V.; Furness, A.; Robb-McGrath, M.; Garlich, J.; Stuart, R. A. Rcf1 and Rcf2, members of the hypoxia-induced gene 1 protein family, are critical components of the mitochondrial cytochrome $bc_1$-cytochrome *c* oxidase supercomplex. *Mol. Cell. Biol.* **2012**, *32*, 1363−1373.
(215) Zhou, S.; Pettersson, P.; Huang, J.; Brzezinski, P.; Pomès, R.; Mäler, L.; Ädelroth, P. NMR structure and dynamics studies of yeast respiratory supercomplex factor 2. *Structure* **2021**, *29*, 275−283 e4.
(216) Zhou, S.; Pettersson, P.; Brzezinski, P.; Ädelroth, P.; Mäler, L. NMR study of Rcf2 reveals an unusual dimeric topology in detergent micelles. *ChemBioChem* **2018**, *19*, 444−447.
(217) Römpler, K.; Müller, T.; Juris, L.; Wissel, M.; Vukotic, M.; Hofmann, K.; Deckers, M. Overlapping role of respiratory supercomplex factor Rcf2 and its N-terminal homolog Rcf3 in *Saccharomyces cerevisiae*. *J. Biol. Chem.* **2016**, *291*, 23769−23778.
(218) Chen, Y. C.; Taylor, E. B.; Dephoure, N.; Heo, J. M.; Tonhato, A.; Papandreou, I.; Nath, N.; Denko, N. C.; Gygi, S. P.; Rutter, J. Identification of a protein mediating respiratory supercomplex stability. *Cell Metab.* **2012**, *15*, 348−360.
(219) Vukotic, M.; Oeljeklaus, S.; Wiese, S.; Vögtle, F. N.; Meisinger, C.; Meyer, H. E.; Zieseniss, A.; Katschinski, D. M.; Jans, D. C.; Jakobs, S.; et al. Rcf1 mediates cytochrome oxidase assembly and respirasome formation, revealing heterogeneity of the enzyme complex. *Cell Metab.* **2012**, *15*, 336−347.
(220) Fischer, F.; Filippis, C.; Osiewacz, H. D. RCF1-dependent respiratory supercomplexes are integral for lifespan-maintenance in a fungal ageing model. *Sci. Rep.* **2015**, *5*, 12697.
(221) Dawitz, H.; Schäfer, J.; Schaart, J. M.; Magits, W.; Brzezinski, P.; Ott, M. Rcf1 modulates cytochrome *c* oxidase activity especially under energy-demanding conditions. *Front. Physiol.* **2020**, *10*, 1555.
(222) Su, C. H.; McStay, G. P.; Tzagoloff, A. The Cox3p assembly module of yeast cytochrome oxidase. *Mol. Biol. Cell* **2014**, *25*, 965−976.
(223) Garlich, J.; Strecker, V.; Wittig, I.; Stuart, R. A. Mutational analysis of the QRRQ motif in the yeast hig1 type 2 protein Rcf1 reveals a regulatory role for the cytochrome *c* oxidase complex. *J. Biol. Chem.* **2017**, *292*, 5216−5226.
(224) Timón-Gómez, A.; Bartley-Dier, E. L.; Fontanesi, F.; Barrientos, A. HIGD-driven regulation of cytochrome *c* oxidase biogenesis and function. *Cells* **2020**, *9*, 2620.
(225) Deckers, M.; Balleininger, M.; Vukotic, M.; Römpler, K.; Bareth, B.; Juris, L.; Dudek, J. Aim24 stabilizes respiratory chain supercomplexes and is required for efficient respiration. *FEBS Lett.* **2014**, *588*, 2985−2992.
(226) Hock, D. H.; Reljic, B.; Ang, C. S.; Muellner-Wong, L.; Mountford, H. S.; Compton, A. G.; Ryan, M. T.; Thorburn, D. R.; Stroud, D. A. HIGD2A is required for assembly of the COX3 module of human mitochondrial complex IV. *Mol. Cell. Proteomics* **2020**, *19*, 1145.
(227) Timón-Gómez, A.; Garlich, J.; Stuart, R. A.; Ugalde, C.; Barrientos, A. Distinct roles of mitochondrial HIGD1A and HIGD2A in respiratory complex and supercomplex biogenesis. *Cell Rep.* **2020**, *31*, 107607.
(228) Hoang, N. H.; Strogolova, V.; Mosley, J. J.; Stuart, R. A.; Hosler, J. Hypoxia-inducible gene domain 1 proteins in yeast mitochondria protect against proton leak through complex IV. *J. Biol. Chem.* **2019**, *294*, 17669−17677.
(229) Schäfer, J.; Dawitz, H.; Ott, M.; Ädelroth, P.; Brzezinski, P. Regulation of cytochrome c oxidase activity by modulation of the catalytic site. *Sci. Rep.* **2018**, *8*, 11397.
(230) Schäfer, J.; Dawitz, H.; Ott, M.; Ädelroth, P.; Brzezinski, P. Structural and functional heterogeneity of cytochrome *c* oxidase in *S. cerevisiae*. *Biochim. Biophys. Acta, Bioenerg.* **2018**, *1859*, 699−704.
(231) Rydström Lundin, C.; Brzezinski, P. Modulation of $O_2$ reduction in *Saccharomyces cerevisiae* mitochondria. *FEBS Lett.* **2017**, *591*, 4049−4055.
(232) Nilsson, T. *Protein and lipid interactions within the respiratory chain: studies using membrane-mimetic systems*. 2019 PhD dissertation, Department of Biochemistry and Biophysics, Stockholm University, Stockholm.
(233) Strogolova, V.; Hoang, N. H.; Hosler, J.; Stuart, R. A. The yeast mitochondrial proteins Rcf1 and Rcf2 support the enzymology of the cytochrome *c* oxidase complex and generation of the proton motive force. *J. Biol. Chem.* **2019**, *294*, 4867−4877.
(234) Rydström Lundin, C.; Von Ballmoos, C.; Ott, M.; Ädelroth, P.; Brzezinski, P. Regulatory role of the respiratory supercomplex factors in *Saccharomyces cerevisiae*. *Proc. Natl. Acad. Sci. U. S. A.* **2016**, *113*, E4476−E4485.
(235) Hayashi, T.; Asano, Y.; Shintani, Y.; Aoyama, H.; Kioka, H.; Tsukamoto, O.; Hikita, M.; Shinzawa-Itoh, K.; Takafuji, K.; Higo, S.; et al. Higd1a is a positive regulator of cytochrome *c* oxidase. *Proc. Natl. Acad. Sci. U. S. A.* **2015**, *112*, 1553−1558.
(236) Varanasi, L.; Mills, D.; Murphree, A.; Gray, J.; Purser, C.; Baker, R.; Hosler, J. Altering conserved lipid binding sites in cytochrome *c* oxidase of Rhodobacter sphaeroides perturbs the interaction between subunits I and III and promotes suicide inactivation of the enzyme. *Biochemistry* **2006**, *45*, 14896−14907.
(237) Vygodina, T. V.; Pecoraro, C.; Mitchell, D.; Gennis, R.; Konstantinov, A. A. Mechanism of inhibition of electron transfer by amino acid replacement K362M in a proton channel of *Rhodobacter sphaeroides* cytochrome *c* oxidase. *Biochemistry* **1998**, *37*, 3053−3061.
(238) Jenney, F. E.; Verhagen, M. F. J. M.; Cui, X.; Adams, M. W. W. Anaerobic microbes: oxygen detoxification without superoxide dismutase. *Science* **1999**, *286*, 306−309.
(239) Lundgren, C. A. K.; Sjöstrand, D.; Biner, O.; Bennett, M.; Rudling, A.; Johansson, A. L.; Brzezinski, P.; Carlsson, J.; Von Ballmoos, C.; Högbom, M. Scavenging of superoxide by a membrane-bound superoxide oxidase. *Nat. Chem. Biol.* **2018**, *14*, 788−793.
(240) Koppenol, W. H.; Rush, J. D.; Mills, J. D.; Margoliash, E. The dipole moment of cytochrome *c*. *Mol. Biol. Evol.* **1991**, *8*, 545−558.
(241) Feng, J. J.; Murgida, D. H.; Kuhlmann, U.; Utesch, T.; Mroginski, M. A.; Hildebrandt, P.; Weidinger, I. M. Gated electron transfer of yeast Iso-1 cytochrome *c* on self-assembled monolayer-coated electrodes. *J. Phys. Chem. B* **2008**, *112*, 15202−15211.
(242) Tian, H.; Sadoski, R.; Zhang, L.; Yu, C. A.; Yu, L.; Durham, B.; Millett, F. Definition of the interaction domain for cytochrome *c* on the cytochrome $bc_1$ complex. Steady-state and rapid kinetic analysis of electron transfer between cytochrome *c* and *Rhodobacter sphaeroides* cytochrome $bc_1$ surface mutants. *J. Biol. Chem.* **2000**, *275*, 9587−9595.
(243) Lange, C.; Hunte, C. Crystal structure of the yeast cytochrome $bc_1$ complex with its bound substrate cytochrome *c*. *Proc. Natl. Acad. Sci. U. S. A.* **2002**, *99*, 2800−2805.
(244) Shimada, S.; Shinzawa-Itoh, K.; Baba, J.; Aoe, S.; Shimada, A.; Yamashita, E.; Kang, J.; Tateno, M.; Yoshikawa, S.; Tsukihara, T. Complex structure of cytochrome *c*-cytochrome *c* oxidase reveals a novel protein-protein interaction mode. *EMBO J.* **2017**, *36*, 291−300.
(245) Capaldi, R. A.; Darley-Usmar, V.; Fuller, S.; Millett, F. Structural and functional features of the interaction of cytochrome *c* with complex III and cytochrome *c* oxidase. *FEBS Lett.* **1982**, *138*, 1−7.
(246) Speck, S. H.; Ferguson-Miller, S.; Osheroff, N.; Margoliash, E. Definition of cytochrome *c* binding domains by chemical modification: kinetics of reaction with beef mitochondrial reductase and functional organization of the respiratory chain. *Proc. Natl. Acad. Sci. U. S. A.* **1979**, *76*, 155−159.
(247) Wennerström, H.; Estrada, E. V.; Danielsson, J.; Oliveberg, M. Colloidal stability of the living cell. *Proc. Natl. Acad. Sci. U. S. A.* **2020**, *117*, 10113−10121.
(248) Moreno-Beltrán, B.; Díaz-Quintana, A.; González-Arzola, K.; Velázquez-Campoy, A.; De La Rosa, M. A.; Díaz-Moreno, I.

Cytochrome c1 exhibits two binding sites for cytochrome *c* in plants. *Biochim. Biophys. Acta, Bioenerg.* **2014**, *1837*, 1717−1729.
(249) Hunte, C.; Solmaz, S.; Lange, C. Electron transfer between yeast cytochrome $bc_1$ complex and cytochrome *c*: a structural analysis. *Biochim. Biophys. Acta, Bioenerg.* **2002**, *1555*, 21−28.
(250) Wilms, J.; Veerman, E. C. I.; König, B. W.; Dekker, H. L.; van Gelder, B. F. Ionic strength effects on cytochrome $aa_3$ kinetics. *Biochim. Biophys. Acta, Bioenerg.* **1981**, *635*, 13−24.
(251) Ferguson-Miller, S.; Brautigan, D. L.; Margoliash, E. Correlation of the kinetics of electron transfer activity of various eukaryotic cytochromes *c* with binding to mitochondrial cytochrome *c* oxidase. *J. Biol. Chem.* **1976**, *251*, 1104−1115.
(252) Speck, S. H.; Dye, D.; Margoliash, E. Single catalytic site model for the oxidation of ferrocytochrome *c* by mitochondrial cytochrome *c* oxidase. *Proc. Natl. Acad. Sci. U. S. A.* **1984**, *81*, 347−351.
(253) Malatesta, F.; Antonini, G.; Nicoletti, F.; Giuffre, A.; D'Itri, E.; Sarti, P.; Brunori, M. Probing the high-affinity site of beef heart cytochrome *c* oxidase by cross-linking. *Biochem. J.* **1996**, *315*, 909−916.
(254) Dethmers, J. K.; Ferguson-Miller, S.; Margoliash, E. Comparison of yeast and beef cytochrome *c* oxidases. Kinetics and binding of horse, fungal, and Euglena cytochromes *c*. *J. Biol. Chem.* **1979**, *254*, 11973−11981.
(255) Gray, H. B.; Winkler, J. R. Electron transfer in proteins. *Annu. Rev. Biochem.* **1996**, *65*, 537−561.
(256) Fuchs, P.; Rugen, N.; Carrie, C.; Elsässer, M.; Finkemeier, I.; Giese, J.; Hildebrandt, T. M.; Kühn, K.; Maurino, V. G.; Ruberti, C.; et al. Single organelle function and organization as estimated from *Arabidopsis mitochondrial* proteomics. *Plant J.* **2020**, *101*, 420−441.
(257) Daldal, F.; Mandaci, S.; Winterstein, C.; Myllykallio, H.; Duyck, K.; Zannoni, D. Mobile cytochrome $c_2$ and membrane-anchored cytochrome $c_y$ are both efficient electron donors to the $cbb_3$-and $aa_3$-type cytochrome *c* oxidases during respiratory growth of *Rhodobacter sphaeroides*. *J. Bacteriol.* **2001**, *183*, 2013−2024.
(258) Myllykallio, H.; Drepper, F.; Mathis, P.; Daldal, F. Membrane-anchored cytochrome $c_y$ mediated microsecond time range electron transfer from the cytochrome $bc_1$ complex to the reaction center in *Rhodobacter capsulatus*. *Biochemistry* **1998**, *37*, 5501−5510.
(259) Andersson, S. G. E.; Zomorodipour, A.; Andersson, J. O.; Sicheritz-Pontén, T.; Alsmark, U. C. M.; Podowski, R. M.; Näslund, A. K.; Eriksson, A. S.; Winkler, H. H.; Kurland, C. G. The genome sequence of *Rickettsia prowazekii* and the origin of mitochondria. *Nature* **1998**, *396*, 133−140.
(260) Berry, E. A.; Trumpower, B. L. Simultaneous determination of hemes *a b* and *c* from pyridine hemochrome spectra. *Anal. Biochem.* **1987**, *161*, 1−15.
(261) Toth, A.; Aufschnaiter, A.; Fedotovskaya, O.; Dawitz, H.; Ädelroth, P.; Büttner, S.; Ott, M. Membrane-tethering of cytochrome *c* accelerates regulated cell death in yeast. *Cell Death Dis.* **2020**, *11*, 722.
(262) Bengtsson, J.; Rivolta, C.; Hederstedt, L.; Karamata, D. Bacillus subtilis contains two small *c*-type cytochromes with homologous heme domains but different types of membrane anchors. *J. Biol. Chem.* **1999**, *274*, 26179−26184.
(263) Megehee, J. A.; Hosler, J. P.; Lundrigan, M. D. Evidence for a cytochrome *bcc-aa*$_3$ interaction in the respiratory chain of *Mycobacterium smegmatis*. *Microbiology* **2006**, *152*, 823−829.
(264) Moreno-Beltrán, B.; Díaz-Moreno, I.; González-Arzola, K.; Guerra-Castellano, A.; Velázquez-Campoy, A.; De La Rosa, M. A.; Díaz-Quintana, A. Respiratory complexes III and IV can each bind two molecules of cytochrome *c* at low ionic strength. *FEBS Lett.* **2015**, *589*, 476−483.
(265) Pérez-Mejías, G.; Guerra-Castellano, A.; Díaz-Quintana, A.; De la Rosa, M. A.; Díaz-Moreno, I. Cytochrome *c*: surfing off of the mitochondrial membrane on the tops of complexes III and IV. *Comput. Struct. Biotechnol. J.* **2019**, *17*, 654−660.
(266) Spaar, A.; Flöck, D.; Helms, V. Association of cytochrome *c* with membrane-bound cytochrome *c* oxidase proceeds parallel to the membrane rather than in bulk solution. *Biophys. J.* **2009**, *96*, 1721−1732.
(267) Gupte, S.; Wu, E. S.; Hoechli, L.; Hoechli, M.; Jacobson, K.; Sowers, A. E.; Hackenbrock, C. R. Relationship between lateral diffusion, collision frequency, and electron transfer of mitochondrial inner membrane oxidation-reduction components. *Proc. Natl. Acad. Sci. U. S. A.* **1984**, *81*, 2606−2610.
(268) De March, M.; Brancatelli, G.; Demitri, N.; De Zorzi, R.; Hickey, N.; Geremia, S. A general exit strategy of monoheme cytochromes *c* and $c_2$ in electron transfer complexes? *IUBMB Life* **2015**, *67*, 694−700.
(269) Trouillard, M.; Meunier, B.; Rappaport, F. Questioning the functional relevance of mitochondrial supercomplexes by time-resolved analysis of the respiratory chain. *Proc. Natl. Acad. Sci. U. S. A.* **2011**, *108*, E1027−E1034.
(270) Baker, N. A.; Sept, D.; Joseph, S.; Holst, M. J.; McCammon, J. A. Electrostatics of nanosystems: application to microtubules and the ribosome. *Proc. Natl. Acad. Sci. U. S. A.* **2001**, *98*, 10037−10041.
(271) *The PyMOL Molecular Graphics System, M.*; Schrödinger, LLC. 2006.
(272) Lobo-Jarne, T.; Nývltová, E.; Pérez-Pérez, R.; Timón-Gómez, A.; Molinié, T.; Choi, A.; Mourier, A.; Fontanesi, F.; Ugalde, C.; Barrientos, A. Human COX7A2L regulates complex III biogenesis and promotes supercomplex organization remodeling without affecting mitochondrial bioenergetics. *Cell Rep.* **2018**, *25*, 1786−1799 e4.
(273) Liu, J.; Barrientos, A. Transcriptional regulation of yeast oxidative phosphorylation hypoxic genes by oxidative stress. *Antioxid. Redox Signaling* **2013**, *19*, 1916−1927.
(274) Poyton, R. O. Models for oxygen sensing in yeast: Implications for oxygen-regulated gene expression in higher eucaryotes. *Respir. Physiol.* **1999**, *115*, 119−133.
(275) Zhou, S.; Pettersson, P.; Huang, J.; Sjöholm, J.; Sjöstrand, D.; Pomès, R.; Högbom, M.; Brzezinski, P.; Mäler, L.; Ädelroth, P. Solution NMR structure of yeast Rcf1, a protein involved in respiratory supercomplex formation. *Proc. Natl. Acad. Sci. U. S. A.* **2018**, *115*, 3048−3053.
(276) Schäfer, J. Doctoral thesis, *Comprehensive summary*; Department of Biochemistry and Biophysics, Stockholm University, 2018.
(277) Guerra-Castellano, A.; Díaz-Quintana, A.; Pérez-Mejías, G.; Elena-Real, C. A.; González-Arzola, K.; García-Mauriño, S. M.; De la Rosa, M. A.; Díaz-Moreno, I. Oxidative stress is tightly regulated by cytochrome *c* phosphorylation and respirasome factors in mitochondria. *Proc. Natl. Acad. Sci. U. S. A.* **2018**, *115*, 7955−7960.
(278) Schägger, H.; Pfeiffer, K. The ratio of oxidative phosphorylation complexes I-V in bovine heart mitochondria and the composition of respiratory chain supercomplexes. *J. Biol. Chem.* **2001**, *276*, 37861−37867.
(279) Lapuente-Brun, E.; Moreno-Loshuertos, R.; Acín-Pérez, R.; Latorre-Pellicer, A.; Colás, C.; Balsa, E.; Perales-Clemente, E.; Quirós, P. M.; Calvo, E.; Rodríguez-Hernández, M. A.; et al. Supercomplex assembly determines electron flux in the mitochondrial electron transport chain. *Science* **2013**, *340*, 1567−1570.
(280) Genova, M. L.; Lenaz, G. A critical appraisal of the role of respiratory supercomplexes in mitochondria. *Biol. Chem.* **2013**, *394*, 631−639.
(281) Blaza, J. N.; Serreli, R.; Jones, A. J. Y.; Mohammed, K.; Hirst, J. Kinetic evidence against partitioning of the ubiquinone pool and the catalytic relevance of respiratory-chain supercomplexes. *Proc. Natl. Acad. Sci. U. S. A.* **2014**, *111*, 15735−15740.
(282) Cogliati, S.; Frezza, C.; Soriano, M. E.; Varanita, T.; Quintana-Cabrera, R.; Corrado, M.; Cipolat, S.; Costa, V.; Casarin, A.; Gomes, L. C.; et al. Mitochondrial cristae shape determines respiratory chain supercomplexes assembly and respiratory efficiency. *Cell* **2013**, *155*, 160−171.
(283) Fedor, J. G.; Hirst, J. Mitochondrial supercomplexes do not enhance catalysis by quinone channeling. *Cell Metab.* **2018**, *28*, 525−531 e4.
(284) Maranzana, E.; Barbero, G.; Falasca, A. I.; Lenaz, G.; Genova, M. L. Mitochondrial respiratory supercomplex association limits production of reactive oxygen species from complex I. *Antioxid. Redox Signaling* **2013**, *19*, 1469−1480.


https://doi.org/10.1021/acs.chemrev.1c00140
*Chem. Rev.* 2021, 121, 9644−9673

(285) Turrens, J. F. Mitochondrial formation of reactive oxygen species. *J. Physiol.* **2003**, *552*, 335−344.
(286) Murphy, M. P. How mitochondria produce reactive oxygen species. *Biochem. J.* **2009**, *417*, 1−13.
(287) Lobo-Jarne, T.; Pérez-Pérez, R.; Fontanesi, F.; Timón-Gómez, A.; Wittig, I.; Peñas, A.; Serrano-Lorenzo, P.; García-Consuegra, I.; Arenas, J.; Martín, M. A.; et al. Multiple pathways coordinate assembly of human mitochondrial complex IV and stabilization of respiratory supercomplexes. *EMBO J.* **2020**, *39*, No. e103912.
(288) Lenaz, G.; Genova, M. L. Structure and organization of mitochondrial respiratory complexes: a new understanding of an old subject. *Antioxid. Redox Signaling* **2010**, *12*, 961−1008.
(289) Postmus, J.; Tuzun, I.; Bekker, M.; Müller, W. H.; Teixeira de Mattos, M. J.; Brul, S.; Smits, G. J. Dynamic regulation of mitochondrial respiratory chain efficiency in *Saccharomyces cerevisiae*. *Microbiology* **2011**, *157*, 3500−3511.
(290) Díaz-Moreno, I.; García-Heredia, J. M.; Díaz-Quintana, A.; De La Rosa, M. A. Cytochrome *c* signalosome in mitochondria. *Eur. Biophys. J.* **2011**, *40*, 1301−1315.
(291) Hüttemann, M.; Pecina, P.; Rainbolt, M.; Sanderson, T. H.; Kagan, V. E.; Samavati, L.; Doan, J. W.; Lee, I. The multiple functions of cytochrome *c* and their regulation in life and death decisions of the mammalian cell: from respiration to apoptosis. *Mitochondrion* **2011**, *11*, 369−381.
(292) Sarewicz, M.; Dutka, M.; Froncisz, W.; Osyczka, A. Magnetic interactions sense changes in distance between heme $b_L$ and the iron-sulfur cluster in cytochrome $bc_1$. *Biochemistry* **2009**, *48*, 5708−5720.
(293) Pettersen, E. F.; Goddard, T. D.; Huang, C. C.; Meng, E. C.; Couch, G. S.; Croll, T. I.; Morris, J. H.; Ferrin, T. E. UCSF ChimeraX: Structure visualization for researchers, educators, and developers. *Protein Sci.* **2021**, *30*, 70.


https://doi.org/10.1021/acs.chemrev.1c00140
*Chem. Rev.* 2021, 121, 9644−9673